Bacterial Adhesion in Structured Environments

by

Ronn S. Friedlander

B.S. Biomedical Engineering and Ecology & Natural Resources, Rutgers University, 2008
M.Phil. Clinical Biochemistry, University of Cambridge, 2009

SUBMITTED TO THE DIVISION OF HEALTH SCIENCES AND TECHNOLOGY
IN PARTIAL FULFILLMENT OF THE REQUIREMENTS FOR THE DEGREE OF

DOCTOR OF PHILOSOPHY IN
MEDICAL ENGINEERING AND MEDICAL PHYSICS
AT THE
MASSACHUSETTS INSTITUTE OF TECHNOLOGY

SEPTEMBER 2014

Signature redacted

Signature of Author:_____
Harvard-MIT Program in Health Sciences and Technology
August 29, 2014

Signature redacted

Certified by:_____
Joanna Aizenberg, Ph.D.
Amy Smith Berylson Professor of Materials Science,
Professor of Chemistry and Chemical Biology,
Harvard School of Engineering and Applied Sciences
Thesis Supervisor

Signature redacted

Accepted by:_____
Emery N. Brown, M.D., Ph.D.
Director, Harvard-MIT Program in Health Sciences and Technology
Professor of Computational Neuroscience and Health Sciences and Technology

Bacterial Adhesion in Structured Environments

by

Ronn S. Friedlander

Submitted to the Harvard-MIT program in Health Sciences and Technology
on August 29, 2014 in partial fulfillment of the requirements for the degree of
Doctor of Philosophy in Medical Engineering and Medical Physics

ABSTRACT

Biofilms—surface-bound communities of microbes—are a major medical concern, as they can be sources of infection that are difficult to eradicate. Their formation starts with the attachment of bacteria to available surfaces—often implantable biomaterials. The development of materials that prevent bacterial adhesion is therefore of paramount importance, and it requires a thorough understanding of the materials and bacterial surface properties that enable adhesive interactions. We herein design model surfaces and examine the interplay between micro-scale geometry, surface energy and bacterial surface properties with respect to adhesion, with the ultimate goal of understanding bacterial adhesion in structured environments, and establishing principles for design of novel surfaces that effectively repel bacteria.

We first study adhesion of *Escherichia coli* to engineered surfaces possessing superficially unfavorable geometries. We show that cells can overcome geometric constraints with the aid of flagella, which are able to reach between narrow crevices, thus improving adhesion and expanding the range of surfaces to which cells can adhere. We examine binding of purified flagella to abiotic surfaces by means of quartz crystal microbalance (QCM) and show that flagella bind preferentially to hydrophobic surfaces, yet they do not appreciably bind to hydrophilic surfaces. Using mutant strains, we investigate the role of flagella in surface attachment of live cells and demonstrate that flagellated cells adhere best to hydrophobic substrates; however flagella may impede cell adhesion to hydrophilic surfaces.

To further explore hydrophilic, structured environments with physiological relevance, we examine mucin—a natural hydrogel that typically harbors microbes in animals, while protecting the host. We purify mucins and use them in their native, three-dimensional configuration to probe bacterial swimming behavior and surface attachment in their presence. We demonstrate that mucins maintain—and possibly enhance—swimming ability for *E. coli* and *Pseudomonas aeruginosa*, and show that they greatly reduce adhesion to underlying substrates.

Finally, we build on our established design principles and construct anti-adhesive surfaces by combining hydrophilic chemistries with topographic features smaller than cellular dimensions. This work suggests a path toward anti-adhesive materials that may be optimized for mechanical robustness, longevity and specific environments of application.

Thesis supervisor: Joanna Aizenberg, Ph.D.
Title: Amy Smith Berylson Professor of Materials Science, Professor of Chemistry and Chemical Biology, Harvard School of Engineering and Applied Sciences

Acknowledgments

When I reflect on the journey I took to get here, I must thank Ashley Winter for showing me the path of biomedical engineering, which combined my love of biological systems with the rigor of engineering principles. Despite our distance in time and space from those early college days, we remain close friends. There was a point in college when I knew I could cut it at a place like MIT. I would say the encouragement and guidance of Charlie Roth at Rutgers was what enabled my confidence to grow; it got me to that point where I could challenge myself to attend the excellent grad programs at Cambridge and MIT/Harvard.

My time in the HST program has been amazing and I must thank those HMS professors who stick out in my mind as making my medical classes invigorating: Rick Mitchell, Shiv Pillai and David Housman. Beyond the classes at HMS and MIT, I was lucky enough to join the lab of Joanna Aizenberg. I am privileged to have spent the last four years in Joanna's lab, working with some of the most creative and intelligent minds I have ever encountered. Joanna took me in as a young student, gave me the tools and freedom to follow my own research path, and enabled me to mature as a scientist. I continue to be impressed by Joanna's ability to drill down to the important points of a research project and very rapidly ask the most poignant questions. I hope some of this has rubbed off on me.

I owe much of my success to my wonderful colleagues who have been friends and collaborators throughout my time at HST. Mike Bucaro was my first mentor in the Aizenberg lab and also made sure everyone was socializing. I won't forget how important he was in helping me find my place in the lab. I soon found Hera Vlamakis, who helped me learn some genetic techniques and was always there to read over and help me with my manuscripts. I am very appreciative of Karen Fahrner for all her wisdom and help as we figured out how to purify flagella. Making the right connections has been so crucial for this research project, due to the numerous academic fields involved. I cannot overstate how important the BASF biofilms group was for helping me to make the right contacts and foster discussions about bacterial behavior among a highly interdisciplinary group of scientists who all wanted to help each other solve problems. Of course, having funding from BASF, the NSF and the Cystic Fibrosis Foundation has enabled much of this work to take place.

Hardly an easy journey, carrying out my PhD work was one of the most challenging tasks I have ever taken on. I could not have done it without mentorship and the support of friends. Research discussions with Katharina Ribbeck were so helpful in building my confidence in the various projects I undertook. I cannot thank her enough for those supportive conversations and collaborations. Having Roberto Kolter as a mentor and thesis committee member was very helpful and enlightening. Also, engaging with other microbiologists and friends through MSI was extremely enjoyable and helpful. Outside of school, I continue to have the constant support of my friends: Alex Bruno, who can always be counted on for a trivia night outing; Jake Brukhman, who always challenges my assumptions and inspires creativity; Eyal Wellisch, who has been there for me since I was 2 years old; my roommates Ben Holmes, Christine Platzek, Dan Rassi and Will Silversmith, who are always around and supportive in things ranging from video gaming to building beverage empires—they help me keep things interesting.

Finally, I thank my family. They made me who I am today. They gave me everything I needed to succeed and the encouragement and tools to be independent. Sandy and my Dad have always encouraged me and been there for me. My mom has been so supportive of me in all that I do and has always inspired me to be curious and question everything. I will continue to do that.

Table of Contents

Chapter 1
Background

CLINICAL IMPACT OF BACTERIAL BIOFILMS

Bacterial infection is a ubiquitous cause of morbidity and mortality that places a considerable burden on our healthcare system. Nearly two million healthcare associated infections (HAIs) per year cost U.S. hospitals between $28 and $45 billion [1]. Of these, ~450,000 are catheter-associated urinary tract infections and 92,000 are central line associated bloodstream infections [1]. In 2002, urinary tract and bloodstream HAIs alone (often via implantation of inert biomaterials) resulted in 13,088 and 30,665 deaths, respectively [2]. In the most insidious HAIs, the contributing bacteria exist in a sessile, protective state called a biofilm. These biofilms form on the surfaces of medical implant materials, such as catheters, heart valves and prostheses, to name only a few [3, 4].

Figure 1.1. Schematic of the steps of biofilm formation. The biofilm life cycle illustrated in three steps: initial attachment events, the growth of complex biofilms, and detachment events by clumps of bacteria or so-called 'seeding dispersal.' Source: Center for Biofilm Engineering, Bozeman, MT.

The standard model for the progression of biofilm development (Figure 1.1) starts with planktonic microbes adhering reversibly to a surface coated with a conditioning film created by

components of the aqueous environment (blood, interstitial fluid, growth medium, etc.) [5, 6]. Once the initial colonizers are present, they can serve to nucleate microcolonies. As these microcolonies reach a threshold size, the microbes begin to secrete matrix and irreversibly attach to a surface [7, 8]. The NIH estimates that 80% of persistent bacterial infections are in the form of biofilms (Figure 1.2) [9, 10]. The overall heterogeneity of gene expression, structure, chemistry and material properties of mature biofilms allows at least parts of them to survive a broad spectrum of assaults [11]. Whether by gene transfer or by antibiotic-induced population bottlenecks that allow resistant 'persister cells' to repopulate biofilms [12], antibiotic susceptibility is greatly reduced in these communities. An early demonstration of this showed *Pseudomonas aeruginosa* biofilms to be viable after treatment with tobramycin concentrations in excess of twenty times the concentration necessary to completely kill planktonic cells of the same strain [13]. There have since been numerous demonstrations of this phenomenon with other species and antibiotics [10, 14–16]. Biofilm populations are extremely dense compared with disseminated swimming bacterial populations. Recent studies show density-dependent antibiotic resistance effects that do not occur in relatively sparse planktonic populations [17, 18]. The matrix enclosure, which can be composed of polysaccharides, protein fibers, surface organelles, and/or nucleic acids, reduces the distance and rate at which antimicrobials can diffuse into the biofilm [9, 19], thus making it very difficult to destroy a biofilm with drug treatments alone. Finally, the sub-lethal doses of antibiotics that do reach the deeper levels of a biofilm will introduce strong selective pressure for resistance [14, 20]. The prevalence and variety of antibiotic-resistant bacterial species is ever increasing, yet the number of antibiotic FDA-approved new molecular entities has steadily dwindled over the past 25 years [21].

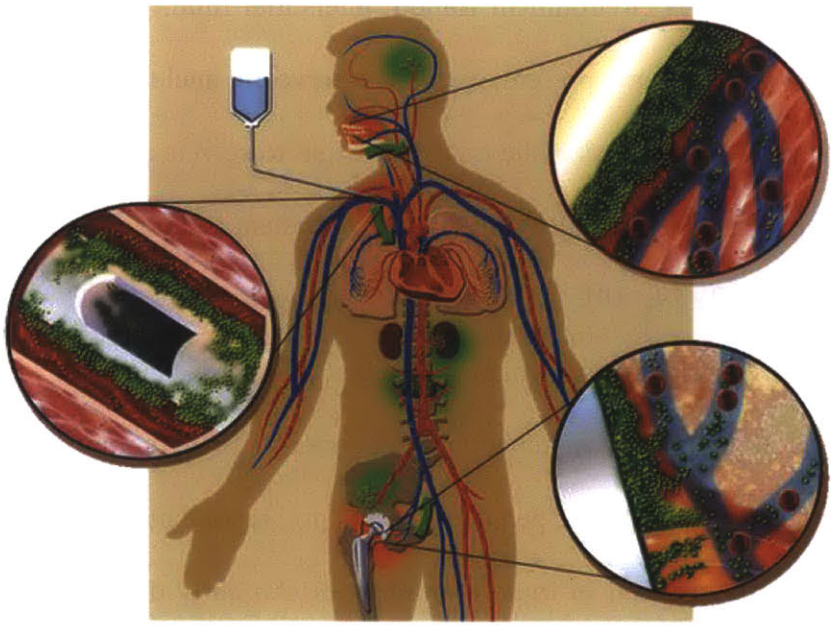

Figure 1.2. Biofilm implant infections. Schematic depiction of implants that can become infected with biofilms and seed new infections in the body. These include catheters, dental implants and hip implants. Source: Center for Biofilm Engineering, Bozeman, MT.

PREVENTION OF BACTERIAL ADHESION TO BIOMATERIALS

Bacterial surface adhesion is a ubiquitous phenomenon in the natural world, and as the first step in biofilm formation, it enables microbes to survive changing environments, chemical and physical assaults and depletion of resources [22, 23]. Due to the survival advantages imparted by the biofilm lifestyle, pristine, unoccupied surfaces provide high-value real estate to bacteria, particularly when conditions favor a survival mode, rather than a proliferative one [9]. Unfortunately, numerous materials applications require the maintenance of pristine surfaces in bacteria-rich environments. Beyond biomedical materials, these also include remote optical sensors and marine vessels, to name a few [8, 9, 24, 25]. These surfaces become exposed to bacteria during use and are ultimately fouled by adhering microbes. Once these microbes progress to mature biofilms, they become difficult or impossible to remove [26]. Researchers

have therefore focused on preventing bacterial adhesion to indwelling medical devices and this has become an important, interdisciplinary field of research.

Two primary methods are currently practiced to reduce bacterial colonization of indwelling materials, both of which involve antimicrobial agents. One common approach is to administer intravenous and topical prophylactic agents before and during implant procedures and to continue an antibiotic regimen for a period after the procedure. This is practiced in conjunction with joint replacement procedures as well as with implantation of some dental prostheses [27]. The result of this antibiotic regimen, combined with strict aseptic techniques and reduced operating times, is a reduction in overall postoperative infection rates. However, prophylaxis has had only weak evidence of efficacy when used for urinary catheterization [28]. Of course, the administration of prophylactic antibiotics will increase the rate of development of resistance. Orthopedic practitioners already debate whether this practice should be continued due to the increased emergence of antibiotic resistant bacteria [29, 30].

Another strategy that has emerged relies on coating or bonding devices with antimicrobial agents to deter biofilm formation. Silicone shunts impregnated with various antibiotics (rifampicin, clindamycin) significantly reduced the survival of *Staphylococcus epidermidis in vitro* [31]. A clinical study of cefazolin-bonded venous and arterial catheters showed a reduction in infection (usually *S. epidermidis*) from 14% of control catheters to 2% of antibiotic-bonded catheters [32]. For urinary catheters, silver alloy coatings have been used as antimicrobials and have been shown to reduce infection, especially during the first week of implantation [33]. These reductions have been modest, with most studies reporting <10% reduction in risk of infection (though one study reported a risk reduction of 32%) [34]. Medicated vascular catheters still have infection rates between 1.2 and 4.8 cases per 1000

catheter days, which is high considering that many patients are catheterized for more than a week at a time [35].

A less popular, but intriguing strategy for biofilm prevention is the probiotic approach. Strong evidence suggests that the presence of some beneficial bacteria in the body can act to inhibit the growth of pathogenic microbes [36, 37]. Furthermore, researchers have shown that specific actions, such as eating yogurt to prevent colonization of laryngeal implants, can reduce incidence of infection [37]. One study demonstrated that the presence of *S. aureus* in human nares could be eliminated by artificial implantation of *Corynebacteria [38]*. In an ongoing phase I clinical trial, non-pathogenic *E. coli* are being used to pre-coat catheters, so as to prevent adhesion of pathogens [39, 40].

A number of promising coatings based on hydrophilic polymers have been shown to reduce bacterial adhesion. These include but are not limited to: polyethylene glycol (PEG) [41–43], chitosan [44, 45], heparin [43], and purified mucin [46]. Mucins are particularly interesting materials as they form the major medium for host-microbe interactions. *In vitro* studies of antifouling mucin coatings have demonstrated varying results in performance. Due to the complexity of these molecules, it is likely that their structural integrity is critical for their antimicrobial properties. Mucins are large glycoproteins with the majority of their molecular weight comprised of oligosaccharides. They are secreted by goblet cells as packets that become hydrated, expand and are crosslinked to form a structured network (Figure 1.3) [47, 48]. It is possible that the structure of this network is related to their ability to regulate the large bacterial populations that reside adjacent to host epithelia (e.g. in the colon). Different methods of preparation and surface tethering utilized in previous studies are perhaps causes for conflicting findings.

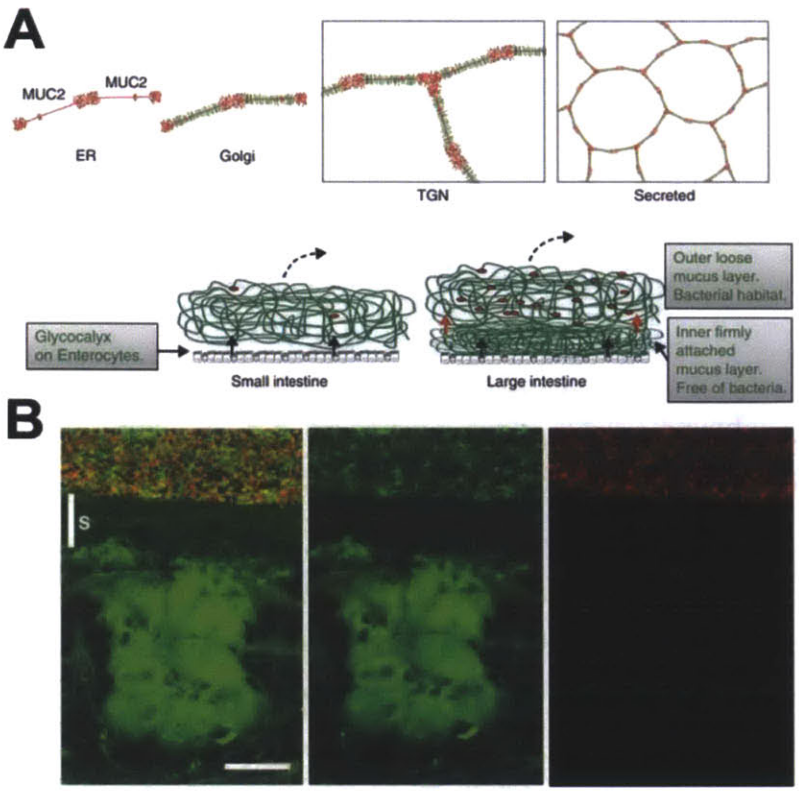

Figure 1.3. Mucins harbor bacteria but protect the host. (*A*) Schematic outline of the Muc2 mucin and its formation of mucus in the small and large intestine. Assembly of the Muc2 mucin (protein core red) into dimeric forms in the endoplasmic reticulum (ER), O-glycosylation (green) in the Golgi apparatus, formation of trimeric forms in the trans Golgi network (TGN) and a schematic picture of the secreted Muc2 polymer in a structured network [49]. (*B*) Combined Muc2 immunostaining (green) and FISH analysis using the general bacterial probe EUB338-Alexa Fluor 555 (red) of distal colon shows Muc2-positive goblet cells and an inner stratified (s) mucus layer on the epithelium. This layer is devoid of bacteria, which can only be detected in the outer mucus layer. The inner mucus generates a spatial separation between the cells and the microflora (Scale bar: 20 μm) [50].

TOPOGRAPHICAL AND GEOMETRICAL APPROACHES TO BIOFILM CONTROL

Given the diversity of bacterial biofilm communities and the ubiquity of conditioning films (which may mask surface chemistry), a more general, physical approach should be taken to prevent adhesion. In the fields of cell biology and tissue engineering, surface architecture has been studied and manipulated extensively in order to achieve a measure of control over tissue

cell behavior [51–55]. Only recently have these techniques been applied for the control of biofilm formation [56].

There is strong evidence that bacteria can respond quite dramatically to surface patterns. Takeuchi *et al.* showed that *E. coli* could be formed into coil shapes by allowing them to grow within toroid trenches [57]. Work by Díaz *et al.* showed that nano-scale trenches reduce migration of surface-bound *Psuedomonas fluorescens* [58]. A study from our lab demonstrated that *E. coli*, *P. aeruginosa* and *Bacillus subtilis* can be patterned in a controllable manner using nano-scale post arrays on a similar size scale to the bacteria. The spacing of the posts can be adjusted to achieve different, predictable patterns [59]. Furthermore, when the posts are sufficiently close together, the bacteria will arrange themselves in a random orientation at the tips of the posts, and not at the base of the substrate.

Micro- and nano-topographies have been used in several studies to determine whether they can influence bacterial adhesion. Campoccia *et al.* compared adhesion of *S. aureus* on an array of 100 nm diameter, 160 nm tall posts spaced 200 nm apart to adhesion on flat surfaces, and was unable to observe a significant influence of this topography [60]. Another study looked at adhesion of multiple cocci and rod-shaped bacteria to surfaces with circular indentations between 0.2 μm and 2 μm; this study showed differential adhesion based on both species and feature size [61]. For the most part, bacteria were retained within the indentations except in the smallest feature sizes. In those cases, the adhesion was similar to adhesion on flat surfaces. One interesting study used shark skin-inspired micro-scale patterns [62] in poly(dimethyl siloxane) (PDMS) elastomer to reduce biofilm formation by *S. aureus* (Figure 1.4) [63, 64]. This same material was originally optimized for reduction of biofouling by zoospores, however it appears to show efficacy in reducing biofilms as well [63, 65].

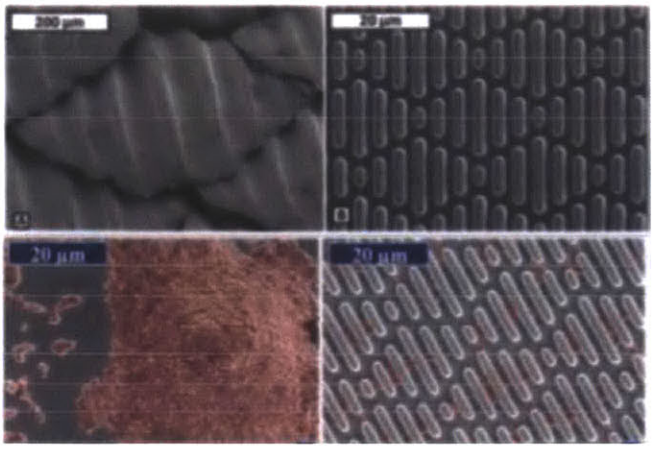

Figure 1.4. Shark skin-inspired surfaces for prevention of biofouling. Clockwise from top: Scales from the spinner shark, Sharklet™ film, *S. aureus* biofilm on flat PDMS (day 14 of culture), and on Sharklet™ PDMS (day 14 of culture). Figure adapted from Chung *et al.* and Scardino *et al.*

Among the studies of bacteria-structure interactions, there are few that address the interplay of structure and chemistry outside the context of superhydrophobic materials. On a microscopic scale, the interfacial features confronting microbes are structural as well as chemical. For example, the cilia and microvilli lining some mammalian epithelial surfaces also have a glycocalyx and secreted mucins that overlay the sub-micron surface structure. Bioinspired antifouling materials have yet to replicate this complexity. Therefore, we aimed to examine the interplay between micro-scale geometry, surface energy and bacterial surface properties with respect to adhesion, with the ultimate goal of understanding bacterial adhesion in structured environments, and establishing principles for design of novel surfaces that effectively repel bacteria.

THESIS ORGANIZATION

The organization of this thesis is designed to reflect the process of discovery during my doctoral work. Each chapter of the thesis serves to ask (and in many cases answer) an important question regarding microbial behavior in structured environments. As in my research, the research findings in one chapter typically motivate the subject of the next. Experiments at the beginning of my studies led me to examine adhesion of *E. coli* to patterned PDMS substrates. Initial analysis hinted at the importance of bacterial appendages, which led me on the path of research described herein.

Chapter 2 examines adhesion of *E. coli* to structured surfaces (Figure 1.5). The surfaces are designed to determine how cells are able to adhere when they cannot fit between micro-structures. We reveal the role of flagella in this process and then further probe their contribution using more directed approaches. By generating mutant strains lacking flagella, we demonstrate the relative contribution of flagella in the adhesive process. We also generate substrates with variable surface feature spacing to determine when cells benefit most from using their surface appendages. We show that flagella improve adhesion to patterned PDMS substrates. Specifically, flagella are able to reach in between crevices where the cell body cannot fit, thus improving adhesion and expanding the range of surfaces to which *E. coli* can adhere.

Understanding the role of flagella in adhesion of bacteria to patterned substrates raises the question of what substrate properties enable nonspecific flagellar surface attachment. Chapter 3 explores this question using self assembled monolayers (SAMs) to generate chemically similar, well defined surfaces that vary in hydrophobicity. Using purified flagella and quartz crystal microbalance (QCM), we examine binding of flagella to abiotic surfaces. We show that flagella bind preferentially to hydrophobic surfaces, and do not appreciably bind to hydrophilic surfaces.

Using SAMs and cells with or without flagella, we also demonstrate that flagellated cells adhere best to hydrophobic substrates, but cells without flagella actually adhere better to hydrophilic substrates than those with flagella, indicating that flagella may impede cell adhesion to hydrophilic surfaces.

In order to further explore hydrophilic, structured environments, Chapter 4 examines mucin—a natural hydrogel that typically harbors microbes in animal hosts, while keeping them in check. We purify mucins and use them in their native, three-dimensional gel configuration to probe bacterial swimming behavior and surface attachment in their presence. We demonstrate that swimming behavior is kept intact—and possibly enhanced—in *E. coli* and *P. aeruginosa* in the presence of mucin. Furthermore, mucin gels greatly reduce adhesion to underlying glass substrates. Cells that are immotile, however, form suspended clumps or flocs that are antibiotic resistant, analogous to those seen in the lungs of cystic fibrosis patients.

In Chapter 5, we begin to examine areas for future study, and present preliminary findings. Part 1 looks at flagellar diversity in *E. coli* across different strains and uses this as a model to ask whether flagellar adhesion to hydrophobic substrates is a more general phenomenon. We clone several flagella genes from various *E. coli* strains, corresponding to different flagellar morphotypes, into the same background strain. Then, we purify these flagella and examine their adhesion to SAMs in QCM experiments. Part 2 focuses on generating new substrates using the knowledge gained in the previous chapters. We generate inverse opal monolayers with structure on the micron scale. We begin to examine pore size and various coatings including mucin and PEG to determine their effects on bacterial adhesion. Parts 1 and 2 of Chapter 5 establish clear lines of inquiry for future studies. This work and preliminary results pave the way for additional research in bacterial adhesion to structured surfaces.

Finally, Chapter 6 examines our findings in the context of existing research. Here, I offer a broader perspective on the research field and extract themes from this thesis and other works in the field. I suggest some approaches that take into account these themes, building on existing strategies and offering new ones, for the improved design of antifouling surfaces.

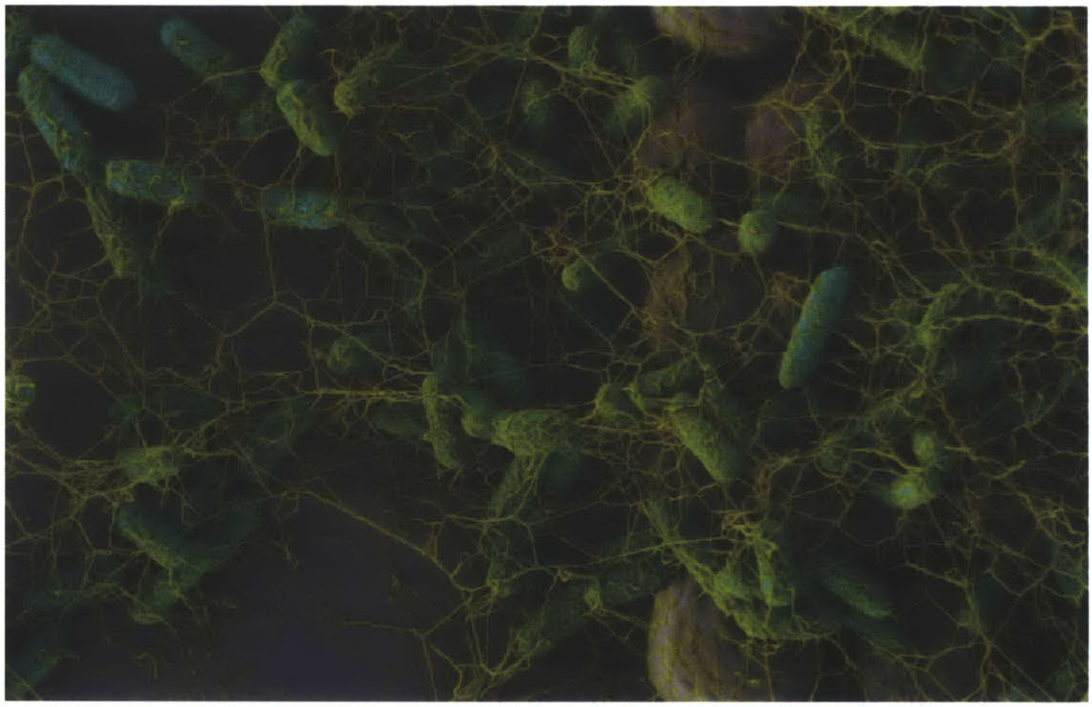

Figure 1.5. *E. coli* on a topographical substrate. False-colored scanning electron micrograph of *E. coli* cells that are adherent to a patterned PDMS substrate. Area shown is where the patterned region meets a flat, unpatterned region. Note the prominence of extracellular fibers (colored yellow)—an abundance of flagella. Coloring courtesy of Michael Bucaro.

BIBLIOGRAPHY

1. Scott R, Detection C (2008) The Direct medical costs of healthcare-associated infections in U.S. hospitals and the benefits of prevention.

2. Klevens R, Edwards, JR, Richards C, et al. (2007) Estimating health care-associated infections and deaths in US hospitals, 2002. Public Health Rep 122:160.

3. Donlan R, Costerton J (2002) Biofilms: survival mechanisms of clinically relevant microorganisms. Clin Microbiol Rev 15:167–193.

4. Schinabeck M, Ghannoum M (2005) 3 Biofilm-Related Indwelling Medical Device Infections.

Biofilms, Infection, and Antimicrobial Therapy 39.

5. Donlan R (2002) Biofilms: microbial life on surfaces. Emerg Infect Dis 8:881–890.

6. Loeb G, Neihof R (1975) Marine conditioning films. Adv Inorg Chem 145:319–335.

7. Bos R, van der Mei HC, Busscher HJ (1999) Physico-chemistry of initial microbial adhesive interactions – its mechanisms and methods for study. FEMS Microbiol Rev 23:179–230.

8. Characklis W (1981) Bioengineering report: Fouling biofilm development: A process analysis. Biotechnol Bioeng 23:1923–1960.

9. Costerton JW, Stewart PS, Greenberg EP (1999) Bacterial biofilms: a common cause of persistent infections. Science 284:1318–1322.

10. Davies D (2003) Understanding biofilm resistance to antibacterial agents. Nat Rev Drug Discov 2:114–122.

11. Stewart P, Franklin M (2008) Physiological heterogeneity in biofilms. Nat Rev Microbiol 6:199–210.

12. Lewis K, Spoering AL, Kaldalu N, et al. 12 Persisters: Specialized Cells Responsible for Biofilm Tolerance to Antimicrobial Agents. Biofilms, Infection 241.

13. Nickel J, Ruseska I, Wright J, Costerton J (1985) Tobramycin resistance of Pseudomonas aeruginosa cells growing as a biofilm on urinary catheter material. Antimicrob Agents Chemother 27:619–624.

14. Gilbert P, Das J, Foley I (1997) Biofilm susceptibility to antimicrobials. Adv Dent Res 11:160–167.

15. Ito A, Taniuchi A, May T, et al. (2009) Increased Antibiotic Resistance of Escherichia coli in Mature Biofilms. Appl Environ Microbiol 75:4093–4100.

16. Høiby N, Bjarnsholt T, Givskov M, et al. (2010) Antibiotic resistance of bacterial biofilms. Int J Antimicrob Agents 35:322–332.

17. Connell J, Wessel A, Parsek M, et al. (2010) Probing prokaryotic social behaviors with bacterial "lobster traps."MBio 1:

18. Butler M, Wang Q, Harshey R (2010) Cell density and mobility protect swarming bacteria against antibiotics. Proceedings of the National Academy of Sciences 107:3776–3781.

19. Epstein A, Pokroy B, Seminara A, Aizenberg J (2011) Bacterial biofilm shows persistent resistance to liquid wetting and gas penetration. Proc Natl Acad Sci U S A 108:995–1000.

20. Kohanski M, Depristo M, Collins J (2010) Sublethal antibiotic treatment leads to multidrug resistance via radical-induced mutagenesis. Mol Cell 37:311–320.

21. Spellberg B, Guidos R, Gilbert D, et al. (2008) The epidemic of antibiotic-resistant infections: a call to action for the medical community from the Infectious Diseases Society of America. Clin Infect Dis 46:155–164.

22. Hall-Stoodley L, Costerton J, Stoodley P (2004) Bacterial biofilms: from the Natural environment to infectious diseases. Nat Rev Microbiol 2:95–108.

23. Costerton J, Cheng K, Geesey G, et al. (1987) Bacterial biofilms in nature and disease. Annu Rev Microbiol 41:435–464.

24. Delauney L, Compère C, Lehaitre M (2010) Biofouling protection for marine environmental sensors. Ocean Sci 6:503–511.

25. Manov DVM, Chang GC, Dickey TD (2004) Methods for Reducing Biofouling of Moored Optical Sensors. Journal of atmospheric and oceanic technology 21:958–968.

26. Dunne W (2002) Bacterial adhesion: seen any good biofilms lately? Clin Microbiol Rev 15:155.

27. Hanssen A, Osmon D (1999) The use of prophylactic antimicrobial agents during and after hip arthroplasty. Clin Orthop Relat Res 124–138.

28. Scott B (2010) Clinical and cost effectiveness of urethral catheterisation: a review. J Perioper Pract 20:235–240.

29. Hanssen A (2004) Prophylactic use of antibiotic bone cement: an emerging standard--in opposition. J Arthroplasty 19:73–77.

30. Edgeworth J (2009) Intravascular catheter infections. J Hosp Infect 73:323–330.

31. Bayston R, Ashraf W, Bhundia C (2004) Mode of action of an antimicrobial biomaterial for use in hydrocephalus shunts. J Antimicrob Chemother 53:778–782.

32. Kamal G, Pfaller M, Rempe L, Jebson P (1991) Reduced intravascular catheter infection by antibiotic bonding. A prospective, randomized, controlled trial. JAMA 265:2364–2368.

33. Francolini I, Donelli G (2010) Prevention and control of biofilm-based medical-device-related infections. FEMS Immunol Med Microbiol 59:227–238.

34. Johnson J, Kuskowski M, Wilt T (2006) Systematic review: antimicrobial urinary catheters to prevent catheter-associated urinary tract infection in hospitalized patients. Ann Intern Med 144:116–126.

35. Maki D, Kluger D, Crnich C (2006) The risk of bloodstream infection in adults with different intravascular devices: a systematic review of 200 published prospective studies. Mayo Clin Proc 81:1159–1171.

36. Cogen AL, Nizet V, Gallo RL (2008) Skin microbiota: a source of disease or defence? Br J

Dermatol 158:442–455.

37. Rickard A, Schooling S (2003) 2.3 Control of Biofilms Associated with Implanted Medical Devices. Medical biofilms: detection, prevention, and control 73.

38. Uehara Y, Nakama H, Agematsu K, et al. (2000) Bacterial interference among nasal inhabitants: eradication of Staphylococcus aureus from nasal cavities by artificial implantation of Corynebacterium sp. J Hosp Infect 44:127–133.

39. Trautner BW, Lopez AI, Kumar A, et al. (2011) Nanoscale surface modification favors benign biofilm formation and impedes adherence by pathogens. Nanomedicine 8:261–270.

40. Trautner BW, Hull RA, Thornby J, Darouiche RO (2007) Coating Urinary Catheters with an Avirulent Strain of Escherichia coli as a Means to Establish Asymptomatic Colonization. Infect Control Hosp Epidemiol 28:92–94.

41. Kingshott P, Wei J, Bagge-Ravn D, et al. (2003) Covalent Attachment of Poly(ethylene glycol) to Surfaces, Critical for Reducing Bacterial Adhesion. Langmuir 19:6912–6921.

42. Wei J, Ravn DB, Gram L, Kingshott P (2003) Stainless steel modified with poly(ethylene glycol) can prevent protein adsorption but not bacterial adhesion. Colloids Surf B Biointerfaces 32:275–291.

43. Park K, Kim Y, Han D, et al. (1998) Bacterial adhesion on PEG modified polyurethane surfaces. Biomaterials 19:851–859.

44. Carlson R, Taffs R, Davison W, Stewart P (2008) Anti-biofilm properties of chitosan-coated surfaces. J Biomater Sci Polym Ed 19:1035–1046.

45. Wang R, Neoh KG, Shi Z, et al. (2011) Inhibition of escherichia coli and proteus mirabilis adhesion and biofilm formation on medical grade silicone surface. Biotechnol Bioeng 109:336–345.

46. Shi L, Ardehali R, Caldwell K (2000) Mucin coating on polymeric material surfaces to suppress bacterial adhesion. Colloids Surf B Biointerfaces 17:229–239.

47. Johansson M, Larsson J, Hansson G (2011) The two mucus layers of colon are organized by the MUC2 mucin, whereas the outer layer is a legislator of host-microbial interactions. Proc Natl Acad Sci U S A 108 Suppl 1:4659–4665.

48. Ambort D, Johansson MEV, Johansson M, et al. (2012) Calcium and pH-dependent packing and release of the gel-forming MUC2 mucin. Proceedings of the National Academy of Sciences 109:5645–5650.

49. Hansson GC (2011) Role of mucus layers in gut infection and inflammation. Curr Opin Microbiol 15:57–62.

50. Johansson M, Phillipson M, Petersson J, et al. (2008) The inner of the two Muc2 mucin-

dependent mucus layers in colon is devoid of bacteria. Proc Natl Acad Sci U S A 105:15064–15069.

51. Berthiaume F, Moghe P, Toner M, Yarmush M (1996) Effect of extracellular matrix topology on cell structure, function, and physiological responsiveness: hepatocytes cultured in a sandwich configuration. FASEB J 10:1471–1484.

52. Curtis A, Wilkinson C (1997) Topographical control of cells. Biomaterials 18:1573–1583.

53. Hui E, Bhatia S (2007) Microscale control of cell contact and spacing via three-component surface patterning. Langmuir 23:4103–4107.

54. Kane R, Takayama S, Ostuni E, et al. (1999) Patterning proteins and cells using soft lithography. Biomaterials 20:2363–2376.

55. Stevens M, George J (2005) Exploring and engineering the cell surface interface. Science 310:1135–1138.

56. Weibel D, DiLuzio W, Whitesides G (2007) Microfabrication meets microbiology. Nat Rev Microbiol 5:209–218.

57. Takeuchi S, DiLuzio W, Weibel D, Whitesides G (2005) Controlling the shape of filamentous cells of Escherichia coli. Nano Lett 5:1819–1823.

58. Díaz C, Schilardi PL, dos Santos Claro PC, et al. (2009) Submicron trenches reduce the Pseudomonas fluorescens colonization rate on solid surfaces. ACS Appl Mater Interfaces 1:136–143.

59. Hochbaum A, Aizenberg J (2010) Bacteria Pattern Spontaneously on Periodic Nanostructure Arrays. Nano Lett 10:3717–3721.

60. Campoccia D, Montanaro L, Agheli H, et al. (2006) Study of Staphylococcus aureus adhesion on a novel nanostructured surface by chemiluminometry. Int J Artif Organs 29:622–629.

61. Whitehead K, Colligon J, Verran J (2005) Retention of microbial cells in substratum surface features of micrometer and sub-micrometer dimensions. Colloids Surf B Biointerfaces 41:129–138.

62. Scardino A, Nys R (2011) Mini review: Biomimetic models and bioinspired surfaces for fouling control. Biofouling 27:73–86.

63. Chung K, Schumacher J, Sampson E, et al. (2007) Impact of engineered surface microtopography on biofilm formation of Staphylococcus aureus. Biointerphases 2:89–94.

64. Reddy S, Chung K, McDaniel C, et al. (2011) Micropatterned surfaces for reducing the risk of catheter-associated urinary tract infection: an in vitro study on the effect of sharklet micropatterned surfaces to inhibit bacterial colonization and migration of uropathogenic

Escherichia coli. J Endourol 25:1547–1552.

65. Schumacher J, Carman M, Estes T, et al. (2007) Engineered antifouling microtopographies - effect of feature size, geometry, and roughness on settlement of zoospores of the green alga Ulva. Biofouling 23:55–62.

Chapter 2

The role of flagella in adhesion of *Escherichia coli* to structured substrates

Parts of this chapter have been previously published as: Friedlander RS, Vlamakis H, Kim P, Khan M, Kolter R, Aizenberg J. Bacterial flagella explore microscale hummocks and hollows to increase adhesion. 2013. *Proc. Natl. Acad. Sci. U. S. A.* 110(14):5624-9.

INTRODUCTION

Among the numerous strategies proposed for antifouling surfaces, physical strategies, particularly the use of rationally designed surface topographies, have gained attention recently as highly nonspecific methods for prevention of attachment without the use of antimicrobials [1–6]. Understanding how bacteria interact with surfaces that have roughness on the micron and sub-micron length-scales (i.e. comparable to the length-scale of the bacteria themselves) is critical to the development of anti-adhesive topographies. Such surfaces are also relevant for a deeper understanding of the native bacterial lifestyle, since most surfaces in nature are not atomically smooth. Indeed, the microvilli of the intestines are between 80 and 150 nm in diameter [7], creating considerable topographic constraints for enteric pathogens that might attempt to colonize the epithelium. Geometric considerations suggest that surfaces with roughness on the bacterial length scale provide less available surface area and fewer attachment points for rigid bacterial bodies than smooth surfaces (Fig. 2.1A). However, the simplistic view of bacteria as rigid rods or spheres ignores the presence of bacterial appendages, such as pili and flagella (Fig. 2.1A, right panel).

Previous work has demonstrated that type I pili and flagella are required for biofilm formation by *E. coli* [8]. Flagella have been suggested to aid in overcoming surface repulsive forces and possibly, to aid in spreading of cells along a surface. Additionally, exopolysaccharides and surface antigens help to develop biofilm morphology [9, 10]. It is possible that such

extracellular features also play important roles in allowing bacteria to adapt and adhere to bumpy surfaces. Using wild-type cells and deletions of several biofilm-associated genes, we herein examine the role of surface appendages on adhesion to patterned substrates and show that flagella in particular appear to aid in attachment to surfaces inaccessible to the cell body, by reaching into crevices and masking surface topography. By measuring adhesion to various surface patterns, we are able to better separate the adhesive role of flagella from their role in improving surface access via swimming motility and to suggest that flagella may provide an additional, structural function in biofilm formation.

RESULTS

E. coli cells form biofilms on surfaces submerged in liquid [11]. A relevant clinical example of this is catheter-associated urinary tract infections by uropathogenic *E. coli*. We asked whether micron-scale surface topography could reduce bacterial adhesion to submerged substrates. By introducing bumps separated by valleys smaller than a cell diameter, we hypothesized that there would be reduced surface area available to cells and thus, adhesion would be diminished compared to smooth surfaces (see Fig. 2.1A). In order to choose an appropriate surface pattern, we first required an accurate measurement of cell diameter. Due to the inadequate resolution of light microscopy and the distortion associated with sample preparations for electron microscopy (EM), we chose to use atomic force microscopy (AFM) to measure the diameters of hydrated cells. Exponential phase *E. coli* (strain ZK2686) cells were imaged on AFM in liquid using contact mode. The measured cell diameters were 0.60 ± 0.10 μm (N=48).

We designed and manufactured silicon wafers with a honeycomb pattern using photolithography. These wafers acted as molds to generate PDMS surfaces with an array of

hexagonal features 2.7 μm in height and 3 μm in diameter, separated by 440 nm trenches (designated as "HEX" patterns; Fig. 2.1B). Notably, the spacing of the trenches was more than one standard deviation (SD) below the measured mean cell diameter. We grew wild-type bacteria on smooth and HEX-patterned PDMS coupons submerged in $M63^{+}$ medium. These static cultures were incubated for 24 h at 37 °C and then prepared for scanning EM imaging (Fig. 2.1C, D). Surprisingly, our observations indicated that there was more surface coverage by the *E. coli* cells on HEX than on flat surfaces. Furthermore, we noted the presence of a dense, fibrous network surrounding the surface-bound cells.

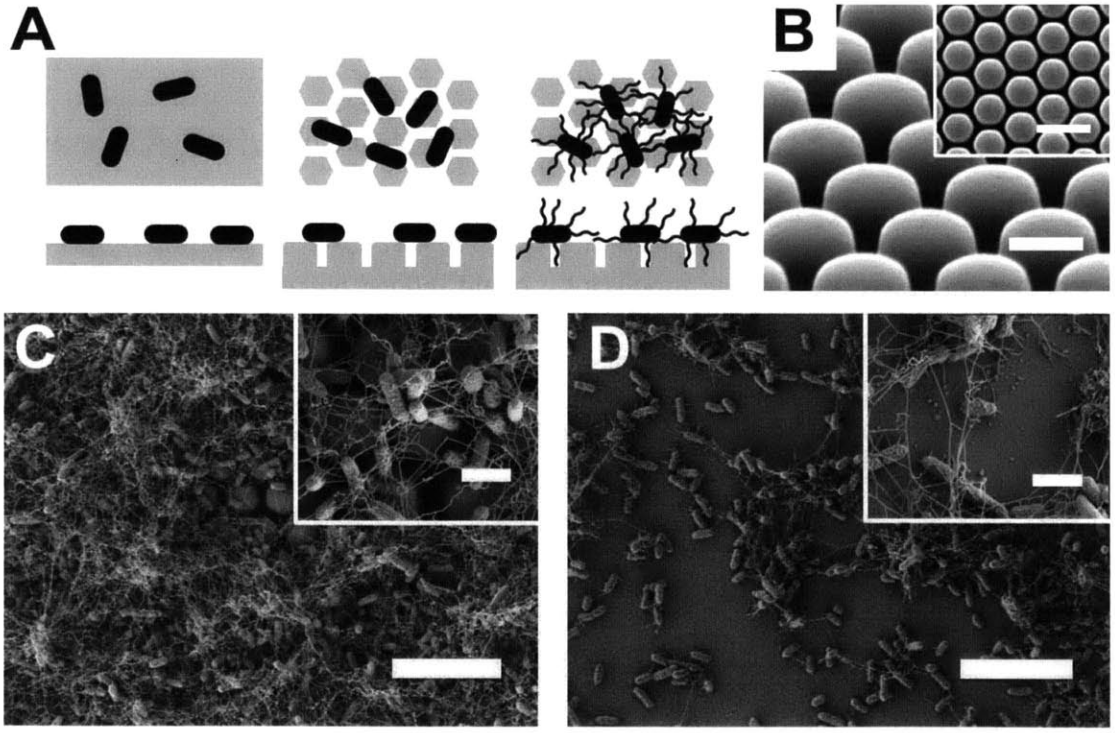

Figure 2.1. Bacterial surface adhesion. (*A*) Schematics of *en face* (top) and cross-sectional (bottom) views of rod-like bacteria adhering to flat (left) or patterned (middle) substrates and attachment of bacteria possessing surface appendages to a patterned substrate (right), when the length scale of surface topography is on the order of the bacterial diameter. (*B*) Scanning EM of a HEX PDMS substrate. Scale bar is 2 μm. Inset is orthogonal view at lower magnification. Inset scale bar is 5 μm. (*C*) Scanning EM of wild-type *E. coli* grown for 24 h at 37°C in $M63^{+}$ on a HEX-patterned PDMS substrate. Inset is higher magnification. (*D*) *E. coli* grown on flat PDMS substrate. Inset is higher magnification. Scale bars in C and D are 10 μm, inset scale bars in C and D are 2 μm.

Matrix components are salient characteristics of most biofilms; indeed, many bacterial species, including *E. coli*, have been shown to produce several kinds of polysaccharide, protein, and DNA elements in their biofilm matrices. Since the *E. coli* cell bodies could not access the entire surface of HEX-patterned substrates, it seemed likely that the observed fibers were helping to augment surface attachment to these topographies. To identify the components of the fibrous material, we constructed and obtained mutants with deletions in known biofilm-associated genes, including: *wcaF*, coding for the polysaccharide colanic acid; *bcsA*, a cellulose gene; *fimA*, coding for type I pili; *csgA*, coding for curlin amyloid fiber subunits; and *flhD*, the master regulator for flagella synthesis. We grew each of these strains on HEX substrates as described above and imaged with a scanning EM (Fig. 2.2). All of the mutants resembled the wild-type, except for Δ*flhD*, which had a clear lack of associated fibers. FlhD is a transcriptional regulator that controls expression of many genes including, but not limited to the flagellar apparatus [12]. To determine if flagella or motility specifically were required for better colonization, we constructed deletion mutants for *fliC*, the flagellin subunit gene and *motB*, a motor protein that enables flagellar rotation (Fig. 2.2). The Δ*fliC* mutant displayed the same phenotype as seen for Δ*flhD*, indicating that the observed effect was due to the absence of flagella. Furthermore, the Δ*motB* motility mutant was able to colonize the surface and it generated fibers similar to the wild type. These findings are consistent with the fibrous material being predominantly composed of flagellar filaments.

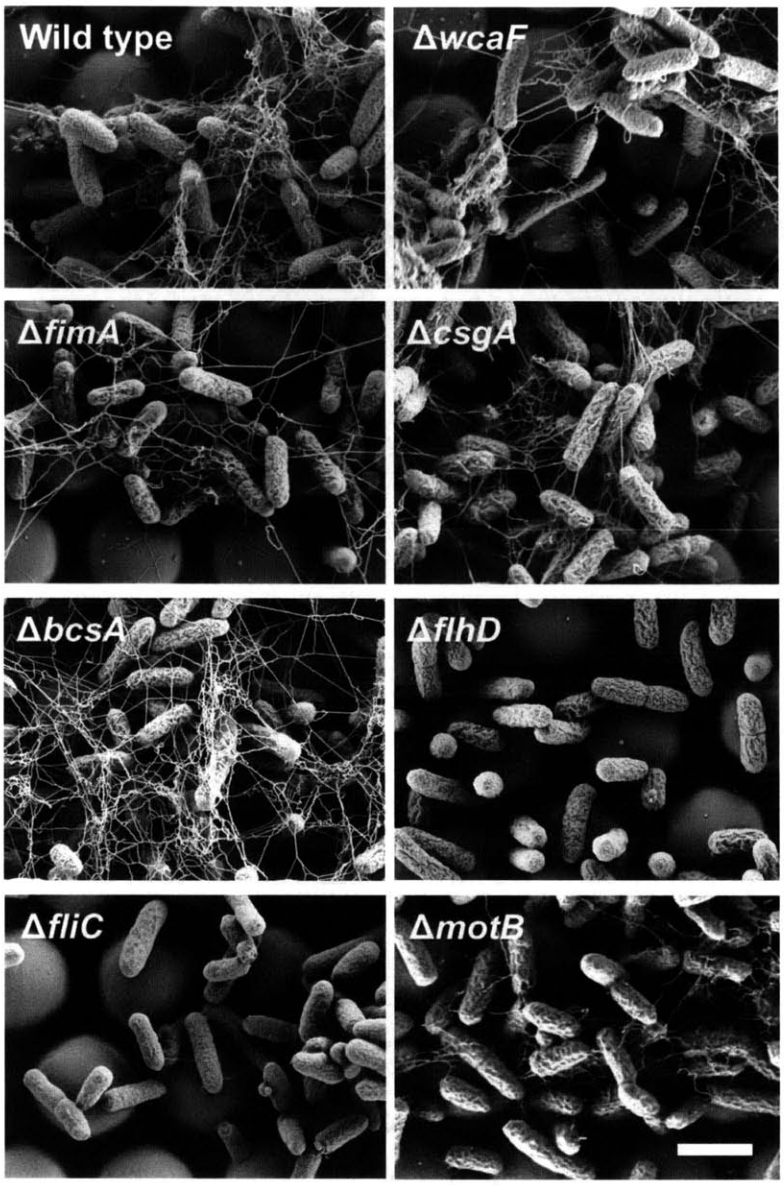

Figure 2.2. Phenotypes of biofilm-associated knockouts on patterned PDMS. Wild-type (ZK2686) and mutant derivatives (as labeled) were grown on topographically patterned PDMS substrates for 24 or 48 h at 37 °C in $M63^{+}$. Scanning EM micrographs depict the morphological properties of each strain. Scale bar is 2 μm.

We examined the time-course of adhesion for wild type and Δ*fliC* mutant on HEX-patterned versus flat surfaces to determine if flagella play a role in the increased adhesion of the wild type to HEX surfaces observed in Figure 2.1B, C. To analyze this, we plotted the ratio of biomass on HEX/flat surfaces at different times over a period of 24 h. For both strains, there was

a reduction in adhesion to the HEX surface versus the flat surface at 2 h, the earliest time analyzed (Fig. 2.3A). At later time points, however, the wild-type cells accumulated more on the HEX surfaces than on the flat surfaces. In contrast, the Δ*fliC* strain showed more biomass on flat surfaces than on HEX surfaces at all time points, though the ratio approached unity toward 24 h. These data suggest that while adherence of wild-type cells appears to benefit from surface patterning, the cells lacking flagella are unable to exploit the additional surface area provided by the micro-topography.

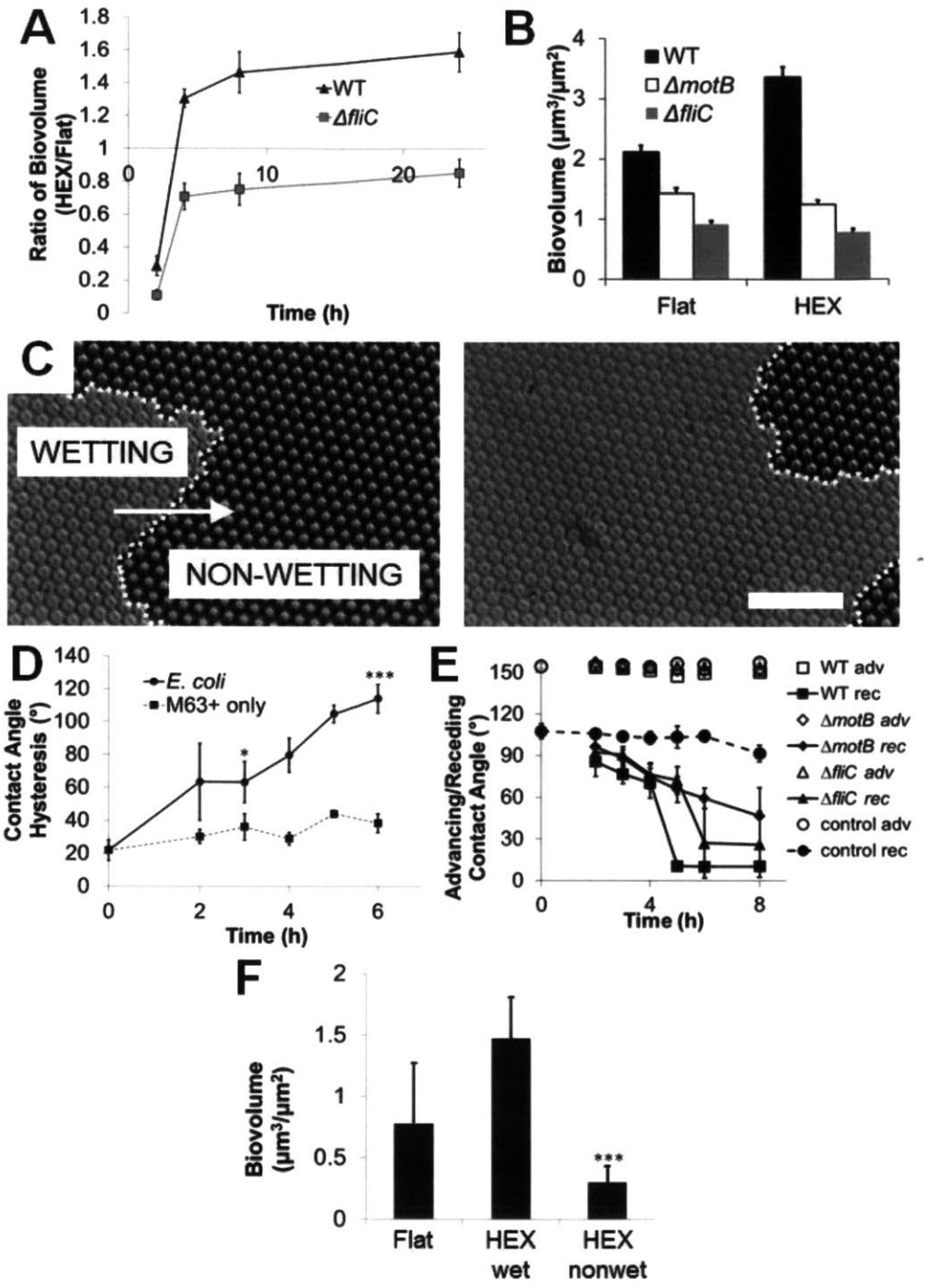

Figure 2.3. Colonization of patterned substrates by wild type and non-motile bacteria and its relationship to surface wetting. (*A*) Time-course of relative biovolume on patterned (HEX) relative to flat substrates for wild type and Δ*fliC* cells at various times. (*B*) Biovolume of cells adherent to submerged flat or HEX-patterned PDMS coupons after 24 h. Error bars indicate SEM of at least 5 independent experiments (5 z-stacks per experiment). ***, $p<0.001$ by Student's two-tailed t-test, compared to WT. (*C*) Optical images of the advancement of the wetting front during culture, at 4 h. The meniscus (dotted line) advances through the patterned

substrate, exposing channels between surface features, thus increasing available surface area for bacterial attachment. The area to the left of the dotted line is fully wetted, whereas the area to the right of the line contains air pockets. The white arrow indicates the direction of the wetting front progression. Thirty minutes have elapsed between the images on the left and right. Scale bar is 20 μm. (*D*) Contact angle hysteresis measurements of substrates that have been exposed to growing *E. coli* cells for increasing incubation periods or $M63^{+}$ medium only, followed by sonication. Error bars represent SD. ***, $p<0.001$ by Student's two-tailed t-test, comparing WT to control at 2h. †††, $p<0.001$ by Student's two-tailed t-test, comparing WT to Δ*fliC* or Δ*motB*. See also Figure 3E. (*E*) Advancing (open symbols) and receding (closed symbols) angles of droplets of distilled water were measured on these substrates after sonication of surfaces to remove adherent bacteria. (*F*) Biovolume of cells adherent to submerged substrates after 2 h of culture. HEX substrates were either force-wet using ethanol followed by rinsing (HEX-wet), or left in their nonwetting state (HEX-nonwet). Error bars represent SD. ***, $p<0.001$ by Student's two-tailed t-test, comparing HEX-wet to HEX-nonwet.

It had previously been shown that mutants lacking flagella (Δ*fliC*) or unable to rotate flagella (Δ*motB*) produce less robust biofilms than wild-type strains on flat surfaces [8]. To determine if this was also the case when cells are grown on patterned surfaces, we compared biofilm production of the wild type to that of the Δ*motB* and Δ*fliC* strains at 24h. These strains were each grown on submerged flat and HEX-patterned PDMS coupons, as above, for 24 h and adherent cells were fixed and quantified by acquiring confocal z-stacks of hydrated cells. Consistent with previous findings [8], the Δ*motB* and Δ*fliC* strains each had significantly less biomass than the wild type regardless of surface topography (Fig. 2.3B). This indicates that motility, not just the presence of flagella *per se* is required for optimal biofilm formation. Interestingly, while still less adhesive than wild type, the Δ*motB* mutant accumulated more biomass than Δ*fliC* on both flat and patterned surfaces suggesting that the presence of flagella, albeit paralyzed ones, may play a role in adhesion (Fig. 2.3B).

While biofilm formation at 24 h was more robust in the wild type, both the flagella mutant and the wild type showed a dramatic preference for adherence to the flat substrate at the earliest (2 h) time point (see Fig. 2.3A). Why was the patterned substrate successful at preventing adhesion at early time points, but not later? To better understand this phenomenon,

we examined the substrates microscopically during the adhesion process. We noted that the HEX surface remained non-wetting, harboring trapped air bubbles within the trenches until approximately 4 h, when the medium began to displace the entrapped air bubbles (Fig. 2.3C). This property, where the liquid phase rests atop a composite interface of air and solid, is termed the Cassie-Baxter wetting state, and is characteristic of superhydrophobic micro or nano-textured surfaces such as the lotus leaf [13, 14]. We observed that this effect was lost over time in the presence of bacteria, resulting in complete wetting of the substrates (termed the Wenzel wetting state).

The difference in wetting properties of sterile medium versus medium with bacteria could be due to a change in surface tension of the medium or due to a change in surface energy of the substrate. Using the pendant drop method [15], we measured the surface tension of the $M63^{+}$ medium to initially be 70.1 ± 0.6 mN/m at 20°C. After 16 h of conditioning with *E. coli*, the medium was extracted by centrifugation and filtration and its surface tension was measured to be 69.1 ± 0.5 mN/m at 20°C. Although measurements were not carried out at culture temperatures, the predicted decrease in surface tension by increasing to 37°C would be unlikely to cause wetting. Furthermore, conditioned medium did not cause wetting of fresh HEX substrates incubated at 37°C.

To determine if bacteria produce a substance that functions to precondition the surface and allow for increased wetting, we measured contact angle hysteresis (CAH) of water on dry HEX substrates after they had been placed in the presence of growing *E. coli* for 0 - 8 h (Fig. 2.3D). CAH is the difference between advancing and receding contact angles, and can be due to changes in surface energy or changes in surface topography. This value changes dramatically during Cassie-Baxter to Wenzel wetting transitions, so serves as a sensitive indicator of wetting

state [16]. All bacteria were removed by sonication before measurements, so as to avoid measuring properties of the bacteria themselves. CAH was significantly increased ($p<0.001$) by 2 h of culture for all strains compared to control and continued to increase over the period measured. The medium-only controls did not wet during this period, resulting in the maintenance of a relatively low CAH. This difference in surface wetting properties indicates that the bacterial modification of the substrate surface energy (rather than modification of the liquid medium) is the dominant contributor to wetting properties. By 5 h, we observed a large increase in CAH for the wild type, but this was still significantly higher than CAH of the two mutant strains ($p<0.001$). A commensurate increase did not happen until 6 or 8 h in the Δ*motB* and Δ*fliC* strains, indicating that the surface wetting brought about by bacteria-surface interactions is aided by the presence of motile flagella. Examining advancing and receding contact angles individually (Fig. 2.3E), we observed that all samples maintained a relatively constant advancing contact angle over time with a slight downward trend, likely due to surface conditioning by bacteria. As the surface transitioned from the Cassie-Baxter to the Wenzel wetting state, there was an increase in drop pinning, which was measured as a decrease in the receding contact angle [16]. It is this receding angle that changed more drastically and differentiated the behavior of the wild-type from that of the mutant strains.

On flat substrates, the lack of microstructure prevents the possibility of a Cassie-Baxter wetting state, thus the surface is entirely available to the cells from the outset. On the structured surfaces, wetting did not significantly occur until after 2 h. During this initial period, only the structure tips (not the trenches) are available to cells, as they cannot penetrate the air-water interface. Only upon wetting does the complete surface become available. We tested this by force-wetting the HEX substrates prior to inoculation with wild-type cells. At 2 h, we measured

adherent biovolume, noting a significant increase in attachment to pre-wet surfaces compared with the untreated HEX substrates (Fig. 2.3F).

We reasoned that if the superior attachment by wild-type cells to HEX substrates is due to the access provided by their flagella, then varying feature size would only affect overall adhesion and biomass insofar as it changes overall surface area. In contrast, the Δ*fliC* cells would experience a reduction in attachment whenever portions of the substrate remained inaccessible to the cell body. We compared attachment of wild-type cells and Δ*fliC* mutants to substrates as we varied the feature diameters and spacings, maintaining a constant pitch (Fig. 2.4A). Indeed, the Δ*fliC* cells increased attachment as the feature spacing became larger, eventually surpassing their adhesion to flat substrates. For wild-type cells, the increased spacing had the opposite effect. Whereas the wild type cells had over four times the biomass of Δ*fliC* cells on HEX-patterned substrates (0.44 μm spacing), this difference was less than 2-fold on substrates with 1.70 μm spacing (Fig. 2.4B).

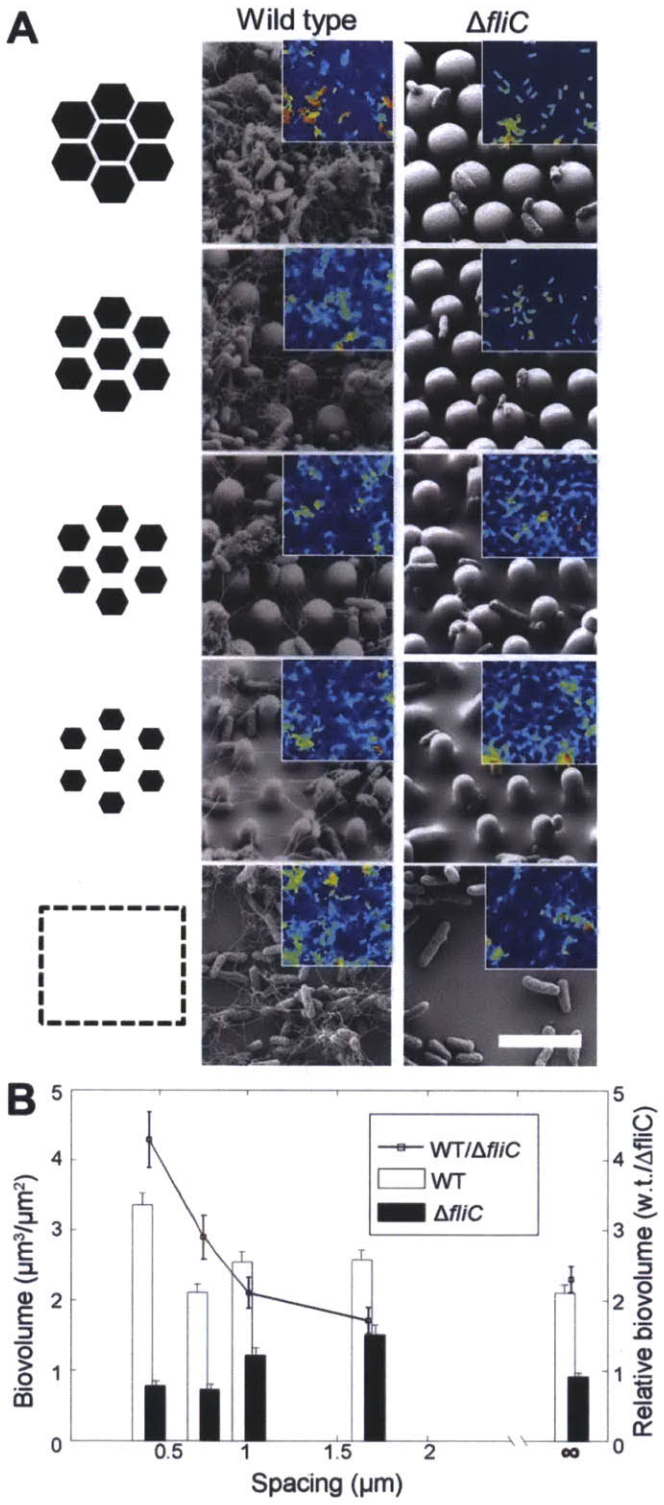

Figure 2.4. Differential response of wild-type and Δ*fliC* cells to changes in surface feature spacing. (*A*) Schematic of underlying surface topography, illustrating increasing spacing with constant pitch (left column) and the scanning EM and confocal images of wild type and Δ*fliC* cells (middle and right columns) grown for 24 h on corresponding PDMS substrates and then fixed. Samples were imaged in the hydrated state using confocal microscopy and then

dehydrated and imaged using scanning EM. Scanning EM images are shown, with thickness maps derived from confocal z-stacks shown in the corresponding inset (color mapping is for clarity and has arbitrary scale). Scale bar is 5 μm. (*B*) Biovolume was quantified for each topographical pattern and normalized to projected surface area. Biovolumes are shown for wild type and Δ*fliC* mutants (plotted as bars), as well as their ratios (black squares connected by lines). Error bars indicate SEM of ≥26 data points.

It appears that the benefit of having flagella is greater during adhesion to substrates with trenches smaller than the cell body than during adhesion to flat substrates or substrates with larger feature spacings. This phenomenon is unlikely to be due solely to the motility provided by flagella, since surface access should have been similar for all substrates tested. To further investigate the role of flagella in adhesion of wild-type cells to topographical substrates, we examined their dynamics in live cells during the adhesion process by fluorescently staining their flagellar filaments [17]. Wild-type *E. coli* cells were placed in contact with HEX substrates and allowed to adhere. During the adhesion process, we observed attachment behavior. We noted that some cells were adhered by their flagella and exhibited tethering behavior (Fig. 2.5A). Additionally, some flagella inserted between surface features and attached within the sub-micron trenches, which was consistent with scanning EM findings, where flagella were observed to adhere between features (Fig. 2.5A-C). After 4 h of incubation, we observed alignment of some flagella with the underlying substrate. There was a tendency of flagella to orient along the planes of symmetry of the substrate (Fig. 2.5D), which implies that the filaments were interacting with the PDMS surface and responding to its topography.

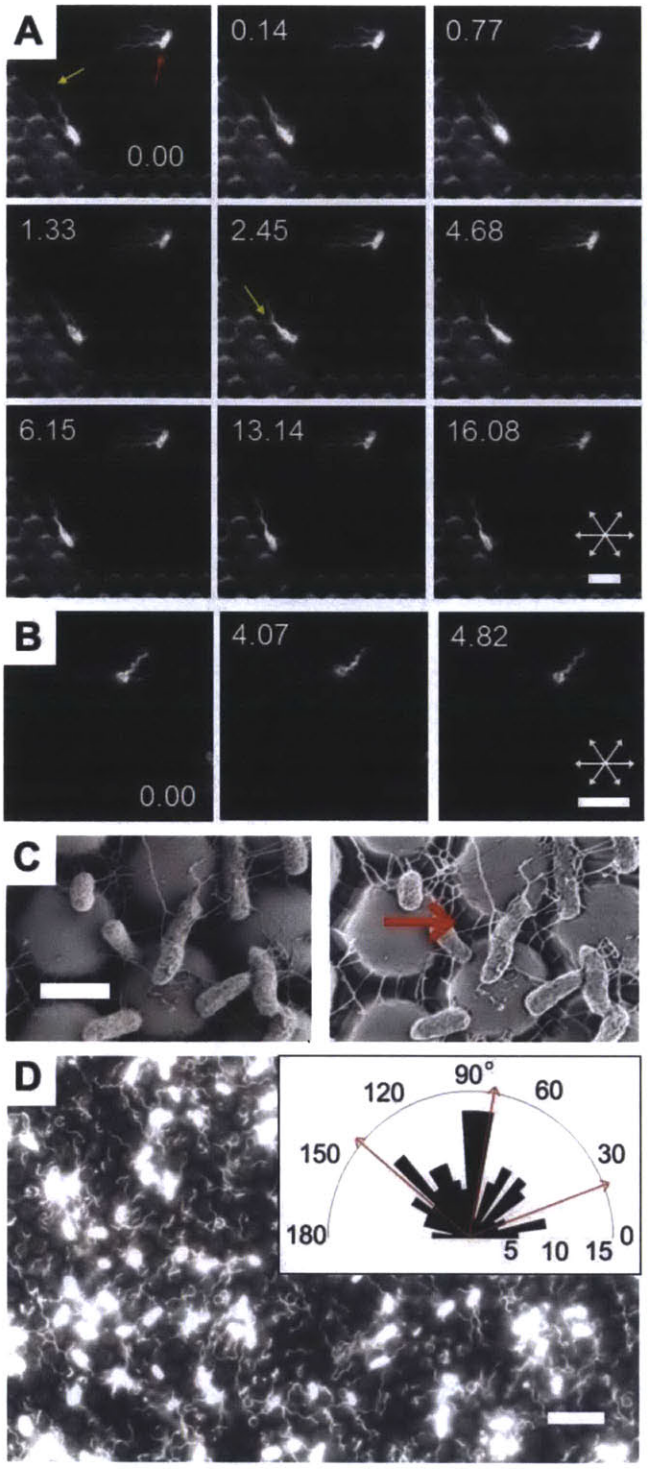

Figure 2.5. Flagellar appendages 'reach' and 'grasp' to improve surface adhesion on patterned surfaces. (*A*) Selected frames from a video of Alexa 594-stained cells taken at 15 frames per second. Times are given (in seconds) in each panel. In frame one, note that the upper cell (red arrow) is fully adherent (it remains stationary throughout the frames). Notably, its middle flagellum is nestled between the surface features slightly out of focus, since it is below

the imaging plane. The other two flagella are resting atop the surface features in the focal plane. The lower bacterium is in the early steps of adhesion, tethered by one flagellum (yellow arrow), also nestled between the surface features. Its remaining free flagella continue to rotate rapidly until 2.45 s, at which time another (short) flagellum makes surface contact (yellow arrow). The cell body continues to slowly reorient as it makes more intimate contact (via other flagella and/or pili) and settles in its final position at 13.14 s. Scale bar is 5 μm. Axes of symmetry of the substrate are indicated by arrows in the bottom-right image. (*B*) Selected frames from a video of Alexa 594-stained cells taken at 15 frames per second. Times are given (in seconds) in each panel. Note that the cell body of *E. coli* is attached and tethered via aligned flagellar filaments along the crystallographic axes of the substrate. The flagellum on the left of the cell continues to move between frames, yet is confined to move within the trench between the surface features. Scale bar is 5 μm. Axes of symmetry of the substrate are indicated by arrows in the bottom-right image. (*C*) Scanning EM images of the same field of wild-type *E. coli* grown on HEX PDMS posts. Images were acquired with secondary electron (left) and inlens detectors (right). The difference in shadowing between the two images highlights the depth of penetration of the flagellar filaments into the channels between the surface features. Note specifically the region indicated by the red arrow. Scale bar is 2 μm. (*D*) Image of Alexa 594-stained cells after initial adhesion to HEX substrate. Scale bar is 10 μm. Inset shows angular histogram of filament orientations of adherent *E. coli*. The histogram illustrates preferential alignment of filaments along the two of the three planes of symmetry of the hexagonal surface pattern. Axes of symmetry of the substrate are indicated with red arrows.

DISCUSSION AND CONCLUSION

We herein set out to characterize the bacterial adhesive response to substrates with regular surface topography. Specifically, we were interested in the role of surface appendages in this response. We tested the hypothesis that surface feature length-scale could, on its own, reduce bacterial attachment by reducing available surface area. Indeed, we observed that sub-micron trenches between features were able to reduce attachment of mutants without flagella. However, the geometric simplification of bacteria as rigid rods becomes invalid when applied to wild-type bacteria possessing surface appendages. Wild-type *E. coli* achieved better adhesion to surfaces with trenches than to flat surfaces. Because their surface appendages could access the trenches, the wild-type cells actually experienced an *increase* in surface area on HEX substrates compared to flat, while the non-flagellated cells experienced the predicted decrease (Figure 2.6). These

results indicate that bacterial adhesion to patterned surfaces is far more nuanced than anticipated by simplistic geometric models.

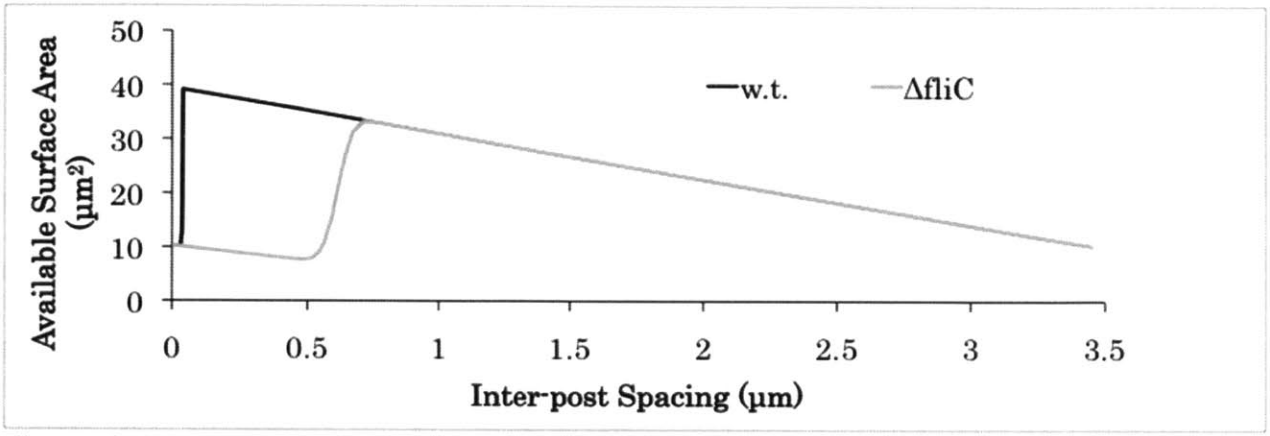

Figure 2.6. Accessible substrate surface area. Simulation of available surface area for wild type and Δ*fliC* strains in a unit cell of HEX substrates with post spacing varying as indicated, based on average diameter and standard deviation. Note that wild-type cells can access inter-post regions using flagella, but Δ*fliC* cells cannot.

During the early adhesion process, we observed that all strains adhered more to flat substrates than to HEX substrates. Upon microscopic inspection, we could observe a wetting front progressing across the sample at 4-6 h into incubation, consistent with an initial Cassie-Baxter wetting state. Similarly, substrates removed from culture at 2 h appeared to be non-wetting and the medium was observed to easily cascade off the substrates. At later time points, the samples remained wet upon removal. These observations were consistent with CAH measurements taken over 8 h of culture, showing a steady increase in hysteresis over time. Given this finding, it appears that for short durations the meniscus forming over each trench prevents bacterial adhesion and reduces surface availability to only the tips of the bumpy surface projections. At that time structured surfaces inhibit bacterial attachment. Δ*fliC* and Δ*motB* mutants were delayed in surface wetting of HEX substrates compared to the wild type, as measured by CAH. We conclude that motile flagella increase the probability of generating

pinning points, thereby resulting in low receding contact angles. This difference in receding contact angle, but similarity in advancing angle between mutants and wild type indicates that their effects on surface chemistry are similar, but they differ in their ability to expose surface features, which act as pinning points. We propose that the motor-driven motion of the flagella and/or cell body provides an input of vibrational energy that disrupts the metastable air-liquid interface and drives the receding of the liquid phase, thus enabling local wetting of trenches. This argument is further supported by microscopic observations of local advancement of the meniscus into trenches in areas where there is notable agitation by bacterial motion (Figure 2.7). Once the trenches are in contact with the culture medium, they can become conditioned with secreted proteins and/or medium components, and they become vacant attachment surfaces.

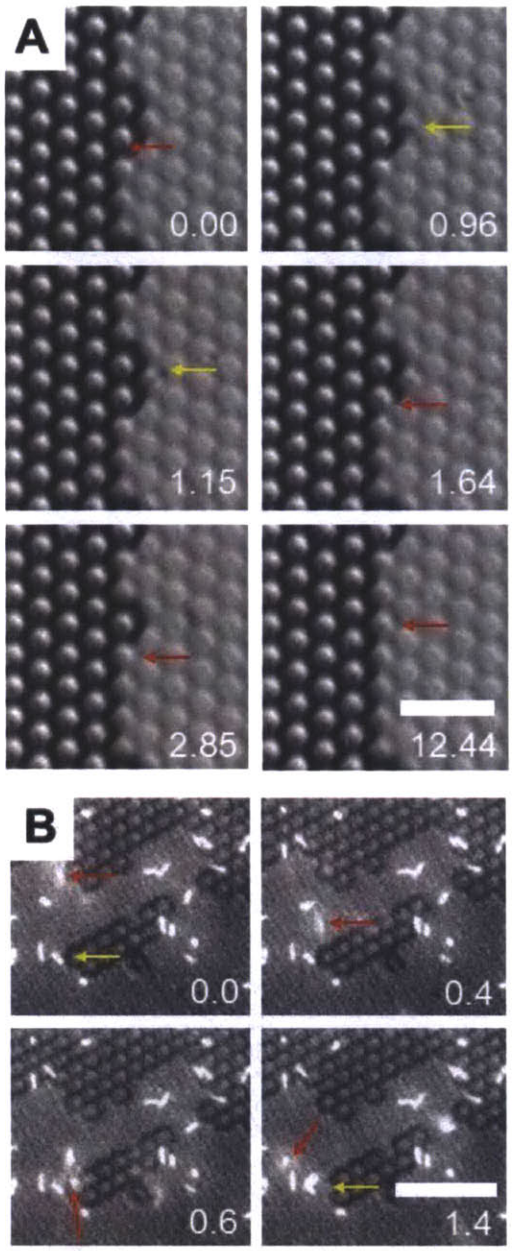

Figure 2.7. Bacterial motion coincides with meniscus advancement. (*A*) Motion of bacteria and wetting front at 6 h into culture, shown using phase contrast imaging. Selected frames from a video taken at 15 frames per second. Times are given (in seconds) in each panel. The frames depict a substrate in the Cassie-Baxter wetting state (left side) and Wenzel state (right side). In frame one, note that the post pointed to by the red arrow is surrounded by an air bubble. By 1.64 s, the meniscus begins to advance to the next post. It reaches the next metastable state by 2.85 s. By 12.44 s, the meniscus has advanced again. Note the faintly visible presence of a cell (yellow arrow) at the interface between these regions right before the meniscus begins to advance, at 0.96 and 1.15 s. Scale bar is 10 μm. (*B*) Motion of bacteria and wetting front at 6 h into culture, shown using bright-field and fluorescence imaging. Selected frames from a video taken at 5 frames per second. Times are given (in seconds) in each panel. As in *A*, parts of the substrate are

in the Cassie wetting state, and parts are in the Wenzel state. Note the motion of a rapidly swimming cell (red arrows) as it approaches the interface between Wenzel and Cassie regions. The cell pauses briefly at 0.6 s and then moves on. During this time, the meniscus has advanced beneath the cell (yellow arrows). Scale bar is 20 μm.

As has been noted in the literature, conditioning films can render surfaces more favorable for bacterial adhesion [18, 19]. In our case, these conditioning films had the added effect of maintaining surface wetting. For the wild-type cells, accessibility of the inter-feature trenches was critical in achieving increased adhesion. Once the initial layer of cells is able to anchor, these cells begin to alter the surface topography by their presence alone and can facilitate further attachment. In a sense, the adhesion of bacteria masks the surface features and acts as a topographical conditioning film, analogous to chemical conditioning films comprised of macromolecules, which mask surface chemistry.

Several studies have reported that flagella are necessary for biofilm formation by *E. coli* and other bacteria such as *Listeria monocytogenes* and *Yersinia enterocolitica* [8, 20, 21]. Furthermore, in addition to the presence of flagellar filaments, motor proteins that cause flagellar rotation are required. It has been suggested that swimming motility allows improved access to surfaces for initial attachment [8, 21]. In low-shear environments, however, McClaine and Ford showed that motility had no effect on attachment of *E. coli* to glass [22]. It has long been known that *E. coli* can adhere to surfaces via flagella [23], and somewhat more recently, several pathogenic strains have been shown to adhere to epithelial tissue using flagella-mediated adhesion [24–26].

Here, we found that the Δ*motB* mutant, which has flagella that are paralyzed, was only marginally better at adhering than the mutant lacking flagella and still had a marked reduction in surface adhesion compared to wild type (Fig. 2.3B). We posit that it is not simply the presence of flagellar filaments that enables access to the inter-feature trenches, but the motion of these

filaments as well. In examining the process of cell adhesion, it is apparent that the wild-type cells are able to rotate their flagella, even after initial attachment (Figure 2.5B). This movement allows the flagella to explore the local geometry. There does not appear to be a strong long-range attractive force between the surface and the flagellar filament, but once the flagella adhere, it seems to be an irreversible process. From a functional standpoint, flagella should not typically be sticky, as this could impede swimming along a surface. Instead there appears to be a low-affinity, high avidity bond between flagella and the surfaces studied. This may be analogous to a cooperative binding event, where the initial binding reduces energy requirements for binding of additional monomers in the flagellar chain by forcing them into proximity with the surface. Still, there is some probability that non-motile filaments would eventually make intimate contact with the substrate, perhaps aided by thermal motion. This possibility may account for the slight increase in biomass attained by Δ*motB* cells over Δ*fliC* cells, despite their ostensibly reduced translational diffusion, owing to the presence of flagella, which increase the effective hydrodynamic radius of the cells [27].

We have herein revealed that the flagella play an important role in surface adhesion, apart from their swimming function. This is supported by the finding that the surface-bound biomass of non-flagellated cells is less than 25% of the biomass of wild-type cells on HEX surfaces, but when inter-feature spacing is large enough to accommodate the cell bodies, the Δ*fliC* cells achieve greater than 50% of the wild-type biomass. Our data indicate that the flagellar filaments, aided by motor-driven rotation, are able to penetrate subsurface features inaccessible to the cell bodies. Furthermore, they may bridge gaps between features, thus weaving a web for improved attachment of additional cells. We speculate that the presence of multiple flagella in a peritrichous arrangement may be of substantial benefit for surface adhesion in topographical

environments. In some species, such as *Aeromonas spp.*, and *Vibrio parahaemolyticus*, lateral flagella are under differential genetic control from their polar flagella [28]. Efforts to isolate their individual functions have led to several interpretations concerning adhesion, virulence and different forms of motility [29]. We note that there are numerous enteric bacterial species possessing peritrichous and/or lateral flagella systems, which may be particularly important in an intestinal environment carpeted with microvilli.

Regardless of physiological interpretations, it is clear that bacterial adhesive abilities have evolved to enable attachment to a vast array of substrates. As the microscopic world tends to be highly structured, it is hardly surprising that bacteria should be able to cope with patterned landscapes. This work highlights the difficulties associated with prevention of bacterial surface colonization, and demonstrates the robustness and versatility of the bacterial adhesion repertoire. In light of this, we must incorporate multiple feature designs to improve anti-fouling surfaces. For example, if surfaces can be created that have stable Cassie-Baxter wetting states in biological settings, their superhydrophobicity may be exploited to reduce bacterial attachment, as we observed at early time points in the current study. The fact that bacteria can reach into small crevices and adhere with their flagella should prompt investigation into surfaces that can minimize flagellar adhesion, but can still be topographically controlled to limit access of the cell body and shorter appendages (such as pili). By increasing our understanding of the physiology of bacterial attachment in general and flagella-substrate interactions in particular, we can improve the parameters for the design of next-generation anti-biofilm surfaces.

EXPERIMENTAL SECTION

Strains and Culture conditions

All strains used in this study are indicated with their sources in Table 2.1. For all adhesion assays, *E. coli* strains were inoculated from Luria Bertani (LB) agar plates into LB broth and incubated at 37 °C overnight with agitation. The overnight cultures were diluted 1:100 in M63 salts plus 0.5% (w/v) casamino acids and 0.2% (w/v) glucose ($M63^+$). PDMS coupons (patterned or flat) were placed at the bottoms of 6- or 12-well tissue culture plates; the overnight cultures diluted in $M63^+$ were used to cover these coupons and the plates were incubated at 37 °C under static conditions for the times indicated in each experiment.

In experiments requiring force-wetting of the HEX substrates, ethanol was used to reduce surface tension and infiltrate the surface microstructures. Ethanol was then displaced with culture medium, which underwent two additional exchanges prior to culture to remove traces of ethanol. When fixation was required, the medium was aspirated at the appropriate time point and the PDMS coupons were rinsed twice in phosphate-buffered saline (PBS). Then, cells were fixed in a modified Karnovsky's fixative (2% glutaraldehyde, 2.5% paraformaldehyde in 0.08 M Sorenson's phosphate buffer) for 15 min and washed twice in PBS prior to imaging. When needed antibiotics were used at the following concentrations: kanamycin, 75 μg/ml; chloramphenicol, 25 μg/ml.

Atomic force microscopy

Overnight cultures of wild-type *E. coli* were diluted 1:100 in $M63^+$ and grown to exponential phase (approximately 4 h, OD_{600} = 0.4). A drop of culture was placed on a flat PDMS coupon and cells were allowed to adhere for 2-4 min. Coupons were then rinsed twice in PBS and examined under a light microscope to ensure a density appropriate for AFM measurements. Cells were fixed as described above for 1 min and rinsed twice again. Cells were imaged in liquid contact mode on an Asylum MFP-3D AFM using a silicon nitride cantilever

with spring constant k = 0.06 N/m. The z-sensor channel was used to determine bacterial diameters.

Substrate fabrication

To fabricate the HEX substrate, we used methods described previously [30, 31]. A negative structure was defined with a photomask/photoresist and etched in a Si wafer using the Bosch process. We deposited a non-stick layer of (tridecafluoro-1,1,2,2-tetrahydrooctyl)-trichlorosilane onto the Si master via vapor-phase deposition and directly molded the PDMS substrates from the coated Si wafers. To produce intermediately-spaced structures, we generated negatives in photo-curable epoxy resin (UVO114, Epotek), using the PDMS samples as molds. These served as masters for structural transformation by electrodeposition on patterned substrates (STEPS), described previously [31, 32]. Briefly, epoxy negatives were sputter-coated with Au to make the surfaces conductive. We immersed the substrates in a bath of 0.1 M sodium dodecyl benzene sulfonate and 0.1 M purified pyrrole and applied a voltage (~600 mV), using the conductive substrate as the working electrode in a standard three-electrode electrodeposition configuration. Samples were slowly withdrawn using a syringe pump, as polypyrrole was conformally electrodeposited. This generated a negative with a gradient of feature sizes. The STEPS-modified gradient samples were then molded in PDMS to obtain substrates with variable spacing/diameter.

Strain	Description	Reference or source
ZK2686	W3110, Δ(*arg*F-*lac*) U169	[9]
ZK2687	ZK2686, Δ*wca*F31::cam	"
JW5665-1	BW25113, F-, Δ(*ara*D-*ara*B)567, Δ*lac*Z4787(::*rrn*B-3), λ-, Δ*bcsA787*::kan, rph-1, Δ(*rha*D-*rha*B)568, *hsd*R514	CGSC
JW4277-1	BW25113, F-, Δ(*ara*D-*ara*B)567, Δ*lac*Z4787(::*rrn*B-3), λ-, Δ*fimA782*::kan, rph-1, Δ(*rha*D-*rha*B)568, *hsd*R514	"
JW1025-1	BW25113, F-, Δ(*ara*D-*ara*B)567, Δ*lac*Z4787(::*rrn*B-3), λ-, Δ*csgA784*::kan, rph-1, Δ(*rha*D-*rha*B)568, *hsd*R514	"
JW1881-1	BW25113, F-, Δ(*ara*D-*ara*B)567, Δ*lac*Z4787(::*rrn*B-3), λ-, Δ*flhD745*::kan, rph-1, Δ(*rha*D-*rha*B)568, *hsd*R514	"
JW1908-1	BW25113, F-, Δ(*ara*D-*ara*B)567, Δ*lac*Z4787(::*rrn*B-3), λ-, Δ*fliC769*::kan, rph-1, Δ(*rha*D-*rha*B)568, *hsd*R514	"
JW1878-4	BW25113, F-, Δ(*ara*D-*ara*B)567, Δ*lac*Z4787(::*rrn*B-3), λ-, Δ*motB742*::kan, rph-1, Δ(*rha*D-*rha*B)568, *hsd*R514	"
RSF31	ZK2686, Δ*bcsA787*::kan	This study
RSF30	ZK2686, Δ*fimA782*::kan	"
RSF28	ZK2686, Δ*csgA784*::kan	"
RSF29	ZK2686, Δ*flhD745*::kan	"
RSF43	ZK2686, Δ*fliC769*::kan	"
RSF41	ZK2686, Δ*motB742*::kan	"

Table 2.1. Strain names, genotypes and sources for all *E. coli* strains used in this chapter. CGSC, Coli Genetic Stock Center (Yale); kan, kanamycin resistance gene; cam, chloramphenicol resistance gene.

Construction of mutants

To generate deletion mutants, we obtained knockout BW25113 *E. coli* strains for the genes of interest from the Keio collection (Coli Genetic Stock Center; Table 2.1; see [33]). These mutations were transferred to the ZK2686 background strain via P1*vir* phage transduction [34]. Strains were selected for kanamycin resistance and transductants were confirmed by polymerase chain reaction using primers internal to the kanamycin gene and upstream of the disrupted gene.

Motility assays were used to confirm the loss of motility in Δ*motA*, Δ*motB*, Δ*flhD*, and Δ*fliC* strains. Cells were stabbed into the center of LB, tryptone broth and $M63^{+}$ plates with 0.3% agar. After overnight growth at 30 or 37 °C, plates were examined for loss of motility compared

to wild type (Figure 2.8). Additionally, exponential phase cells were examined by microscopy for swimming behavior.

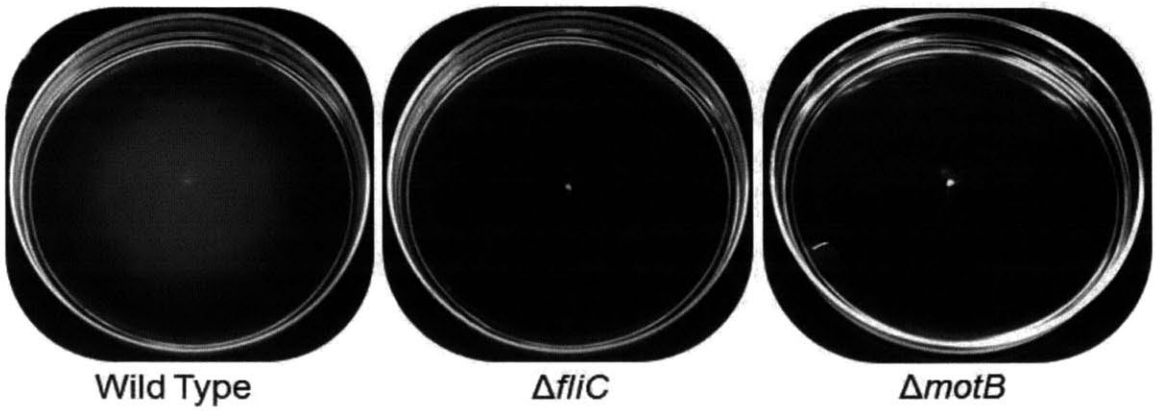

Figure 2.8. Motility assays. Representative images of motility agar plates after overnight growth of the strains indicated. These images are from $M63^{+}$ motility plates. Note that wild-type cells generate a hazy disc, but Δ*fliC* and Δ*motB* strains do not.

Scanning electron microscopy

Cells were cultured on PDMS coupons as described above. After fixation, coupons were rinsed 2 times in PBS and then dehydrated in an ethanol series of 25%, 50%, 75%, 95%, 100%, 100%, 100% ethanol (dilutions were in deionized water) for 10 min each. Samples were then critical point-dried and sputter coated with gold. Samples were mounted on aluminum stubs with carbon tape and conductive paths were painted with colloidal silver. Micrographs were obtained on a Zeiss Supra 55VP FE-SEM using a secondary electron Everhart-Thornley or inlens detector.

Quantification of biofilms with confocal microscopy

Biofilms grown on PDMS coupons were rinsed and fixed as described above. Cells were permeabilized with 0.1% triton-X in PBS for 15 min. Samples were then rinsed with PBS and stained with 5 μg/mL 4',6-diamidino-2-phenylindole, dihydrochloride for 15 min. The stain was

removed and samples were rinsed in PBS. Biofilms were imaged in PBS using a water immersion lens mounted on a Zeiss LSM 710 upright confocal microscope. We obtained ≥5 z-stacks per sample from random locations on the surface.

Bio-volume was quantified using a Matlab script modified from Comstat [35], in which a Canny edge detector was used to locate edges of biofilms in the stack slices and generate a binary image of edges. These edges were dilated and eroded and the binary images were then despeckled, followed by thickening of the edges. This image was used as a mask to determine the median pixel intensity for the areas occupied by bacteria. The slice with the maximum median value was used and averaged with its two adjacent slice medians to determine the threshold intensity value for the z-stack. Z-stacks were then thresholded and voxels were counted and scaled to determine total volume of bacteria within the stack. These volumes were normalized to projected surface area to give average thicknesses for the stacks.

Measurement of liquid surface tension and surface contact angles

To obtain conditioned medium for surface tension measurements, liquid was aspirated from 16 h cultures of *E. coli* biofilms and spun down, preserving the supernatant. This was passed through a 0.2 μm sterile filter and loaded into a Hamilton syringe. The syringe was inverted and droplets of approximately 10 μL were imaged with a goniometer. Surface tension was determined using the pendant drop method [15].

To measure contact angles of PDMS substrates, *E. coli* cultures were grown on HEX substrates as described above. At the time points indicated (Fig. 2.3D), PDMS substrates were removed, rinsed in deionized water, and then sonicated for 10 min. in deionized water to remove adherent bacteria (bacterial detachment was confirmed by crystal violet staining and microscopic examination after contact angle measurements were completed). PDMS coupons were used for

contact angle measurements after drying under N_2 gas. Advancing and receding contact angles were measured using a contact angle goniometer to image deionized water on the substrate surfaces. Receding angles lower than 10° or those that were too small to be measured were assumed to be 10°, a conservative lower limit for the goniometer. The difference in these angles was the contact angle hysteresis.

Live imaging of flagella

To observe the movement and orientation of flagella, live cells were fluorescently stained with Alexa Fluor carboxylic acid succinimidyl esters as described previously [17]. We used both Alexa 488 and Alexa 594 for this application. Briefly, exponential-phase cells grown in $M63^+$ were centrifuged at 2000 rcf for ten minutes and medium was removed. The pellet was resuspended gently in a wash buffer of 0.01 M KPO_4, 0.067 M NaCl, 10^{-4} M ethylenediaminetetraacetic acid, pH-adjusted to 7.0 with HCl, and then spun down. After two additional rinses, cells were incubated with 0.5 mg/mL Alexa Fluor carboxylic acid succinimidyl ester for 1 h at room temperature, gently rocking. After staining cells were washed twice, as above, to remove residual dye and cells were resuspended in $M63^+$ for imaging.

Stained cells were imaged using fluorescence microscopy. After approximately 3 h of incubation of bacteria on substrates, images were taken to visualize flagellar orientation. To measure orientation, lines were drawn manually on images along the main axis of flagellar orientation. The angles of these lines with the horizontal were measured and used to generate a histogram (Fig. 2.5D). For videos, the samples were prepared as above and the dynamic adhesion process was recorded at 15-20 frames/s using a QImaging Exi Blue monochrome CCD camera.

Statistical Analysis

Values are reported in the text as value ± SD. For statistical comparisons between groups with normal distributions, the Student's two-tailed t-test was used. Error bars in figures are either SD or SEM, as indicated in the legends.

BIBLIOGRAPHY

1. Chung K, Schumacher J, Sampson E, et al. (2007) Impact of engineered surface microtopography on biofilm formation of Staphylococcus aureus. Biointerphases 2:89–94.

2. Xu L-C, Siedlecki CA (2011) Submicron-textured biomaterial surface reduces staphylococcal bacterial adhesion and biofilm formation. Acta Biomater 8:72–81.

3. Díaz C, Schilardi P, Salvarezza R, Fernández Lorenzo de Mele M (2007) Nano/microscale order affects the early stages of biofilm formation on metal surfaces. Langmuir 23:11206–11210.

4. Reddy S, Chung K, McDaniel C, et al. (2011) Micropatterned surfaces for reducing the risk of catheter-associated urinary tract infection: an in vitro study on the effect of sharklet micropatterned surfaces to inhibit bacterial colonization and migration of uropathogenic Escherichia coli. J Endourol 25:1547–1552.

5. Campoccia D, Montanaro L, Agheli H, et al. (2006) Study of Staphylococcus aureus adhesion on a novel nanostructured surface by chemiluminometry. Int J Artif Organs 29:622–629.

6. Singh AV, Vyas V, Patil R, et al. (2011) Quantitative Characterization of the Influence of the Nanoscale Morphology of Nanostructured Surfaces on Bacterial Adhesion and Biofilm Formation. PLoS One 6:e25029.

7. Brown A (1962) Microvilli of the human jejunal epithelial cell. J Cell Biol 12:623–627.

8. Pratt L, Kolter R (1998) Genetic analysis of Escherichia coli biofilm formation: roles of flagella, motility, chemotaxis and type I pili. Mol Microbiol 30:285–293.

9. Danese P, Pratt L, Dove S, Kolter R (2000) The outer membrane protein, Antigen 43, mediates cell- to- cell interactions within Escherichia coli biofilms. Mol Microbiol 37:424–432.

10. Danese P, Pratt L, Kolter R (2000) Exopolysaccharide production is required for development of Escherichia coli K-12 biofilm architecture. J Bacteriol 182:3593.

11. O'Toole G, Pratt L, Watnick P, et al. (1999) Genetic approaches to study of biofilms. Methods Enzymol 310:91–109.

12. Liu X, Matsumura P (1994) The FlhD/FlhC complex, a transcriptional activator of the Escherichia coli flagellar class II operons. J Bacteriol 176:7345–7351.

13. Cassie A, Baxter S (1944) Wettability of porous surfaces. Trans Faraday Soc 40:546–551.

14. Barthlott W, Neinhuis C (1997) Purity of the sacred lotus, or escape from contamination in biological surfaces. Planta 202:1–8.

15. Stauffer C (1965) The measurement of surface tension by the pendant drop technique. J Phys Chem 69:1933–1938.

16. Lafuma A, Quéré D (2003) Superhydrophobic states. Nat Mater 2:457–460.

17. Turner L, Ryu W, Berg H (2000) Real-time imaging of fluorescent flagellar filaments. J Bacteriol 182:2793–2801.

18. Murga R, Miller JM, Donlan R (2001) Biofilm Formation by Gram-Negative Bacteria on Central Venous Catheter Connectors: Effect of Conditioning Films in a Laboratory Model. J Clin Microbiol 39:2294–2297.

19. Banerjee I, Pangule RC, Kane RS (2011) Antifouling Coatings: Recent Developments in the Design of Surfaces That Prevent Fouling by Proteins, Bacteria, and Marine Organisms. Adv Mater 23:690–718.

20. Duan Q, Zhou M, Zhu L, Zhu G (2012) Flagella and bacterial pathogenicity. J Basic Microbiol 53:1–8.

21. Lemon K, Higgins D, Kolter R (2007) Flagellar motility is critical for Listeria monocytogenes biofilm formation. J Bacteriol 189:4418.

22. Mcclaine J, Ford R (2002) Characterizing the adhesion of motile and nonmotile Escherichia coli to a glass surface using a parallel-plate flow chamber. Biotechnol Bioeng 78:179–189.

23. Meadows P (1971) The attachment of bacteria to solid surfaces. Arch Mikrobiol 75:374–381.

24. Yamamoto T, Fujita K, Yokota T (1990) Adherence characteristics to human small intestinal mucosa of Escherichia coli isolated from patients with diarrhea or urinary tract infections. J Infect Dis 162:896–908.

25. Erdem A, Avelino F, Xicohtencatl-Cortes J, Girón J (2007) Host protein binding and adhesive properties of H6 and H7 flagella of attaching and effacing Escherichia coli. J Bacteriol 189:7426–7435.

26. Girón J, Torres A, Freer E, Kaper J (2002) The flagella of enteropathogenic Escherichia coli mediate adherence to epithelial cells. Mol Microbiol 44:361–379.

27. Tavaddod S, Charsooghi MA, Abdi F, et al. (2011) Probing passive diffusion of flagellated and deflagellated Escherichia coli. Eur Phys J E Soft Matter 34:1–7.

28. Mccarter L (2004) Dual flagellar systems enable motility under different circumstances. J Mol Microbiol Biotechnol 7:18–29.

29. Kirov S (2003) Bacteria that express lateral flagella enable dissection of the multifunctional roles of flagella in pathogenesis. FEMS Microbiol Lett 224:151–159.

30. Pokroy B, Epstein A, Persson-Gulda M, Aizenberg J (2009) Fabrication of Bioinspired Actuated Nanostructures with Arbitrary Geometry and Stiffness. Adv Mater 21:463–469.

31. Kim P, Adorno-Martinez W, Khan M (2012) Enriching libraries of high-aspect-ratio micro- or nanostructures by rapid, low-cost, benchtop nanofabrication. Nat. Protoc.

32. Kim P, Epstein A, Khan M, et al. (2011) Structural Transformation by Electrodeposition on Patterned Substrates (STEPS): A New Versatile Nanofabrication Method. Nano Lett.

33. Baba T, Ara T, Hasegawa M, et al. (2006) Construction of Escherichia coli K-12 in-frame, single-gene knockout mutants: the Keio collection. Mol Syst Biol 2:1–11.

34. Thomason L, Costantino N, Court D (2007) E. coli genome manipulation by P1 transduction. Curr Protoc Mol Biol Chapter 1:Unit 1.17.

35. Heydorn A, Nielsen A, Hentzer M, et al. (2000) Quantification of biofilm structures by the novel computer program COMSTAT. Microbiology 146 (Pt 10):2395–2407.

Chapter 3
Flagellar adhesion to abiotic surfaces

Collaborator: Nicolas Vogel

Flagella play an important role in adhesion to patterned substrates. In Chapter 2, we showed that in the presence of surface topography, the presence of flagella can greatly improve adhesion. Indeed, flagella can be greater than 10 μm long with a diameter of approximately 20 nm, which can enable access to deep and narrow crevices [1]. Of course, in order for flagellar access to translate into cellular surface adhesion, the interactions between the flagella themselves and the substrate must be enable anchoring of the cell body. The adhesive force between flagella and abiotic surfaces is dependent on material properties, such as surface energy. Because our previous work was carried out entirely on PDMS surfaces, we wanted to extend our research to include the full range of surfaces to which bacterial flagella could adhere.

INTRODUCTION

The design of superhydrophobic surfaces appears to be a promising starting point to non-specifically prevent bacteria from adhering. By combining hydrophobic surface chemistry with micro- or nano-scale topography, surfaces become extremely repellent since water is prevented from coming into contact with the complete topography and resides on a metastable composite air/solid interface at the top of the structures [2–5]. As a result, the contact area between liquid and surface is minimized, leading to ease of removal of the droplet. Unfortunately, we have found that the combination of hydrophobicity and structure does not work as expected in repelling water-borne bacteria [6]. On the contrary, bacteria can adsorb, cover the surface and degrade the metastable air/solid interfaces at the top of the microstructures, leading to the loss of

superhydrophobicity and an increase in available surface area. As a result, such surfaces actually increase bacterial adhesion compared to flat ones.

Since bacterial adhesion is a complex process that depends on the specific environments, materials and species involved, as well as temporal variations in cell surface composition, it is difficult to generalize performance of antifouling materials. The Derjaguin-Landau-Verwey-Overbeek (DLVO) theory describing colloidal particle interaction forces, for example, does not adequately describe or predict bacterial adhesion in many cases [7–11]. Therefore, a detailed understanding of the mechanisms of adhesion, cell surface features and physical properties is of paramount importance in order to advance our ability to design anti-adhesive materials and predict performance.

In the process of adhesion, bacteria can rely on either specific adhesive organelles or proteins (e.g. pili, lipopolysaccharide, non-fimbrial adhesin-1), or nonspecific interactions with surfaces such as van der Waals, electrostatic, and hydrophobic interactions [12–14]. *Escherichia coli* has been well studied as a as a laboratory model organism in general, and in adhesion and biofilm formation in particular. It has been shown that specific flagellar isoforms can enable attachment of certain *E. coli* strains to mammalian antigens. For example the flagellar filament of *E. coli* Nissle 1917 adheres to porcine mucin 2 [15], and a secreted protein, EtpA, can mediate adhesion between the tips of enterotoxigenic *E. coli* flagella and host cell surface receptors [16]. Characterizations of other specific adhesive interactions have exposed new potential targets for anti-adhesive strategies. For example, some studies of *E. coli* adhesion as it relates to virulence have focused on type I pili [12, 17–19], which can bind to mannose on eukaryotic cell surfaces. Pilus-mediated adhesion has been specifically targeted by the development of pilicides, which block pili biogenesis [20]. *E. coli* can also secrete extracellular polymeric substances, such as

curli (an amyloid fiber) and colanic acid or cellulose (polysaccharides). These substances can act as virulence factors by enabling cells to improve adhesion to tissues and assemble biofilms [21–24]. Similar in strategy to pilicides, curlicides have also been developed to inhibit curli biogenesis [25]. Such strategies target virulence rather than microbial death, which results in reduced selection pressure for drug resistance (a major and growing concern in public health) relative to antibiotics. While promising, pilicides and curlicides target specific organelle-mediated cell-host interactions but do not directly address nonspecific bacterial adhesion to inert biomaterials, which can act as portals and reservoirs for infection.

Some surface organelles and molecules have been examined for their nonspecific adhesive properties. For example, a study of type I fimbriae indicated that these organelles strengthened adhesion to hydrophobic surfaces, but reduced adhesion to hydrophilic surfaces [26]. Another study focusing on lipopolysaccharide (LPS) showed that the length and charge of LPS molecules on the surface of *E. coli* K12 strains did not directly correlate with adhesion to quartz particles [27]. We recently showed that bacterial flagella can improve adhesion to abiotic surfaces with topography, enabling bacteria to overcome geometrical constraints imposed by the size and shape of the cell body relative to surface features [6]. However, the role of flagella in adhesion to biomaterials and abiotic surfaces more generally has not been well described.

Bacterial flagella are complex organelles that improve cell motility, enable chemotaxis, contribute to biofilm structure [28], and aid in mucin adhesion for a number of species [15, 29–33]. Flagella are the longest extensions from the cell surface and as such, they mediate many important interactions, both advantageous for the bacterium (e.g. epithelial cell adhesion) and deleterious (e.g. stimulation of innate immunity of higher organisms through Toll-like receptor-5) [34, 35]. By characterizing and quantifying the ability of flagella to adhere to abiotic surfaces

and relating this to overall cell adhesive ability, we sought to better understand the diverse functionality of flagella, particularly by elucidating their functions beyond motility.

In this chapter, we aim to shed light on the role of flagella for *E. coli* adhesion via non-specific interactions by quantifying attachment of isolated flagella to surfaces with different hydrophobicities. We show that purified flagella adhere to hydrophobic surfaces, and that cells possessing flagella demonstrate increased adhesion to hydrophobic surfaces compared to their non-flagellated counterparts. We also quantify adhesion of whole cells to hydrophobic and hydrophilic surfaces, comparing strains with and without surface appendages. We show that flagella increase cell surface activity at hydrophobic interfaces. Surprisingly, we also see that flagella adhere poorly to hydrophilic surfaces and reduce adhesion of the cell to these interfaces, contrasting with the widely held view that flagella categorically improve adhesion and biofilm formation of *E. coli* on immersed surfaces [12, 36–38]. This work highlights and elucidates the important role that flagella play in surface adhesion, beyond their role in cell motility.

RESULTS AND DISCUSSION

In order to isolate the effects of flagellar adhesion from other adhesive phenomena related to the cell body or other surface appendages, we purified flagellar filaments from *E. coli* ZK2686 (Figure 3.1) and used them for quartz crystal microbalance with dissipation (QCM-D) measurements. QCM-D uses changes in resonance frequency of a quartz crystal and is extremely sensitive to changes in adsorbed mass (~ng/cm^2), allowing us to precisely determine extent of flagella binding to the crystal surface [39]. In order to control surface hydrophobicity, we used gold-coated crystals and generated self-assembled monolayers (SAMs) with thiol-bearing molecules [40, 41]. We chose 11-mercapto-1-undecanol as a hydrophilic, uncharged

functionality (water contact angle 28°) and dodecanethiol as a hydrophobic functionality (water contact angle 112°) and mixed them in different ratios to achieve intermediate hydrophilicities (Figure 3.2A-C). This blend of thiols enabled us to vary hydrophobicity without significantly altering other aspects of the surface, such as chemical structure or charge. It has been shown that such mixed monolayers do not show phase separation and can generate a homogeneous surface coating [42–44]. Since the size of the two molecules is similar, no topographic effects (i.e. shielding of one function by the other, larger molecule) are expected. It has previously been shown that dodecanethiol is preferentially incorporated from solution into mixed SAMs with 11-mercapto-1-undecanol [44]. This is consistent with our observation of high contact angles until the mole fraction of 11-mercapto-1-undecanol exceeds approximately 0.5.

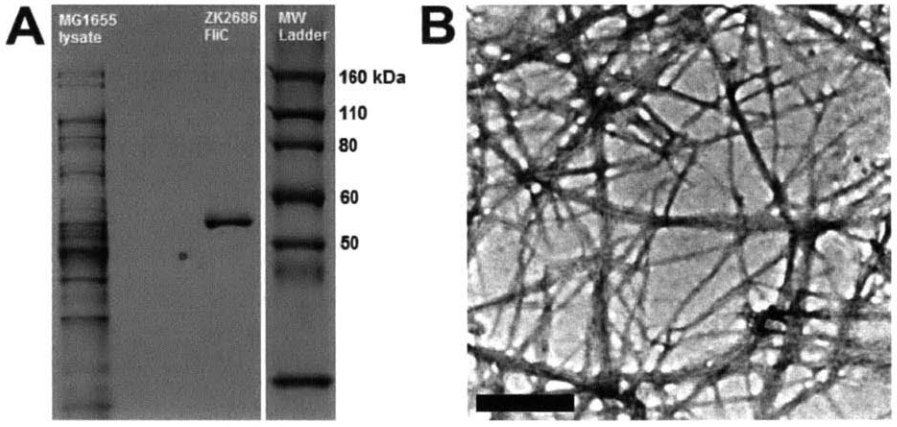

Figure 3.1. Flagella are purified in filamentous form. (*A*) Sodium dodecyl sulfate polyacrylamide gel electrophoresis of MG1655 whole cell lysate (for comparison) and purified flagellin, stained with Coomassie Blue. Molecular weights (MW) as indicated in MW ladder. (*B*) TEM image of purified flagellar filaments negatively stained with 1% phosphotungstic acid. Scale bar is 500 nm.

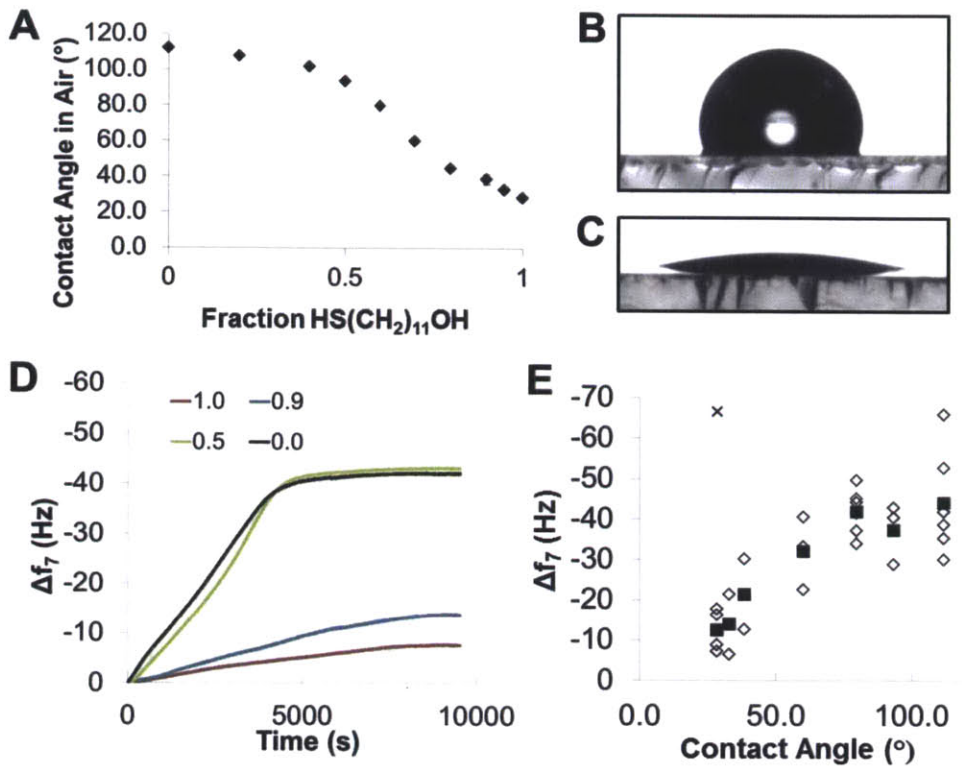

Figure 3.2. Increasing surface hydrophobicity improves adhesion of isolated flagella. (*A*) Contact angle of a water droplet on mixed thiol SAM surfaces, in air. SAMs are composed of a blend of 11-mercapto-1-undecanol and dodecanethiol in the fractions indicated. Water droplets are shown on (*B*) the most hydrophobic (100% dodecanethiol) SAM surface, and (*C*) the most hydrophilic (100% 11-mercapto-1-undecanol) SAM surface. (*D*) Frequency change of QCM resonance (7^{th} overtone) during flow of isolated flagella. Mole fraction 11-mercapto-1-undecanol for each SAM (as in *A*) is indicated for each trace in the legend. (*E*) Final frequency changes in 7^{th} overtone of QCM resonances for surfaces of varying hydrophobicity. Contact angle of each surface is plotted against the corresponding frequency change from several individual experiments per condition. Individual experiments are plotted as diamonds and means are plotted as squares. Outlier is indicated with an "x".

Quartz crystals with SAMs representing the full range of available hydrophobicities were chosen for flagellar adhesion experiments. Crystals were placed in flow chambers and solutions of 5 μg/mL of purified flagella in phosphate buffered saline (PBS) were flowed over the crystals at 10 μL/min. Frequency changes were monitored during flow until these values saturated (Figure 3.2D). After several experiments for each condition, the final change in frequency, Δf, was averaged and plotted against the water contact angle of the SAM-modified surface as a

measure of its hydrophobicity. We observed a general increase in adsorbed mass as hydrophobicity of the surfaces increased (Figure 3.2E). The mean frequency shift saturated at approximately -40 Hz, which was achieved for surfaces with contact angles of 80° and greater (SAMs assembled from a solution of 0.4 or greater mole fraction of dodecanethiol blended with 11-mercapto-1-undecanol). The most hydrophilic surfaces allowed only very low flagellar adhesion.

The viscoelasticity of the adsorbed material in our QCM measurements causes damping of the crystal vibrations, which is measured with QCM-D. In general, a softer or less tightly bound material will show stronger dissipation compared to a stiff film [45]. In the case of our filamentous flagella, more tightly bound filaments should result in less dissipation than loosely bound ones, which would increase drag and energy dissipation. Examining dissipation versus frequency (Figure 3.3A), we observe that the relationship is nearly linear for hydrophilic surfaces, but for hydrophobic surfaces, dissipation levels off at higher frequency changes. This indicates that the flagella become more tightly bound to hydrophobic interfaces. Normalizing for the total adsorbed mass (measured as Δf), we can also examine dissipation caused by bound flagella over the course of an experiment (Figure 3.3B). These plots indicate that on hydrophilic surfaces energy dissipation is highest at the onset of adhesion, and decreases exponentially. The more hydrophobic surfaces have distinct maxima of dissipation, followed by a decrease to a steady state. This corresponds to a more complex adhesive process with a changing dissipation profile.

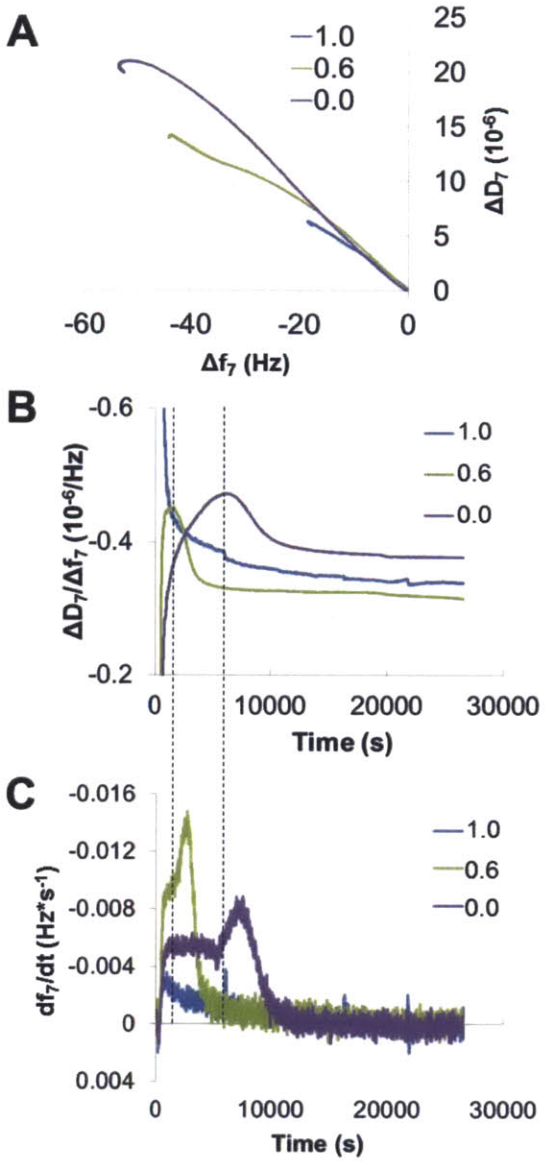

Figure 3.3. Energy dissipation and rate of adhesion of flagella. (*A*) Energy dissipation change plotted against frequency change for representative experiments. (*B*) Normalized energy dissipation from QCM-D. (*C*) Rate of change of QCM resonance frequency during flow of flagella over surface. Fraction 11-mercapto-1-undecanol for each SAM is indicated for each trace in the legend. Traces of corresponding colors in all panels are from the same experiments. Dashed lines indicate times of peak normalized energy dissipation.

We used the time-derivative of the frequency change to examine kinetics of adsorption throughout the QCM experiments (Figure 3.3C). We observe a monotonic decay of adsorption rate of flagella to hydrophilic surfaces over time, indicating surface saturation. For more

hydrophobic crystals there is a complex behavior consisting of an increase to a plateau value, followed by a peak and decay of adsorption rate. The maximal rate of adsorption tended to increase with hydrophobicity, but the overall maximum rate observed was to surfaces with contact angles of ~80°, which decreased with higher contact angles. The peaks in adhesion rates observed for more hydrophobic surfaces can be interpreted in the context of frequency and dissipation data. As normalized dissipation begins to drop, there is a brief and coincident increase in rate of frequency change to a peak value (see dotted lines in Figure 3.3), which may indicate that the surface configuration of flagella adhering to hydrophobic surfaces is changing. Overall energy dissipation does not generally decrease—only normalized dissipation decreases, indicating a decrease in average energy dissipation per attached flagellum.

We interpret the difference between attachment to hydrophilic and hydrophobic surfaces to be a single versus multistep adhesion process. On hydrophilic surfaces, flagella adhere and are loosely bound to the surface and the tethered filaments continue to vibrate in random thermal motion and obstruct additional attachment after adsorption of an initial layer, comparable to a steric repulsion process observed on polymers tethered to the surfaces of colloids [46, 47] (Figure 3.4). This type of adsorption process would translate into a monotonic decay in adsorption rate and a linear relation between dissipation and frequency change as we observe in the QCM-D experiments. On hydrophobic surfaces however, we speculate that flagella are first attaching loosely; as in the case of hydrophilic surfaces. Over time, they seem to change their conformation and may "zip" onto the surface, becoming more tightly bound, most likely by increasing van-der-Waals attractions between flagella proteins and surface. This tighter binding would translate into a drop in normalized dissipation – as we observe in QCM-D. As the flagella "zip" onto the surface, the volume above the surface they shield by thermal motion is decreased,

allowing additional flagella to gain access and adsorb to the surface. Consistent with this interpretation, the decrease in dissipation we observe in QCM-D is followed by an increase in adhesion rate. We and others have previously observed flagellar entanglement in biofilms as well as highly flagellated strains at the substrate interface [6, 28], which is consistent with such an interaction.

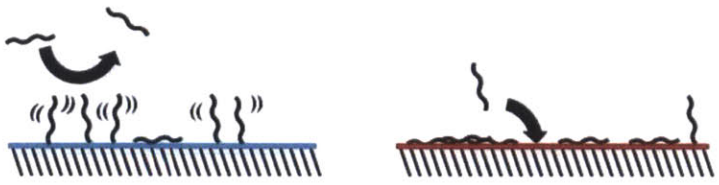

	Hydrophilic	Hydrophobic
Δf	++	+++
ΔD	+++	+

Figure 3.4. Schematic of adhesion process of flagella to hydrophilic and hydrophobic surfaces, based on QCM data. Flagella adhere to hydrophilic surfaces, but do not bind as tightly as to hydrophobic surfaces. This is measured as greater dissipation and an overall lower frequency change than observed for hydrophobic surfaces. On hydrophobic surfaces, flagella "zip" onto the surface for tighter binding, reduced dissipation, and reduced obstruction of additional adhesion.

Regardless of the exact mechanism of the flagella-surface interaction, we have shown that flagella can adhere directly to surfaces of a hydrophobic nature and do not adhere as readily to hydrophilic surfaces. This information allows us to better correlate findings of live-cell adhesion experiments with cell surface properties. To isolate the role of flagella in whole cell adhesion, we used mutants lacking flagellar filaments (Δ*fliC*). We also used mutants lacking type I pili (Δ*fimH*), or both flagella and pili (Δ*fliC*Δ*fimH*) so as to isolate the adhesive properties of the cell body from this other large surface appendage. All strains were derived from *E. coli* ZK2686 (Table 3.1), and growth curves were shown to be comparable (Figure 3.5). To simplify, we constrained our experiments to the assessment of cell adhesion on purely hydrophilic and

hydrophobic substrates, prepared by SAMs of dodecanethiol (hydrophobic) or 11-mercapto-1-undecanol (hydrophilic) on gold-coated microscope slides. Substrates were submerged in $M63^+$ medium and sample wells were inoculated with each *E. coli* strain. After 4 h, samples were washed with PBS using a peristaltic pump to control shear, while avoiding sample dewetting, as passage of an air-liquid interface can result in shear forces 100-1000 times greater than fluid flow alone [13, 48], which would distort the measured quantity of attached cells. Samples were then fixed and imaged with a light microscope for cell counts (Figure 3.6).

Strain	Description	Reference or source
ZK2686	W3110, Δ(*arg*F-*lac*) U169	[49]
ZK2695	ZK2686, Δ*fimH*::cam	"
JW1908-1	BW25113, F-, Δ(*ara*D-*ara*B)567, Δ*lac*Z4787(::*rrn*B-3), λ-, Δ*fliC769*::kan, rph-1, Δ(*rha*D-*rha*B)568, *hsd*R514	CGSC
RSF43	ZK2686, Δ*fliC769*::kan	[6]
RSF41	ZK2686, Δ*motB742*::kan	"
RSF99	ZK2695, Δ*fliC769*::kan	This study

Table 3.1. Strain names, descriptions and sources for all *E. coli* strains used in this chapter. CGSC, Coli Genetic Stock Center (Yale); kan, kanamycin resistance; cam, chloramphenicol resistance; amp, ampicillin resistance.

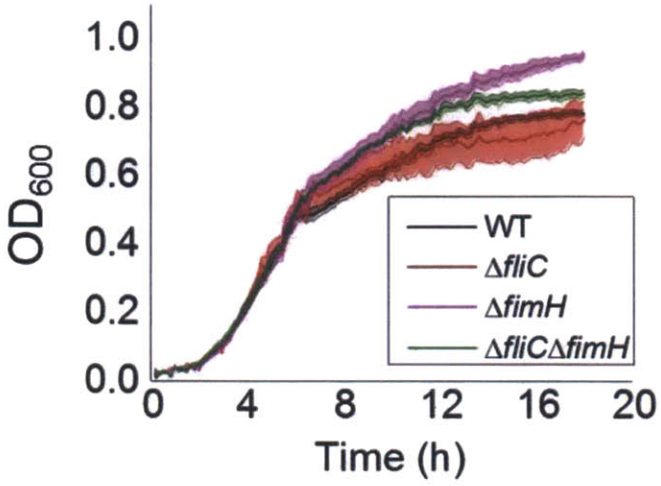

Figure 3.5. Growth curves. Cells were inoculated in $M63^{+}$ in a plate reader and OD_{600} was plotted over 18 h for the strains indicated. Shaded areas correspond to the standard deviation of 3-4 growth curves.

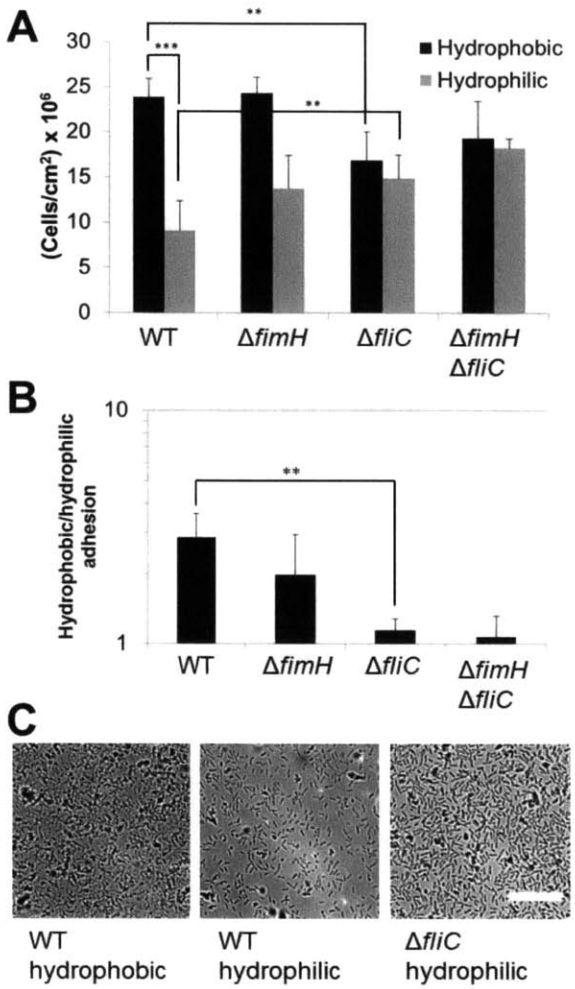

Figure 3.6. Flagella augment cell adhesion to hydrophobic surfaces, but reduce adhesion to hydrophilic surfaces. (*A*) Number of adherent cells after 4 h of culture and rinsing of hydrophobic (dodecanethiol) and hydrophilic (11-mercapto-1-undecanol) SAM surfaces. (*B*) Ratio of adherent cells per unit area on hydrophobic *versus* hydrophilic SAM surfaces for the genotypes indicated. Each data point is the ratio of adherent cells from a hydrophobic sample to the corresponding hydrophilic sample in the same well. Significance in *A* and *B* was assessed using Student's two-tailed t-test; ***, $p<0.001$; **, $p<0.01$. (*C*) Transmitted light optical microscope images of adherent *E. coli*, with conditions as indicated. These are representative images from those used for quantification. Scale bar is 25 μm.

As shown previously [6], wild-type cell counts were highest on hydrophobic surfaces, and nearly 3-fold higher than cell counts on hydrophilic surfaces. Interestingly, loss of type I fimbriae did not negatively affect the ability of cells to adhere to hydrophobic surfaces, and possibly improved adhesion to hydrophilic surfaces. Loss of flagella strongly reduced the

capacity of wild-type *E. coli* to adhere to hydrophobic surfaces, but significantly improved cell adhesion to hydrophilic surfaces, indicating an inhibitory effect of flagella in cell attachment to hydrophilic surfaces. For Δ*fliC* cells, adhesion to hydrophilic and hydrophobic surfaces was nearly equal. Surprisingly, Δ*fliC*Δ*fimH* cells were the most adherent strain for hydrophilic substrates. They also demonstrated similar levels of adhesion to hydrophilic and hydrophobic surfaces. We interpret these results to mean that the cell surface properties enable adhesion to hydrophilic surfaces, but the presence of flagella (which do not adhere well to hydrophilic surfaces) hinder this interaction, possibly due to their large size, movement and peritrichous arrangement. Nonetheless, wild-type cells adhere to hydrophobic surfaces better than Δ*fliC* mutants, demonstrating a quantifiable advantage for possessing flagella in scenarios where hydrophobic surfaces are present.

Given that flagella displayed increased adhesion to hydrophobic surfaces and that cells lacking flagella or fimbriae had improved adhesion to hydrophilic surfaces, we wanted to know whether the presence of flagella imparted an overall amphiphilicity to the cells. To test this, we adapted a traditional method called "microbial adhesion to hydrocarbons" [50]. We mixed exponential phase cultures with dodecane to create a two-phase system. We emulsified the two phases by vortexing and investigated the stability of the emulsion over time (Figure 3.7). Indeed, we observed a stable emulsion over 2 h, created in the presence of wild-type cells. Cells lacking flagella (Δ*fliC*) did not create stable emulsions, and complete phase separation was observed within 5-10 min. We further examined the wild-type emulsions using optical microscopy (Figure 3.7C,D). Wild-type cells mixed with dodecane were enriched around the perimeters of large droplets, and formed clusters of cells that surrounded and stabilized smaller droplets. This result

indicates that the flagella become embedded in the dodecane phase, and the more hydrophilic cell bodies remain associated with the aqueous phase, creating a living analog of a surfactant.

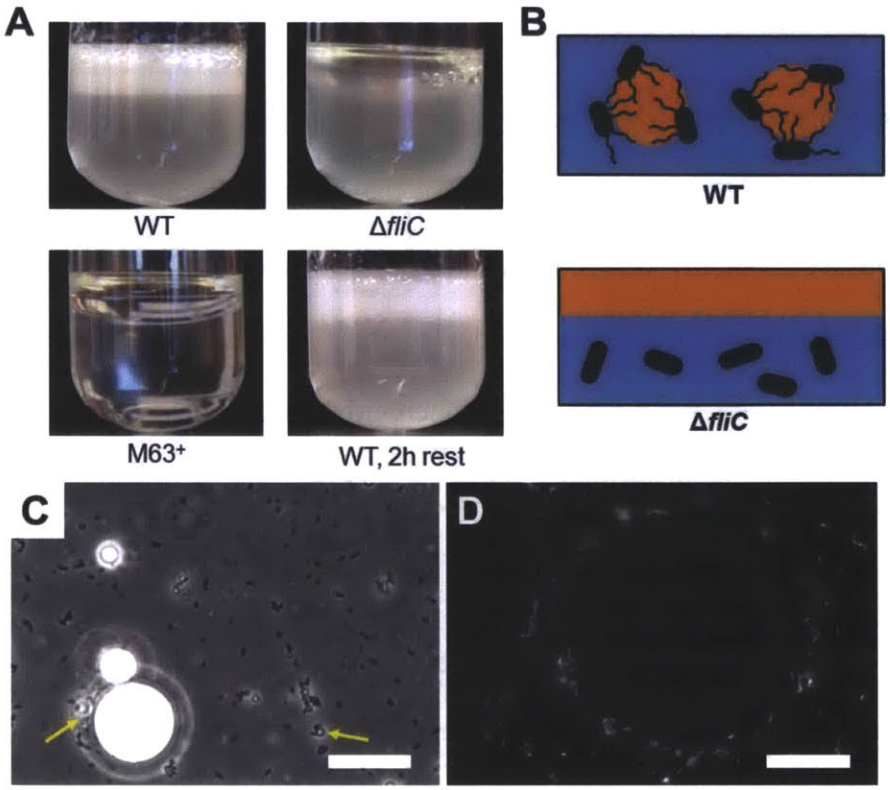

Figure 3.7. Bacterial emulsions demonstrate overall amphiphilicity of flagellated cells and hydrophilicity of Δ*fliC* mutants. (*A*) Exponential phase aqueous bacterial cultures (lower phase) were mixed with dodecane (upper phase) and vortexed for 60 s. After a ten minute rest, tubes were photographed. WT cells were photographed again after 2 h, as indicated. (*B*) Schematic illustration of WT bacterial emulsions (upper panel) and phase separation of Δ*fliC* cultures. (*C*) Phase contrast optical micrograph of WT, exponential-phase *E. coli* from a dodecane-aqueous emulsion. The left arrow is pointing to an area of cell enrichment surrounding a large droplet of dodecane. The right-most arrow is pointing to a small droplet of dodecane stabilized by bacteria. (*D*) Fluorescence micrograph of Syto9-stained *E. coli* surrounding a large dodecane droplet. Note the enrichment of bacteria around the droplet and the lack of cells within the droplet. Scale bars in *C* and *D* are 25 μm.

Based on our QCM-D findings as well as our results that cells lacking flagella adhere better to hydrophilic surfaces than wild-type cells, we can think of these cells as having hydrophobic flagellar filaments that interact with the hydrocarbon phase, and hydrophilic cell bodies, that preferentially interact with the aqueous phase. Essentially, the entire cell can act as a

surfactant when it expresses flagella. In general, this property may improve surface activity of the cells, which is favorable for attachment and biofilm formation.

Our findings emphasize the importance of characterizing both materials and cell properties during adhesion studies. The finding that flagella decrease adhesion to hydrophilic samples belies the concept that flagella generally improve adhesion. The interplay between surface properties and bacterial physiology is complex and often unpredictable. Native environments provide variation in surface chemistry, topography, shear forces, pressures, osmolarity, ionic strength and nutrients. These properties are all likely to affect adhesion and thus, there is no adequate substitute for testing materials in their intended environments. Nonetheless, a deeper understanding of the material properties that relate to adhesion can be reached by abstracting material properties into relevant experimental systems, such as the hydrophobic-hydrophilic spectrum described here.

As large, extracellular appendages, flagella require significant cell resources and must therefore provide a substantial selective advantage to the cell, particularly for cells possessing multiple flagella, such as *E. coli*. We have shown that flagella have a complex and significant role in surface adhesion, which is in addition to their function in cell motility. This may increase the return on investment cells receive from their flagella. With this in mind, we may think of flagella as multifunctional appendages that increase the cell's overall Darwinian fitness in multiple ways. Our description of flagella adhesive properties improves understanding of this complex and well-studied organelle and contributes insight to the lifestyle of *E. coli*.

EXPERIMENTAL SECTION

Strains and culture conditions

All strains used in this study are indicated with their sources in Table 3.1. For all adhesion assays, overnight cultures of *E. coli* were grown in LB shaking at 220 RPM at 37 °C. Overnight cultures were diluted 1:100 in M63 salts plus 0.5% (w/v) casamino acids and 0.2% (w/v) glucose ($M63^+$). When needed, kanamycin was used at 75 μg/ml. Gold-coated glass coupons with thiol SAMs were placed at the bottoms of 4-well rectangular plates, so that each well contained one hydrophobic and one hydrophilic coupon in a randomized position. The overnight cultures diluted in $M63^+$ were used to cover these coupons and the plates were incubated at 37 °C under static conditions for the times indicated in each experiment. At the endpoints, coupons were rinsed with phosphate-buffered saline (PBS) so as to remove loosely adherent cells. In order to avoid dewetting of the surfaces, PBS was flooded into the wells in one direction and allowed to overflow and dilute the medium. Throughout processing of samples, passage of an air-water interface over the samples was strictly avoided. In cases where this occurred, samples were discarded. To keep shear forces consistent between experiments, wells were rinsed using a peristaltic pump at a flow rate of 100 mL/min/well. Each well was rinsed with a total of 600 mL of PBS. After rinsing, half of the liquid volume in each well was removed and 2x fixative was added (4% glutaraldehyde, 5% paraformaldehyde in 0.16 M Sorenson's phosphate buffer), to obtain 1x fixative in the well. This protocol enables the samples to remain immersed in liquid at all times and reliably avoids dewetting of hydrophobic samples. Fixative was incubated for 15 min and then rinsed with 20 volumes of PBS with a peristaltic pump at 100 mL/min/well, again avoiding dewetting.

Growth Curves

To ensure the various strains of *E. coli* grew at comparable rates under the same conditions, we measured growth curves for each. Stationary phase cultures (from overnight growth) were inoculated at an effective optical density measured at 600 nm (OD_{600}) of 0.05 in 150 μL of medium of interest per well of a honeycomb well plate (Growth Curves USA). Plates were incubated in a Bioscreen C (Growth Curves USA) plate reader and set to shake continuously at high amplitude at 37 °C for 18 h. OD_{600} readings were taken every 10 minutes.

Purification of flagella

Methods for isolating flagella were adapted from Crawford et al., 2010 and Erdem et al., 2007 [33, 51]. Cells were grown to exponential phase in 2.4 L of $M63^+$ medium ($OD_{600}\approx0.6$), at which point cells were harvested and centrifuged at 8000 rcf for 15 min. A small sample of cells was also examined under phase contrast microscope to check for motility. Supernatant was discarded and cells were resuspended in 250 mL PBS. The centrifugation step was repeated and cells were then resuspended in approximately 50 mL PBS. This suspension was blended for 60 s in a Waring commercial blender to shear off flagella. Cells were checked for loss of motility under microscope. Cell/flagella suspension was then centrifuged at 9000 rcf for 20 min and then the supernatant was removed and spun at 12000 rcf for 30 min. Supernatant was removed and ammonium sulfate was slowly added to 45% saturation. This solution was incubated at 4 °C overnight. The next day, the solution was centrifuged at 12000 rcf for 1 h. The pellet was resuspended in a small volume (2-6 mL) of PBS while rocking at 4 °C for 8 h. This solution was dialyzed against PBS using several buffer changes over 4 days. Concentration was measured using Coomassie Brilliant Blue G and standard curves obtained from BSA. If sample needed additional concentration, we used a Macrosep centrifugal device (Pall Corp.) with a 10 kDa molecular weight cutoff, following manufacturer's instructions. Purity was verified using SDS-

PAGE with SimplyBlue Safe stain (Life Technologies). Morphology of purified flagellar filaments was examined using transmission electron microscopy.

Gold-thiol SAMs

We prepared stock solutions of 11-mercapto-1-undecanol and dodecanethiol with a concentration of 100 mmol/L in ethanol. For the individual samples, we used these stock solutions to mix the two thiols in molar ratios as specified in the text and Figure 3.2 with a total concentration of 2 mmol/L in ethanol. We coated microscope slides with 2 nm titanium and 30 nm of gold using a Cressington 308 evaporator (Ted Pella, USA). The titanium served as an adhesion promoter to prevent delamination of the gold film. For bacterial adhesion experiments, we cut the slides into 1x1 cm^2 coupons and immersed them for 18 h in the thiol solutions. For the QCM-D experiments, we used commercially available gold-coated QCM-D crystals (Biolin Scientific, Inc.). To remove excess thiols, we rinsed the samples twice in ethanol and dried them under a stream of nitrogen gas immediately before using them in bacterial adhesion experiments.

Transmission electron microscopy (TEM)

Samples of purified flagella were loaded onto a carbon-coated TEM grid. Grids were negatively stained with 1% phosphotungstic acid for ten seconds, and then rinsed twice with deionized water. Grids were allowed to dry prior to TEM imaging. TEM images were acquired using a JEOL 2100 microscope with an operating voltage of 200 kV. High resolution images were taken using a Gatan Osiris digital camera.

Contact angle measurements

Static water contact angles were measured using a goniometer (CAM 101, KSV Instruments) at ambient condition with a 3 µl droplet of water and evaluated with the provided software. All measurements were repeated at least five times on different areas of the substrates and averaged.

QCM-D

Gold-coated quartz crystals were obtained from Biolin Scientific, Inc. Prior to functionalization, crystals were cleaned by 10 min UV ozone exposure, followed by a 10 min bath in 5:1:1 H_2O: H_2O_2:NH_4OH, and then another 10 min UV ozone exposure. Thiol SAMs were then assembled on the surfaces (see "Gold-thiol SAMs") to obtain surfaces with a range of hydrophobicity. Crystals were rinsed in 100% ethanol and dried under a stream of N_2. Crystals were loaded into flow cell chambers of a Q-Sense E4 QCM-D and chambers were flushed with PBS. Purified flagella were diluted in PBS to a concentration of 5 µg/mL. During measurements, flagella solution was flowed through the chambers at 10 µL/min until frequency change saturated and stabilized. Chambers were then flushed with PBS.

Construction of mutants

To generate deletion mutants, genes of interest were replaced with kanamycin resistance cassettes, as described in Friedlander et al., 2013 [6]. Briefly, mutations were transferred from Keio collection knockouts to the ZK2686 background strain via P1*vir* phage transduction [52]. Transductants were confirmed by polymerase chain reaction using primers internal to the kanamycin gene and upstream of the disrupted gene. For double deletion mutants, second deletions were introduced via another round of P1*vir* phage transduction as described above, with a different selection marker.

Quantification of cell adhesion

After cell growth on SAMs for 4 h, cells were rinsed and fixed as described in "Strains and culture conditions". Fixed cells in PBS were imaged on an inverted microscope with a water immersion lens. For each sample, 4-7 images were taken and cells were counted on each image and normalized to the surface area of the images. Each condition was repeated at least 4 separate times.

Two-phase cell mixtures

E. coli were grown overnight in LB, shaking at 220 RPM at 37 °C. The next day, cells were diluted 1:100 into $M63^{+}$ and grown for ~4.5 h shaking at 220 RPM at 37 °C to obtain an OD_{600} of 1.0. Wild-type cells were checked for motility by phase contrast microscopy. 2 mL of this exponential phase cell suspension was placed in a glass culture tube. To this, 400 µL of dodecane was added and tubes were vortexed on high speed for 1 min. Tubes were allowed to rest for 10 min and were then photographed to image extent of phase re-separation. For microscopic imaging, emulsions were spotted onto glass slides and imaged using a phase contrast microscope. Certain samples of cells were stained with Syto9 live cell stain prior to emulsifying. These emulsions were imaged using fluorescence microscopy.

BIBLIOGRAPHY

1. Kim M, Bird JC, Van Parys AJ, et al. (2003) A macroscopic scale model of bacterial flagellar bundling. Proc Natl Acad Sci U S A 100:15481–15485.

2. Cassie A, Baxter S (1944) Wettability of porous surfaces. Trans Faraday Soc 40:546–551.

3. Bhushan B, Jung Y (2011) Natural and biomimetic artificial surfaces for superhydrophobicity,

self-cleaning, low adhesion, and drag reduction. Prog Mater Sci 56:1–108.

4. Quéré D (2005) Non-sticking drops. Rep Prog Phys 68:2495–2532.

5. Liu K, Yao X, Jiang L (2010) Recent developments in bio-inspired special wettability. Chem Soc Rev 39:3240–3255.

6. Friedlander RS, Vlamakis H, Kim P, et al. (2013) Bacterial flagella explore microscale hummocks and hollows to increase adhesion. Proc Natl Acad Sci U S A 110:5624–5629.

7. Ong Y-L, Razatos A, Georgiou G, Sharma MM (1999) Adhesion Forces between E. coli Bacteria and Biomaterial Surfaces. Langmuir 15:2719–2725.

8. Hermansson M (1999) The DLVO theory in microbial adhesion. Colloids Surf B Biointerfaces 14:105–119.

9. Derjaguin B, Landau L (1941) The theory of stability of highly charged lyophobic sols and coalescence of highly charged particles in electrolyte solutions. Acta Physicochim. URSS

10. Poortinga AT, Bos R, Norde W, Busscher HJ (2002) Electric double layer interactions in bacterial adhesion to surfaces. Surf Sci Rep 47:1–32.

11. Verwey E, Overbeek J, Van K (1948) Theory of the stability of lyophobic colloids: the interaction of sol particles having an electric double layer.

12. Pratt L, Kolter R (1998) Genetic analysis of Escherichia coli biofilm formation: roles of flagella, motility, chemotaxis and type I pili. Mol Microbiol 30:285–293.

13. Bos R, Mei H, Busscher H (1999) Physico- chemistry of initial microbial adhesive interactions–its mechanisms and methods for study. FEMS Microbiol Rev 23:179–230.

14. Ahrens R, Ott M, Ritter A, et al. (1993) Genetic analysis of the gene cluster encoding nonfimbrial adhesin I from an Escherichia coli uropathogen. Infect Immun 61:2505–2512.

15. Troge A, Scheppach W, Schroeder BO, et al. (2012) More than a marine propeller – the flagellum of the probiotic Escherichia coli strain Nissle 1917 is the major adhesin mediating binding to human mucus. Int J Med Microbiol 302:304–314.

16. Roy K, Hilliard G, Hamilton D, et al. (2009) Enterotoxigenic Escherichia coli EtpA mediates adhesion between flagella and host cells. Nature 457:594–598.

17. Thomas WE, Nilsson LM, Forero M, et al. (2004) Shear-dependent "stick-and-roll" adhesion of type 1 fimbriated Escherichia coli. Mol Microbiol 53:1545–1557.

18. Müller CM, Aberg A, Straseviçiene J, et al. (2009) Type 1 fimbriae, a colonization factor of uropathogenic Escherichia coli, are controlled by the metabolic sensor CRP-cAMP. PLoS Pathog 5:e1000303.

19. Schwartz DJ, Kalas V, Pinkner JS, et al. (2013) Positively selected FimH residues enhance

virulence during urinary tract infection by altering FimH conformation. Proceedings of the National Academy of Sciences. doi: 10.1073/pnas.1315203110

20. Pinkner JS, Remaut H, Buelens F, et al. (2006) Rationally designed small compounds inhibit pilus biogenesis in uropathogenic bacteria. Proceedings of the National Academy of Sciences 103:17897–17902.

21. Gophna U, Barlev M, Seijffers R, et al. (2001) Curli fibers mediate internalization of Escherichia coli by eukaryotic cells. Infect Immun 69:2659–2665.

22. Norinder BS, Lüthje P, Yadav M, et al. (2011) Cellulose and PapG are important for Escherichia coli causing recurrent urinary tract infection in women. Infection 39:571–574.

23. Connell I, Agace W, Klemm P, et al. (1996) Type 1 fimbrial expression enhances Escherichia coli virulence for the urinary tract. Proc Natl Acad Sci U S A 93:9827–9832.

24. Olsén A, Jonsson A, Normark S (1989) Fibronectin binding mediated by a novel class of surface organelles on Escherichia coli. Nature 338:652–655.

25. Cegelski L, Pinkner JS, Hammer ND, et al. (2009) Small-molecule inhibitors target Escherichia coli amyloid biogenesis and biofilm formation. Nat Chem Biol 5:913–919.

26. Otto K, Elwing H, Hermansson M (1999) The role of type 1 fimbriae in adhesion of Escherichia coli to hydrophilic and hydrophobic surfaces. Colloids Surf B Biointerfaces 15:99–111.

27. Walker SL, Redman JA, Elimelech M (2004) Role of Cell Surface Lipopolysaccharides in Escherichia coli K12 adhesion and transport. Langmuir 20:7736–7746.

28. Serra DO, Richter AM, Klauck G, et al. (2013) Microanatomy at Cellular Resolution and Spatial Order of Physiological Differentiation in a Bacterial Biofilm. MBio 4:e00103–13.

29. Sánchez B, López P, González-Rodríguez I, et al. (2011) A flagellin-producing Lactococcus strain: interactions with mucin and enteropathogens. FEMS Microbiol Lett 318:101–107.

30. Arora S, Ritchings B, Almira E, et al. (1998) The Pseudomonas aeruginosa flagellar cap protein, FliD, is responsible for mucin adhesion. Infect Immun 66:1000.

31. Tasteyre A, Barc M, Collignon A, et al. (2001) Role of FliC and FliD flagellar proteins of Clostridium difficile in adherence and gut colonization. Infect Immun 69:7937.

32. Zgair AK, Chhibber S (2011) Adhesion of Stenotrophomonas maltophilia to mouse tracheal mucus is mediated through flagella. J Med Microbiol 60:1032–1037.

33. Erdem A, Avelino F, Xicohtencatl-Cortes J, Girón J (2007) Host protein binding and adhesive properties of H6 and H7 flagella of attaching and effacing Escherichia coli. J Bacteriol 189:7426–7435.

34. Hayashi F, Smith KD, Ozinsky A, et al. (2001) The innate immune response to bacterial flagellin is mediated by Toll-like receptor 5. Nature 410:1099–1103.

35. Miyamoto Y, Iimura M, Kaper JB, et al. (2006) Role of Shiga toxin versus H7 flagellin in enterohaemorrhagic Escherichia coli signalling of human colon epithelium in vivo. Cell Microbiol 8:869–879.

36. Genevaux P, Muller S, Bauda P (1996) A rapid screening procedure to identify mini-Tn10 insertion mutants of Escherichia coli K-12 with altered adhesion properties. FEMS Microbiol Lett 142:27–30.

37. Wood T, González Barrios A, Herzberg M, Lee J (2006) Motility influences biofilm architecture in Escherichia coli. Appl Microbiol Biotechnol 72:361–367.

38. Domka J, Lee J, Bansal T, Wood TK (2007) Temporal gene-expression in Escherichia coli K-12 biofilms. Environ Microbiol 9:332–346.

39. Sauerbrey G (1959) Verwendung von Schwingquarzen zur Wägung dünner Schichten und zur Mikrowägung. Z Physik 155:206–222.

40. Bain CD, Troughton EB, Tao YT, et al. (1989) Formation of monolayer films by the spontaneous assembly of organic thiols from solution onto gold. J Am Chem Soc 111:321–335.

41. Love JC, Estroff LA, Kriebel JK, et al. (2005) Self-assembled monolayers of thiolates on metals as a form of nanotechnology. Chem Rev 105:1103–1169.

42. Bertilsson L, Liedberg B (1993) Infrared study of thiol monolayer assemblies on gold: preparation, characterization, and functionalization of mixed monolayers. Langmuir 9:141–149.

43. Laibinis PE, Nuzzo RG, Whitesides GM (1992) Structure of monolayers formed by coadsorption of two n-alkanethiols of different chain lengths on gold and its relation to wetting. J Phys Chem 96:5097–5105.

44. Arima Y, Iwata H (2007) Effect of wettability and surface functional groups on protein adsorption and cell adhesion using well-defined mixed self-assembled monolayers. Biomaterials 28:3074–3082.

45. Höök F, Rodahl M, Brzezinski P, Kasemo B (1998) Energy dissipation kinetics for protein and antibody-antigen adsorption under shear oscillation on a quartz crystal microbalance. Langmuir

46. Bevan MA, Prieve DC (2000) Forces and Hydrodynamic Interactions between Polystyrene Surfaces with Adsorbed PEO–PPO–PEO. Langmuir 16:9274–9281.

47. Owen RJ, Crocker JC, Verma R, Yodh AG (2001) Measurement of long-range steric repulsions between microspheres due to an adsorbed polymer. Phys Rev E Stat Nonlin Soft

Matter Phys 64:011401.

48. Boks NP, Norde W, van der Mei HC, Busscher HJ (2008) Forces involved in bacterial adhesion to hydrophilic and hydrophobic surfaces. Microbiology 154:3122–3133.

49. Danese P, Pratt L, Dove S, Kolter R (2000) The outer membrane protein, Antigen 43, mediates cell- to- cell interactions within Escherichia coli biofilms. Mol Microbiol 37:424–432.

50. Rosenberg M, Gutnick D (1980) Adherence of bacteria to hydrocarbons: a simple method for measuring cell-surface hydrophobicity. FEMS

51. Crawford R, Reeve K, Gunn J (2010) Flagellated but not hyperfimbriated Salmonella enterica serovar Typhimurium attaches to and forms biofilms on cholesterol-coated surfaces. J Bacteriol 192:2981–2990.

52. Thomason L, Costantino N, Court D (2007) E. coli genome manipulation by P1 transduction. Curr Protoc Mol Biol Chapter 1:Unit 1.17.

Chapter 4

Antiadhesive properties of three-dimensional mucin gels

Parts of this chapter have been previously published as: Caldara M*, Friedlander RS*, Kavanaugh NL, Aizenberg J, Foster KR, Ribbeck K. Mucin biopolymers prevent bacterial aggregation by retaining cells in the free-swimming state. 2012. *Current Biology*. 22(24): 2325-2330. (*These authors contributed equally to this work).

INTRODUCTION

Our studies of bacterial adhesion to abiotic surfaces provide biological insight into the mechanisms and underlying trends in adhesion. Understanding the roles of surface hydrophobicity and various adhesive organelles can help to direct the design of effective antifouling materials. For inspiration we can also look to existing biological systems wherein microbes are kept in check. One such example is the mammalian epithelial surfaces, which harbor numerous bacteria that do not typically cause harm. Mucus, the hydrogel overlying all wet epithelia in the body, can prevent bacterial contact with the underlying tissue. The digestive tract, for example, is lined by a firmly adherent mucus layer that is typically devoid of bacteria, followed by a second, loosely adherent layer that contains numerous bacteria [1]. In fact, the human body is home to trillions of microbes that persist without causing infection. It is clear that the mucus layer is important to prevent microbial disease, as evidenced by diseases in which a compromised mucus barrier is found concurrently with microbial infection, such as cystic fibrosis, irritable bowel disease and peptic ulcers [2–4]. However, the mechanisms by which the mucus confers protection from microbial infections are poorly understood.

In order to study the interactions between microbes and mucus, we use an *in vitro* system in which purified native mucus components are used to reconstitute mucin gels. The principle gel-forming component of mucus, namely the glycoprotein mucin, is purified and suspended in

liquid media to produce mucus-like gels in vitro. The purification and study of mucins is paramount, as these molecules are the main components of mucus and provide many of the rheological and barrier properties observed therein.

Mucins are large glycoproteins, whose sugar components comprise up to 70% of their molecular mass. Mucins may form crosslinked networks, which help to provide structure to the mucus layer. Additionally, the sugar moieties on mucin molecules allow for mucin networks to retain large amounts of water, giving mucus its swollen, jelly-like consistency. In order to understand how mucin interactions and structure relate to function, purification must be carried out in a manner that retains post-translational modifications as well as supramolecular structure. In fact, many industrially purified mucins do not form gels as native mucins do, ostensibly due to the loss of structural integrity [5, 6]. Therefore, when studying mucins, it is important to carefully and thoroughly purify them. Here, we use mucins purified in-house to investigate mucus's role as a principal arena for host-microbe interactions and attempt to better understand its role in modulating bacterial adhesion and swimming behavior with the ultimate goal of inspiring novel antifouling surfaces.

RESULTS AND DISCUSSION

Mucins reduce surface adhesion and biofilm formation of *P. aeruginosa*

To begin to dissect mucin-bacterial interactions, we developed an *in vitro* assay that uses defined concentrations of native mucins. As a source of mucins we purified native porcine gastric mucus to obtain an extract composed predominantly of MUC5AC, which is one of the major gel-forming components of mucus in the lungs and stomach [7]. The use of natively purified mucins is decisive for the utility of this assay, as commercially available mucins are processed and have lost the ability to form viscoelastic hydrogels, as are generated by the native

polymers [5, 6]. The second critical feature for this assay is the presentation of mucins in solution, as they exist in the secreted lung mucus, instead of depositing them onto a surface. This detail is important as the surface deposition of mucins is likely to adsorb functional groups, thereby partially dehydrating and altering the biochemical activity of the polymer.

First, we tested the effect of mucins on the ability of bacteria to colonize an immersed surface. A glass coverslip was immersed in culture medium that contained physiological concentrations of mucins [8]. Using the motile, opportunistic pathogen *Pseudomonas aeruginosa,* we quantified firm attachment by inoculating exponential-phase cells in the mucin-bearing medium and imaging the coverslip using phase contrast microscopy. Cells that adhered to the surface and fully arrested (based on overlaying pairs of images separated by 2 s) were considered firmly attached, and were counted at 20-minute intervals (Figure 4.1A).

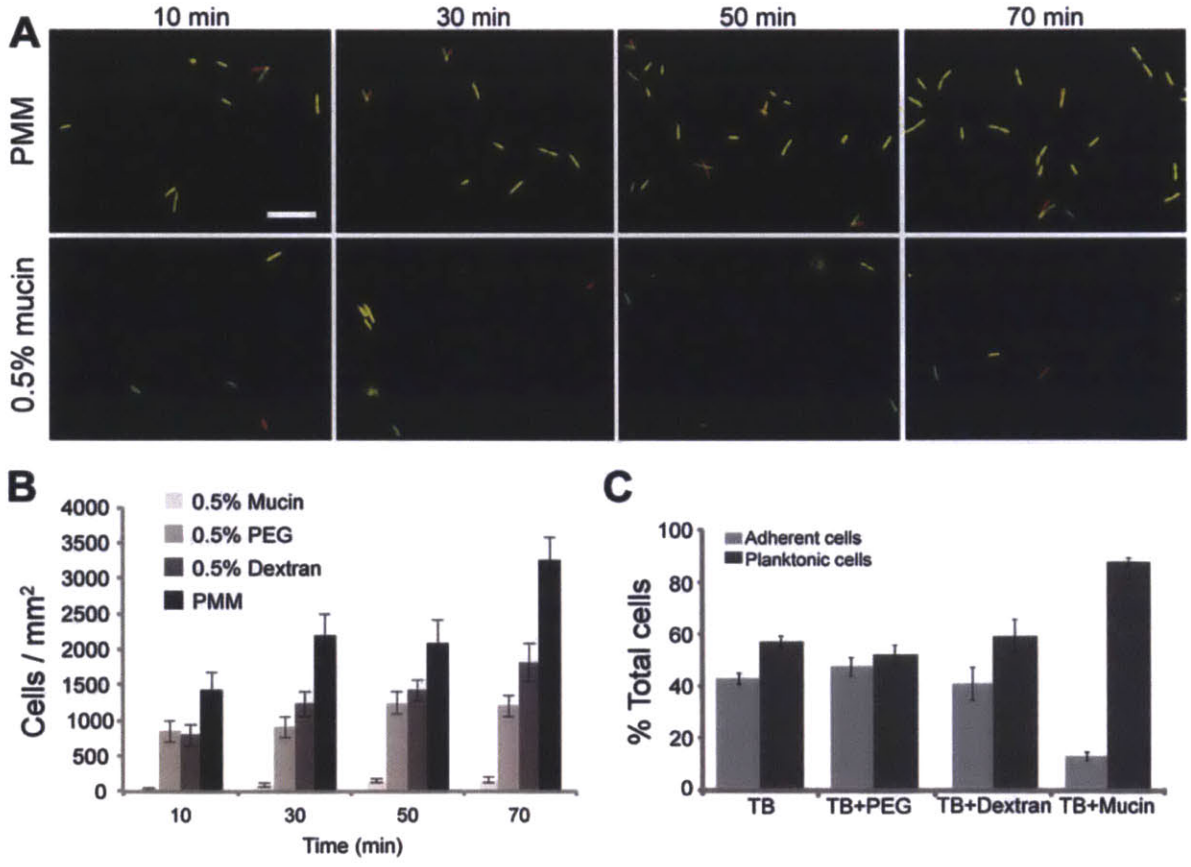

Figure 4.1. Mucins block *P. aeruginosa* attachment to surfaces. (*A*) Images of coverglass surfaces at the indicated time points, depicting cell adhesion. Cells in PMM or PMM plus mucins were photographed at 2 s intervals at each time point. Images from these intervals were false-colored red and green, respectively, and overlaid, allowing visualization of active cell motility or Brownian motion, versus firm adhesion. Scale bar is 10 μm. (*B*) Number of wild-type cells firmly adherent to coverglass in PMM, or PMM supplemented with PEG, dextran or mucins after the indicated incubation periods. Error bars indicate SEM of 8-11 different data points. (*C*) PAO1 wild-type bacteria were grown in polypropylene tubes containing TB or TB plus 1% (w/v) PEG, dextran, or mucin. After 6 h, the relative amount of planktonic versus surface-attached cells was quantified using MTT staining. Error bars represent the standard deviation.

We found that mucins reduced bacterial surface adhesion by 20-fold over a 70 minute period (Figure 4.1B). To test if this inhibitory effect was specific to the mucins, or a generic result of the presence of polymers, we compared the effects of mucins to solutions of polyethylene glycol (PEG), a polymer often used as an anti-adhesive coating [9], and dextran, a branched, high molecular weight polysaccharide. In comparison to mucins, PEG and dextran demonstrated only mild reductions in bacterial adhesion at these early time points, indicating that mucins have singular effects that cannot be attributed to their polysaccharide or soluble polymeric attributes alone. At 6 h, a time at which biofilms have begun to form, approximately 90% of *P. aeruginosa* cells remained planktonic in the presence of mucins, compared with 50-60% in tryptone broth (TB) alone or TB plus PEG or dextran (Figure 4.1C).

Mucin gels maintain or augment bacterial swimming motility

It is tempting to speculate that bacteria failed to access the underlying surface because they were trapped within the mucin network. If this is true, we should expect to see a measurable decrease of motility within the mucin hydrogel. First, to test if motion was hindered in the presence of mucins we tracked the movements of *P. aeruginosa* cells that carried a deletion in the flagellar hook gene (*flgE*), and were thus deficient in self-propulsion. These cells demonstrated a significant decrease in diffusivity ($p<0.001$) in mucin environments, from 2.4 ±

0.2×10^{-9} cm^2/s to $1.0 \pm 0.1 \times 10^{-9}$ cm^2/s ($n \geq 96$ cells), reflecting a higher apparent viscosity of mucin-containing gels, and suggesting that geometric hindrance was present. However, the wild-type cells remained highly motile in the presence of the mucins. The distribution of velocities of swimming cells in mucins is similar to that in liquid medium, despite the differences in apparent viscosity (Figure 4.2A,B). This effect was apparent when we compared cells in *Pseudomonas* minimal medium (PMM) as well as in TB with or without mucins. To test whether this effect is specific for *P. aeruginosa*, or if it is a more general phenomenon that affects other swimming bacteria, we tracked a different motile bacterium, *E. coli*. Despite a significant decrease in diffusivity ($p<0.001$) of non-flagellated cells (Δ*fliC*) in mucins, from $2.2 \pm 0.2 \times 10^{-9}$ cm^2/s to $0.7 \pm 0.1 \times 10^{-9}$ cm^2/s ($n \geq 92$ cells), the wild-type cells had significantly increased swimming velocities in mucins compared with medium-only (Figure 4.2C,D).

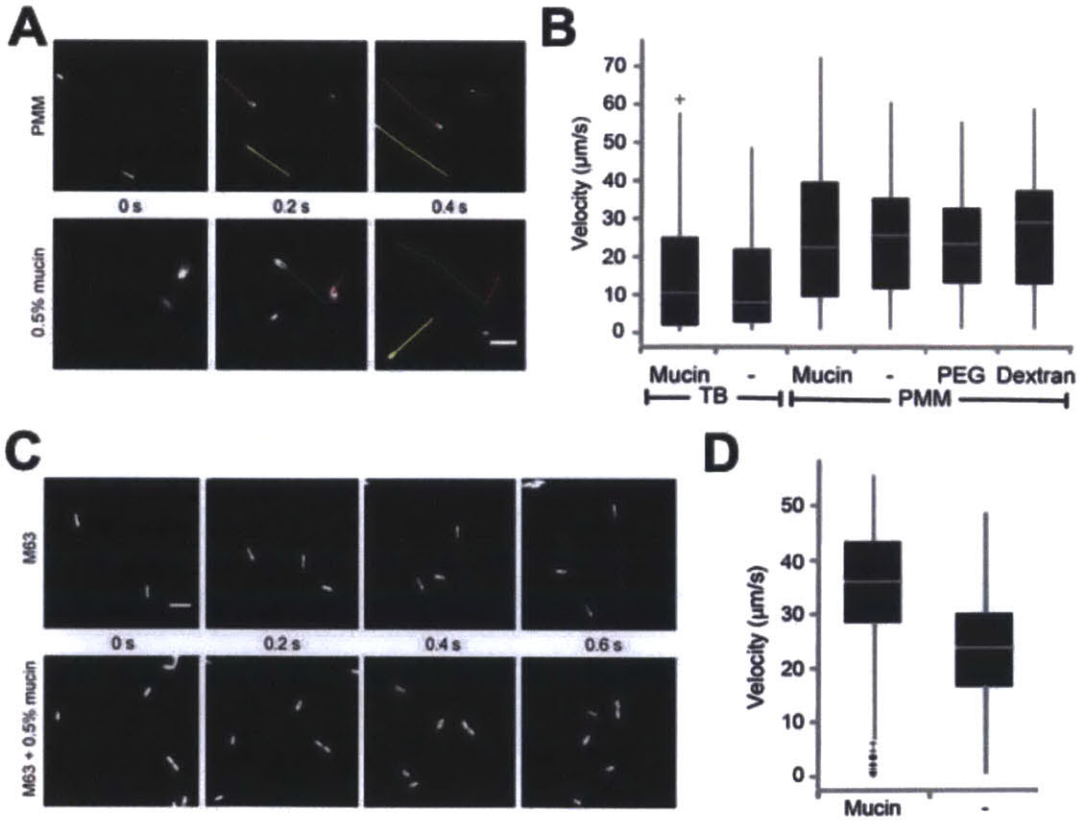

Figure 4.2. Swimming velocity of bacteria is increased in the presence of mucins. (*A*) Time-lapse images of swimming *P. aeruginosa* in 50% PMM or 50% PMM + 0.5% mucin. (*B*) Boxplots depicting swimming velocities of *P. aeruginosa* in various conditions. Cells were grown in the media indicated, but swimming experiments were in 50%-strength media. Velocities were obtained from particle tracking analyses of 20-s swimming videos obtained at 20 frames per second. (*C*) Time-lapse images of swimming *E. coli* in 50% M63 (upper) or 50% M63 + 0.5% mucin (lower). (*D*) Mean swimming velocities of *E. coli* in 50% M63 with or without 0.5% mucins. Velocities were obtained from particle tracking analyses of 20-s swimming videos obtained at 20 frames per second. In (*A* & *C*), images are at 0.2 s intervals and individual cell tracks are marked. Scale bars are 5 μm. For all boxplots, boxes extend from the 25th to the 75th percentile, the central line is the median, and whiskers extend to the data point nearest to 1.5 times the interquartile range above and below the box. Outliers are plotted as plus signs.

Immotile *P. aeurginosa* cells can form suspended flocs in mucin gels

If mucins can prevent surface colonization by maintaining cellular motility, we speculated that cells lacking motility may be able to overcome this dispersion effect and succeed in adhesion and biofilm formation in mucin environments. This line of inquiry may have direct physiological relevance, as isolates of *P. aeruginosa* from cystic fibrosis (CF) mucus are often non-motile [10]. As with the wild-type, mucins detectably reduced surface adhesion of non-motile cells (Δ*flgE*), which are already poorly adherent (Figure 4.3; compare to Figure 4.1B). To look beyond surface adhesion in the presence of mucin, we observed the bacteria in the volume of the mucin gel after 20 h of incubation. The wild-type cells remained largely as individual cells or small, suspended colonies (Figure 4.4A, B) of up to 20 μm^2 (this corresponds roughly to clusters of 10-20 cells) distributed throughout the volume of the mucin medium. Increasing mucin concentration did not visibly increase cellular cluster size (Figure 4.4C). However, when observing the Δ*flgE* mutant, we noticed a striking difference compared to the behavior of wild-type cells. The flagella mutant formed large aggregated flocs of up to 250 μm^2 (Figure 4.4A, B). These differences are not likely due to variations in cellular populations in the mucin medium, as PAO1 displayed similar growth rates in the presence and absence of mucins (Figure 4.4D). A

similar behavior was found for two additional flagella mutants, Δ*flgK*, which lack a hook filament junction protein, and Δ*fliD*, which lack an adhesive protein at the tip of the flagellar filament (Figure 4.4A, B) but not for Δ*pilB* which lack pilus-mediated adhesion and twitching motility (Figure 4.4A, B). The ability of cells to form suspended flocs was inversely correlated with their ability to form surface biofilms in mucin-free environments (Figure 4.4E, compare with 4.4B). For example, wild-type and Δ*pilB* cells formed substantial surface biofilms, but failed to form large suspended flocs in the presence of mucins. Conversely, the various flagellar mutants formed large flocs, but had reduced surface biofilms in the absence of mucins. All mutants tested displayed similar growth rates (Figure 4.4F). The flocs formed by Δ*flgE* strains increased in maximum size with increasing mucin concentration (Figure 4.4G).

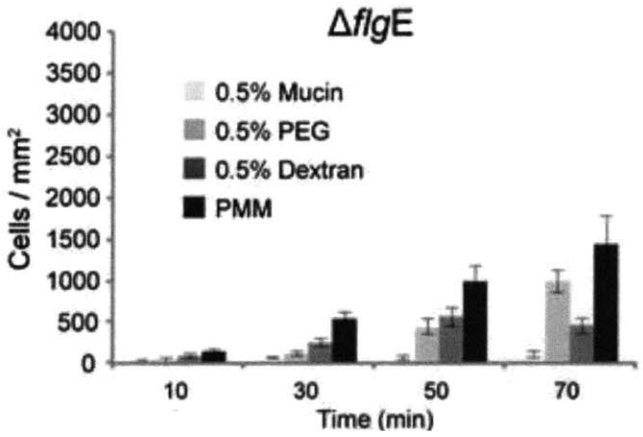

Figure 4.3. Adhesion of non-motile cells. Number of Δ*flgE* cells firmly adherent to coverglass in PMM, or PMM supplemented with PEG, dextran or mucins after the indicated incubation periods. Error bars indicate SEM for 4-11 data points.

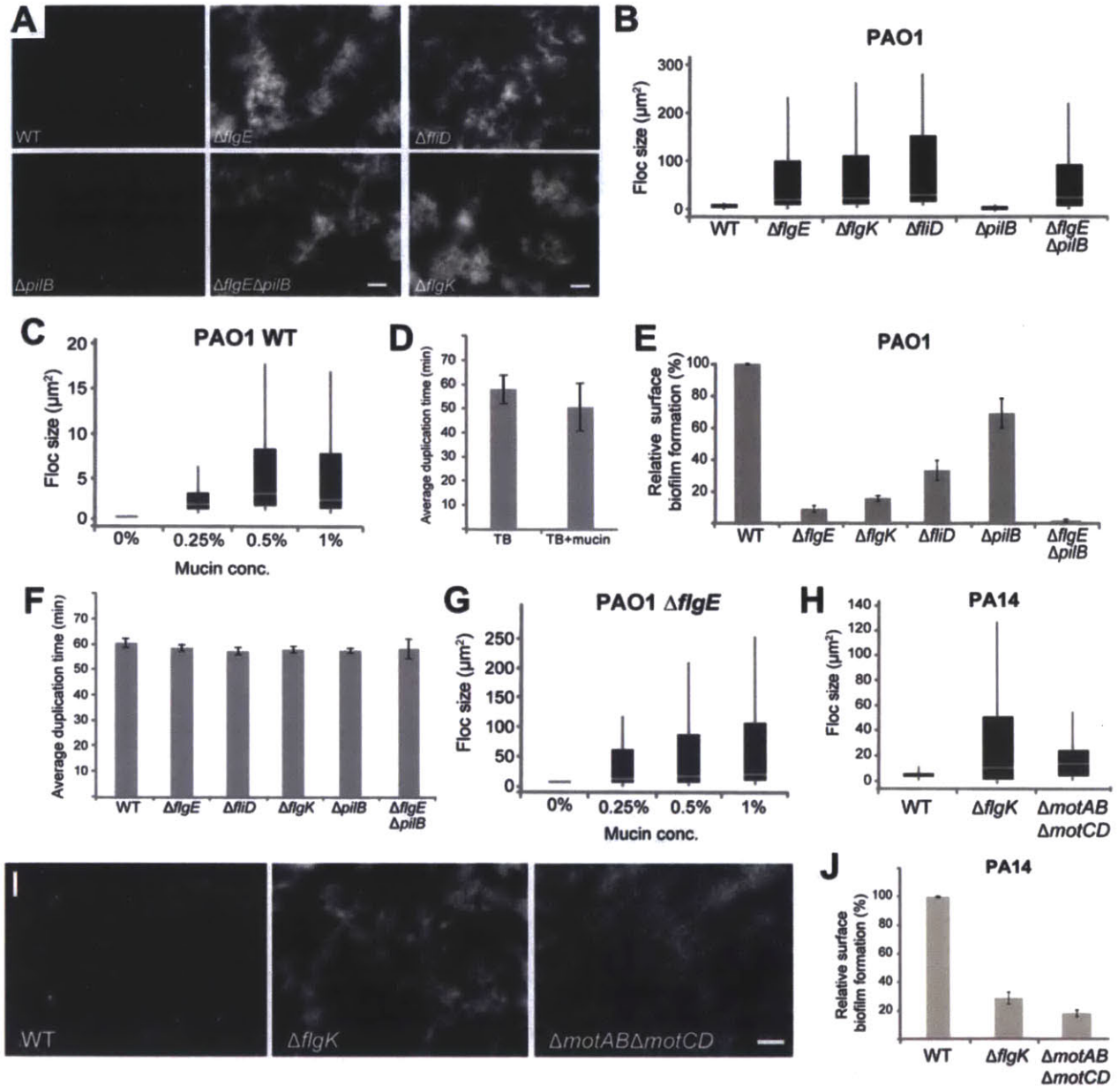

Figure 4.4. Non-motile flagella mutants, but not their motile counterparts, form flocs in mucin environments. (*A*) Floc formation of wild-type cells, flagella mutants (Δ*flgE*, Δ*fliD*, Δ*flgK*), a pili mutant (Δ*pilB*), and double flagella and pili mutant (Δ*flgE*Δ*pilB*) in PMM with 1% mucins after 20 h of incubation. Images are of cells in suspension only. Scale bar is 20 μm. (*B*, *C*, *G*, *H*) Boxplots quantifying floc size of wild type, flagella, pili and matrix and motility mutants for the strains indicated, after 20 h of growth in 1% mucin (unless otherwise indicated). For details on the quantification method see experimental procedures. For all boxplots, boxes extend from the 25th to the 75th percentile, the central line is the median, and whiskers extend to the data point nearest to 1.5 times the interquartile range above and below the box. Outliers are plotted as plus signs. (*D*) The average duplication time of PAO1 in TB or TB plus mucins was determined over a time span of 6 h by CFU counting. Error bars represent standard deviation. (*E*,

J) Surface attached biofilm formation was quantified by crystal violet (CV): liquid cultures of the strains indicated were inoculated in 96-well plates at an OD_{600} of 0.01, and incubated for 7 h at 37°C. The biofilms that formed were quantified by staining with 0.1% CV as described previously [11]. After staining, each plate was rinsed, and the remaining CV was destained with 33% acetic acid for 15 min and measured using a plate reader (OD_{595}). Data are presented as percent biofilm formation relative to wild type for the strains indicated. The error bars represent standard deviation. (*F*) Exponential phase cultures were added to PMM containing 1% mucins at a final concentration of 50-100 cells/μL. The initial number of cells was determined by measuring the CFU. The culture was then incubated at 37°C for 20 hrs. At the end of the incubation the culture was bead bashed and diluted with PBS to determine the final number of cells by CFU. Knowing the initial and final number of cells present in the mix, we could estimate the average duplication time of each strain. Each sample was inspected by microscopy to ensure that no aggregates were present. (*I*) Fluorescence micrographs depicting floc formation of wild-type PA14 cells and flagella/motility mutants (Δ*flgK*, Δ*motAB*Δ*motCD*) in 1% mucins after 20 h of incubation. Scale bar is 20 μm. *This figure and data courtesy of Nicole Kavanaugh and Marina Caldara.*

We hypothesized that loss of flagellar motility (rather than other properties of flagella, such as adhesion) was the dominant contributor to the observed aggregation. To test this, we measured mucin-dependent flocculation by a PA14 strain that carries a fully assembled flagellum, but is paralyzed due to deletions in all four stators in the motor complex (Δ*motAB*Δ*motCD*). This mutant formed substantially larger flocs (up to 60 μm^2) than the wild-type (Figure 4.4H, I), but the structures were smaller than those formed by the Δ*flgK* strain. Again, floc-forming ability in mucins tended to be negatively correlated with surface biofilm formation in medium-only environments (Figure 4.4J). Both a loss of motility and loss of the flagella itself, therefore, appear to contribute to mucus colonization. Complementing the *flgE* deletion in PAO1 Δ*flgE* restored swimming motility and diminished the capacity of the bacteria to form flocs in mucin, indicating that it is indeed the lack of flagella that caused the formation of flocs (Figure 4.5A, B).

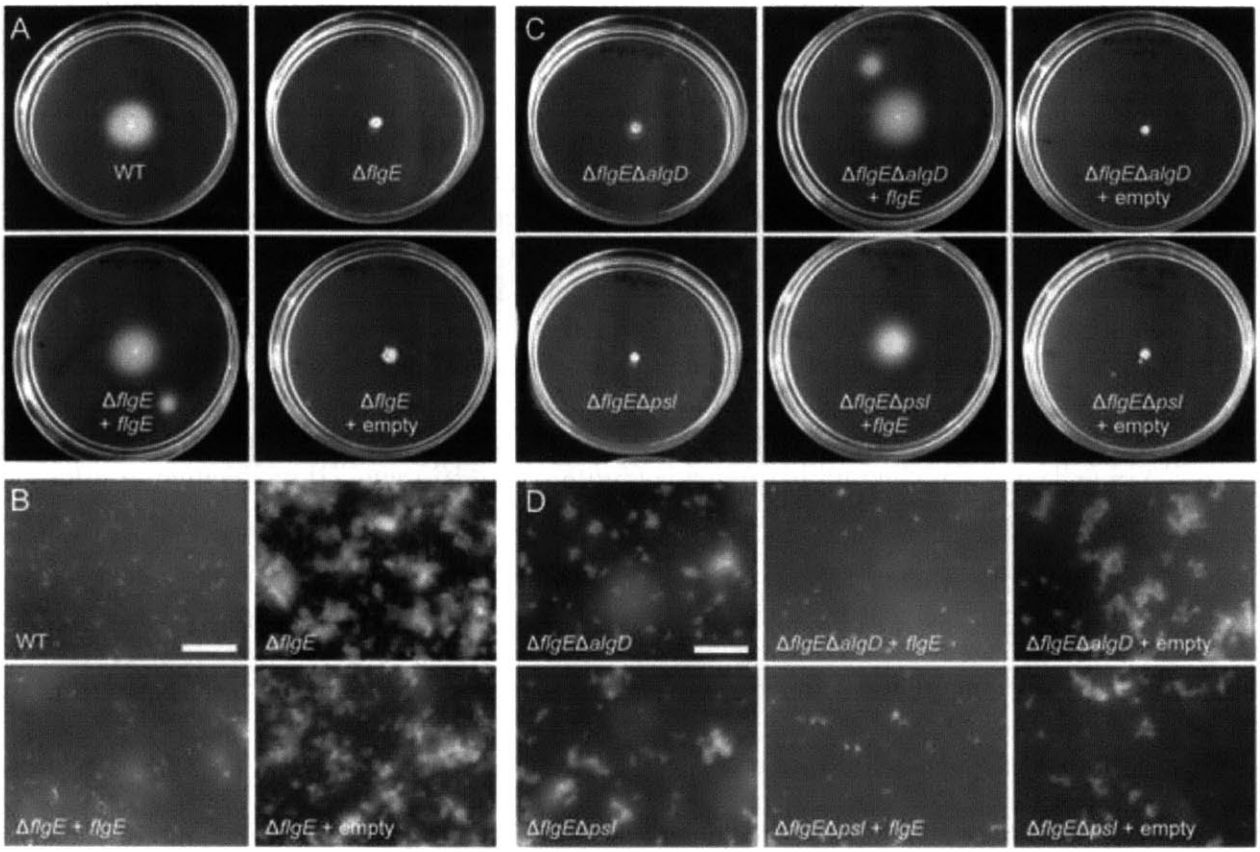

Figure 4.5. Complementation of Δ*flgE* strains restores swimming motility and abolishes floc formation in mucin. The Δ*flgE* mutants were complemented using the plasmid pMQflgE (pMQ80 containing the *flgE* gene). As a control, pMQ80 plasmid without *flgE* was used ("empty"). (*A*) Swimming motility of the genetically complemented Δ*flgE* mutant. The center of the agar plate is inoculated with bacteria. Only those cells that can swim will spread out from the center. (*B*) Growth of the *flgE* complemented Δ*flgE* mutant in mucin. Scale bar is 50mm. (*C*) Swimming motility of the Δ*flgE*Δ*algD* and Δ*flgE*Δ*psl* double mutants. (*D*) Growth of *flgE*-complemented Δ*flgE*Δ*algD* and Δ*flgE*Δ*psl* double mutants in mucin. Scale bar is 50 μm. *This figure and data courtesy of Nicole Kavanaugh.*

Our data suggest that mucins are highly effective at preventing swimming cells from surface attachment and from forming suspended aggregates. Previous work has indicated that fliD is an adhesin for mucin [12], yet it does not appear to be required for the aggregative phenotype (Figure 4.4A, B). How then do the flagella mutants achieve aggregate formation? It appears that their lack of motility enables cells to form clonal outgrowths of individual cells within the mucus. This was supported by culturing mixtures of fluorescent and non-fluorescent immotile cells in mucin medium. Over the course of 20 h small homogeneous patches of ten to

twenty cells emerged and further expanded (Figure 4.6). Notably, floc formation did not occur in PEG, dextran or industrially purified mucins (Figure 4.7A). It appears that this phenomenon depends on specific features unique to native mucins.

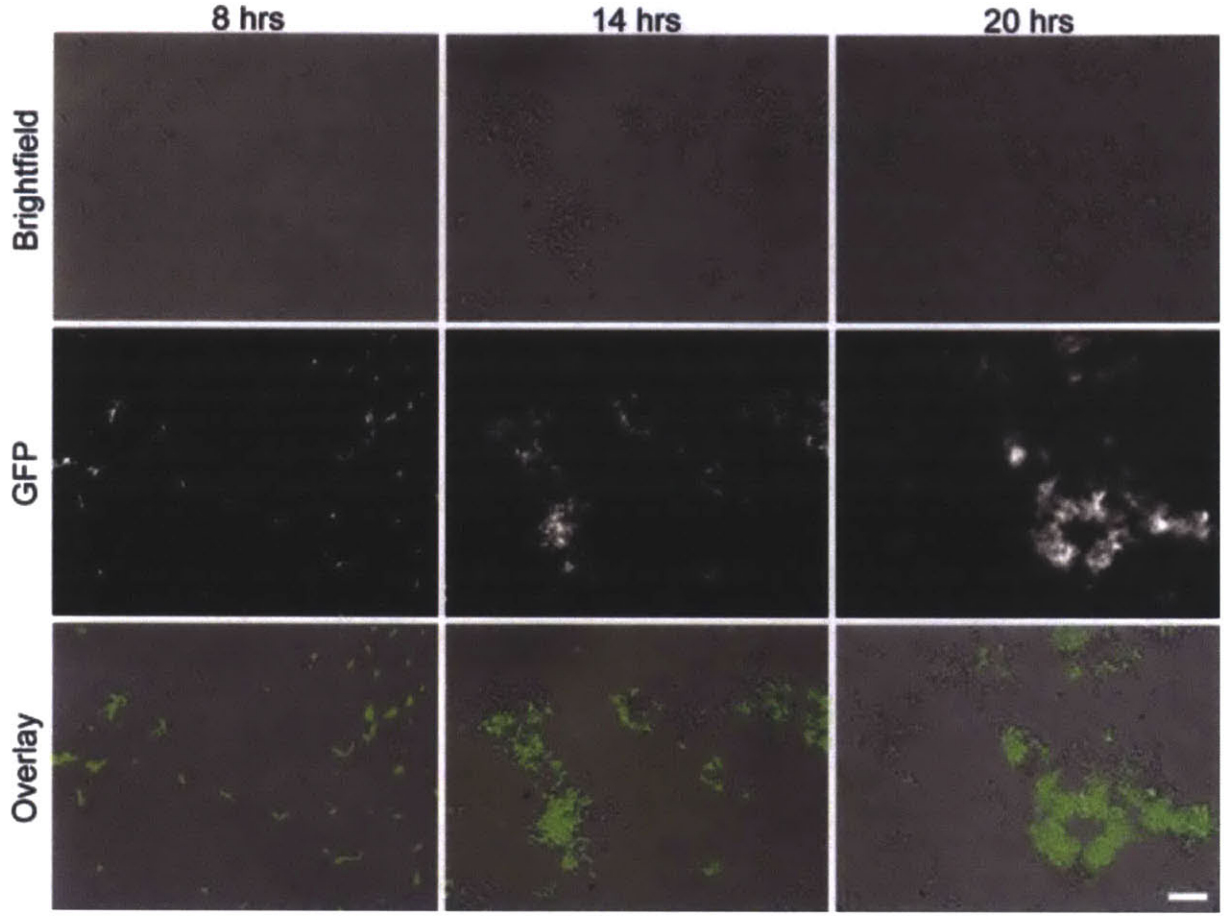

Figure 4.6. Non-motile flagella mutants form clonal flocs in mucin environments. A GFP-tagged Δ*flgE* mutant was mixed 1:1 with the un-tagged strain, and the mixture was inoculated in PMM containing 1% mucins. Images were taken after 8, 14 and 20 h. The top panels are visualized by bright field, the middle panels by fluorescence microscopy, and the bottom panels show overlays of the two channels. Scale bar is 20 μm. *This figure and data courtesy of Nicole Kavanaugh and Marina Caldara.*

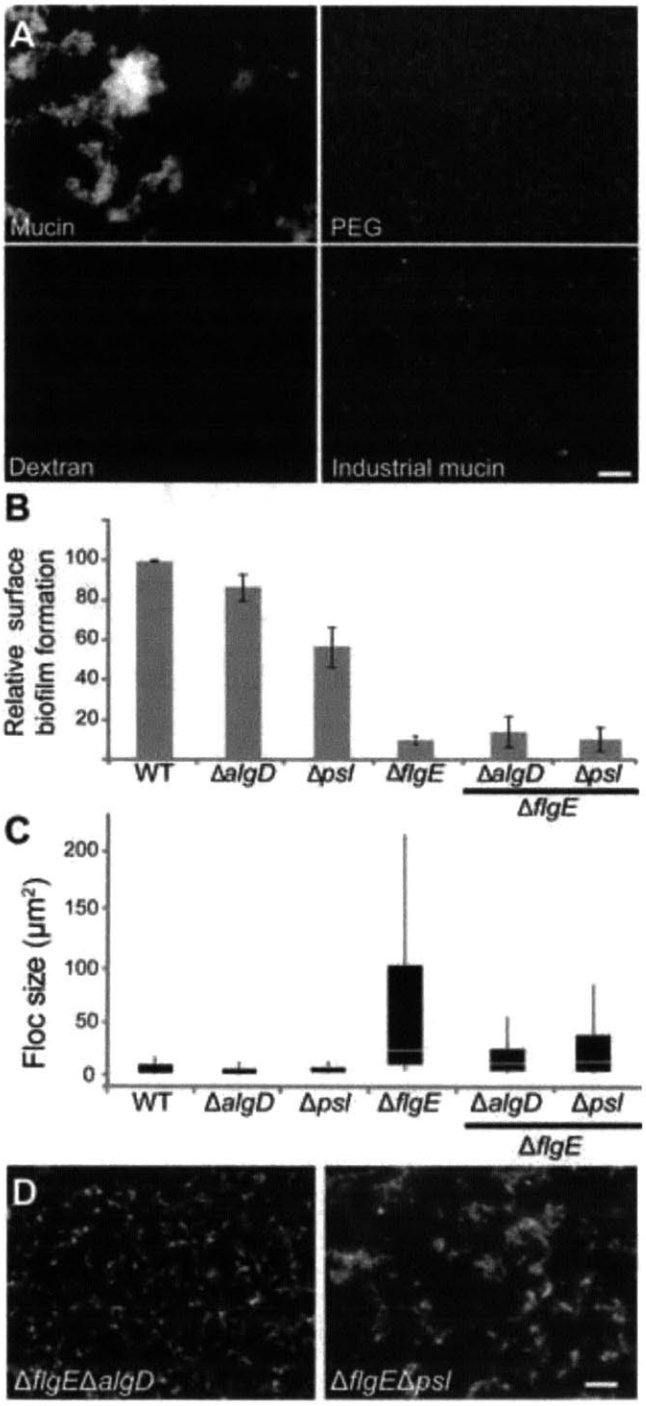

Figure 4.7. Flocs formed in mucin environments are exopolysaccharide-dependent. (*A*) Δ*flgE* strains were grown for 20 h in PMM containing 1% (w/v) either PEG, dextran or industrially purified mucins (NBS Biologicals). Only in the presence of native mucins is floc formation observed. Scale bar is 20 μm. (*B*) Liquid cultures of EPS secretion mutants and motility mutants were quantified by CV, as described in Figure 4.4. The experiments were performed in triplicate. The error bars represent the standard deviations. (*C*) Boxplots of floc size

of wild-type cells and the indicated motility and matrix mutants in PMM with 1% mucins after 20 h of incubation. For all boxplots, boxes extend from the 25th to the 75th percentile, the central line is the median, and whiskers extend to the data point nearest to 1.5 times the interquartile range above and below the box. Outliers are plotted as plus signs. (*D*) Fluorescence micrographs depicting floc formation of wild-type cells and flagella/matrix mutants (Δ*flgE*Δ*algD*, Δ*flgE*Δ*psl*) in 1% mucins after 20 h of incubation. Scale bar is 20 μm. *This figure and data courtesy of Nicole Kavanaugh and Marina Caldara.*

P. aeruginosa floc formation is dependent on the production of Psl-and alginate

Flagella loss appears to allow bacteria to effectively colonize mucus in a manner reminiscent of surface attached biofilms. Just how similar are these two forms of bacterial aggregation? To address this, we tested if floc formation by non-motile cells required extracellular matrix, a hallmark of biofilms. Specifically, we looked at Psl, which plays a structural role in the maturation of surface-attached biofilms [13] and alginate, which appears to play only a minor role in biofilm formation (Figure 4.7B, [14]) but is overexpressed in colonies adapted to growth in CF lung mucus [15, 16]. Using previously characterized single *algD* and *psl* mutant strains [13, 17], we introduced additional *flgE* mutations to study the importance of the extracellular matrix on the immotile flocs. Complementation of the double mutants with *flgE* was able to restore motility (Fig. 4.5C, D). We found that both polymers, particularly alginate, were important for floc formation (Figure 4.7C, D). This phenotype may be relevant to CF pathology, where the formation of *P. aeruginosa* flocs inside the lung mucus is associated with the rise of antibiotic resistance [18]. In sum, our data suggest that mucin-based flocs and biofilms have the same broad reliance on extracellular matrix but the mechanistic details differ in important ways. Specifically, flocs rely on alginate and flagella loss in a manner not seen in surface attached biofilms.

P. aeruginosa flocs that emerge in mucin gels are antibiotic resistant

Last, we asked whether floc formation can provide bacteria with a selective advantage. Again by analogy with biofilms, we hypothesized that the immotile cellular aggregates that emerge in the presence of mucins also have a higher resistance toward antibiotics. We grew wild-type and the non-motile Δ*flgE* cells in mucin media for 20 h, and then subjected both strains to two clinically relevant antibiotics that differ in their mode of action (Figure 4.8). This experiment revealed two points: first, both wild-type and Δ*flgE* bacteria were systematically more resistant to colistin in the presence of mucins as compared to liquid culture without mucins. This suggests that the mucins themselves have the capacity to reduce the efficacy of colistin, regardless of whether cells are planktonic (wild-type) or form flocs (Δ*flgE*). Second, it appeared that the floc-forming Δ*flgE* cells were more resistant to both antibiotics in the mucin medium than the motile wild type cells. To test for this possibility we determined the percent survival of the bacteria in either condition, by normalizing to the cell numbers in the untreated samples in liquid and mucin. Inside the mucin medium, the non-motile flagella mutants were on average 14 times more resistant to colistin (Figure 4.8B) and approximately 6 times more resistant to ofloxacin (Figure 4.8C) than wild-type cells, both of which are statistically significant differences. We conclude that the aggregates that emerge upon loss of motility indeed have an increased resistance compared to motile wild-type cells, possibly due to the presence of an altered composition or quantity of extracellular matrix components, or due to a protective effect of increased cell density [19].

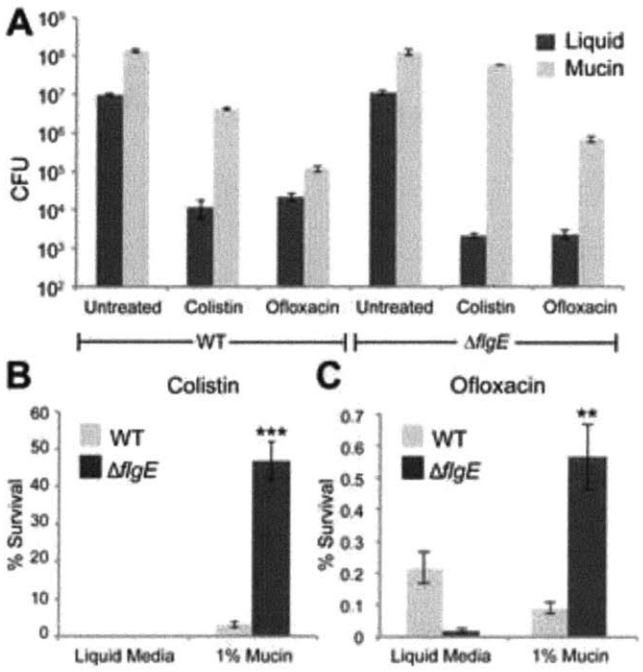

Figure 4.8. Flocs grown in mucin environments are antibiotic resistant. (*A*) Wild-type and Δ*flgE* cells were grown in liquid culture or in 1% mucin for 20 h and then exposed to colistin and ofloxacin. After 3 h of antibiotic exposure, the cells were plated to determine the number of surviving cells. (*B*, *C*) Data from (*A*) replotted as survival of antibiotic treated cells as a percentage of CFUs of untreated cells. Each trial was repeated at least 3 times. Error bars represent SEM. **, $p<0.01$; ***, $p<0.001$, comparing survival of Δ*flgE* to wild type in 1% mucins. *This figure and data courtesy of Nicole Kavanaugh and Marina Caldara.*

Conclusions and Outlook

Here we have found that mucin polymers provide a candidate solution to inhibit biofilm formation. Critically, our results demonstrate that mucins can limit bacterial surface attachment and biofilm formation without killing or trapping bacteria, which will help to limit selective pressure for resistance (Figure 4.9). Indeed, our only evidence for a resistance phenotype comes in the form of non-motile cells, which are likely to be strongly limited in other modes of virulence [10, 20]. Our observations of motility and reduced adhesion in mucin media are similar to findings for *Campylobacter jejuni* in mouse intestinal crypts. In a previous study, extracted epithelial scrapings from *C. jejuni*-colonized gnotobiotic mice demonstrated a lack of adhesion

and unhindered motility within the crypts [21]. Similar to this, a recent study showed that when supplemented in agar plates, mucins appear to increase motility of *P. aeruginosa* [22]. At first sight these and our findings contrast with reports on surface-immobilized mucins, which arrest [12, 23] and can cause large aggregate formation of *P. aeruginosa* cells [24]. However, these findings can be reconciled if one considers that the effects of mucins on motility may depend on their native three dimensional structure and hence biophysical properties such as viscoelasticity and lubricity, which are preserved in native mucus and presumably inside agar gels, but not when adsorbed to a two-dimensional surface [22]. The gel-forming mucin MUC2 has an ordered repeating ring structure [25], and we speculate that also other gel-forming mucins, such as the MUC5AC used in our experiments, display three dimensional features that affect their interactions with bacteria. Indeed, Berg and Turner have observed that certain structured viscous solutions allow increased velocities of motile bacteria by providing a rigid framework for generating propulsive forces [26]. We anticipate that studying mucins in their native three-dimensional form will reveal valuable novel information about bacterial behavior that cannot be captured by collapsed mucin monolayers.

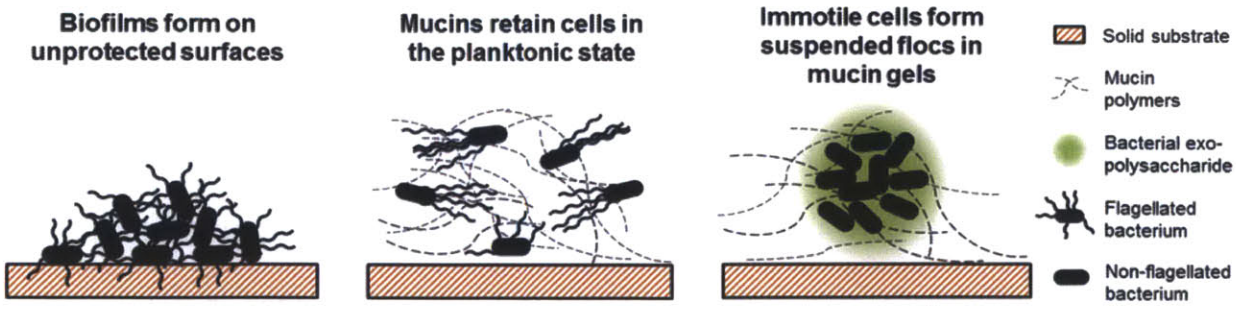

Figure 4.9. Schematic summary of bacterial response to mucin gels.

EXPERIMENTAL SECTION

Mucin purification

The source for purification of native MUC5AC was pig stomachs (Figure 4.10A), which secrete MUC5AC, homologous to the human glycoprotein [27]. Porcine gastric mucins were purified as described previously, with the omission of the CsCl density gradient centrifugation [28]. Stomachs were opened (Figure 4.10B) and the lumens were gently rinsed of adherent food and debris with water. The mucosal surfaces were scraped to obtain thick mucus gel (Figure 4.10C). Scrapings were collected into a large beaker on ice (Figure 4.10D). Scrapings were diluted 1:5 using 0.2 M NaCl and 0.04% NaN_3 (Sodium azide is added as a bacterial growth inhibitor). We adjusted pH to 7.4 using 1N NaOH and added protease inhibitors as follows: 5mM Benzamidine HCl, 1mM dibromoacetophenone, 1mM phenylmethylsulfonylfluoride, 5mM EDTA pH 7. The mixture was stirred gently overnight at 4 °C to solubilize mucus. The samples were then centrifuged at 7,000 rpm (SLA 3,000) for 30 minutes at 4 °C (Figure 4.10E). The supernatant was collected and then centrifuged at 10,000 rpm (SLA 3000) for 30 minutes at 4 °C. The supernatant was again collected and ultracentrifuged at 45,000 rpm for 1 h at 4 °C (PC bottles 355618). Supernatant was then removed carefully. Sample was then filtered on a PD10 sephadex column to remove any remaining particulate matter. This sample was then loaded on a Sepharose (CL2B) column that was equilibrated with filtered 0.2 M NaCl. Fractions were collected based on positive periodic acid-Schiff staining (Figure 4.10F). 45-9 mL fractions were collected (Figure 4.10G) and transferred to a stirred cell concentrator with a deionized water-soaked membrane and the sample was concentrated to 50 mL in preparation for washing (Figure 4.10H). This sample was diluted 1:20 in deionized water so that final salt concentration was less

than 20 mM NaCl. The sample was again concentrated to 50 mL and aliquoted into 1 mL samples. These were snap frozen in liquid nitrogen and lyophilized (Figure 4.10I).

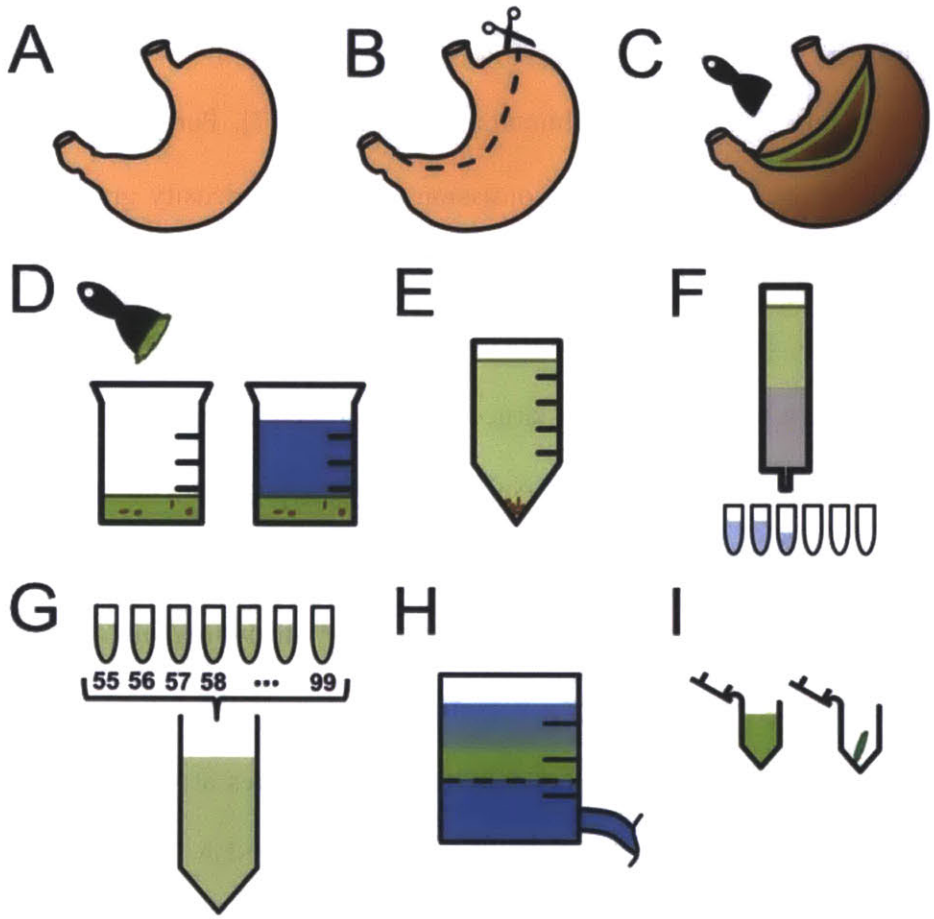

Figure 4.10. Purification of porcine gastric mucins. (*A*) Pig stomachs are obtained from an abattoir for mucin purification. (*B*) An incision is made along the body of the stomach to expose the inner contents of the stomach. (*C*) Loose chyme and food particles are first removed and then the luminal epithelial surface is scraped gently to remove mucus. (*D*) The mucus from up to 30 stomachs is collected in a beaker, and diluted 5-fold using 0.2 M NaCl and 0.04% NaN_3. pH is adjusted to 7.4 using NaOH and several protease inhibitors are added. (*E*) After this mixture is thoroughly mixed, the sample is centrifuged several times to remove particulate matter. (*F*) Samples are then loaded on a Sepharose column and 9 mL fractions are collected. (*G*) Based on a Schiff assay, 45 fractions with glycoproteins are collected and combined. (*H*) These fractions are placed in a stirred cell concentrator to concentrate mucin glycoprotein. (*I*) Samples are aliquoted and lyophilized for storage at -80 °C.

Mass spectrometry analysis was used to determine the composition of the mucin preparation as described previously [29]. Briefly, the analysis was performed at the Harvard

Microchemistry and Proteomics Analysis Facility by microcapillary reverse-phase HPLC nanoelectrospray tandem mass spectrometry on a Thermo LTQ-Orbitrap mass spectrometer. The spectra were analyzed using the algorithm Sequest [30]. The analysis showed that MUC5AC was the predominant mucin present in our purified extract, which also contained MUC2, MUC5B and MUC6 as well as other proteins including histones, actin and albumin. In addition, its quality was tested by rheology as described in [6, 28], which confirmed that the isolated mucins displayed viscoelastic properties similar to native mucus.

Microbial adhesion assays

For adhesion experiments, PAO1 wild-type and PAO1 Δ*flgE* were inoculated in LB and grown overnight at 37°C, shaking. Overnight cultures were diluted 1:100 into PMM and grown shaking at 37°C for 4 h. 1 ml of exponential phase cells (OD_{600} = 0.4 to 0.45) were centrifuged and cells were resuspended in 400 µL sterile PMM. These cells were diluted 1:10 in PMM and then further diluted 1:10 into the medium to be tested (PMM only, 0.5% mucin, 0.5% PEG 3350, or 0.5% dextran). 40 µL of this mixture was pipetted onto glass slides with shallow spherical depressions, covered with a glass coverslip and inverted. Pairs of images were taken 2 s apart in multiple fields for each sample at 10, 30, 50 and 70 min. Image pairs were compared to differentiate firmly attached cells from moving cells in each frame. Adherent cells were counted for each time point. Pairs of dividing cells were counted as single cells.

Quantification of biofilm formation in mucin gels

Freshly growing cells at an OD_{600} of 0.01 were inoculated in polypropylene PCR tubes and incubated at 37°C in TB or in TB containing 0.5% (w/v) mucins. After 6 h the planktonic cells were removed for quantification, and the adherent cells in the tubes were washed 2 times

with PBS to remove non-adherent cells. Planktonic and adherent cells were stained with 5 mg/ml MTT (3-(4,5-Dimethylthiazol-2-yl)-2,5-diphenyltetrazolium bromide) for 2 h at 37°C, and subsequently destained with 20% sodium dodecyl sulfate in 50% dimethylformamide (adjusted to pH = 4.7) overnight at 37°C. The resulting solutions were quantified using a plate reader (OD_{595}).

Particle tracking

For measurement of cell velocities, bacteria were grown to exponential phase as described above, stained with Syto9 live cell stain by adding Syto9 1:1000 into the culture, and incubated for 10 minutes at room temperature. The stained cells were diluted 1:10 into a 50% strength solution of growth medium or growth medium supplemented with mucin, dextran or PEG. These solutions were mixed and dispensed into chambers for visualization. Videos of cells were taken on an inverted fluorescent microscope at 20 frames per second to obtain trajectories. The trajectories obtained were processed using Matlab to determine velocities and diffusivities. Diffusivities were based upon mean squared displacement values for a range of lag times. Trajectories were also examined visually to ensure accuracy.

Antibiotic treatment

To determine the antibiotic resistance of flocs grown in mucin-media, cells were grown in PMM with 1% (w/v) mucin. After 20 h, the number of cells was determined by counting CFU; this number was used as the reference number prior to treatment. The antibiotics ofloxacin and colistin were added to the cultures at final concentrations of 20 μg/ml, and the cultures were grown at 37°C for 3 h. After treatment, the number of survivors was estimated by measuring the CFU. To avoid aggregates, we bead-bashed each sample for 30 s before diluting and plating.

Each experiment was carried out in triplicate. To determine the resistance of cells grown in the absence of mucins, an exponential phase culture was adjusted to contain the same number of cells as had grown in 1% mucin in 20 h, and challenged with antibiotics as described above.

Strains and growth conditions

All strains, plasmids, and their sources are listed in Table 4.1. *Pseudomonas aeruginosa* PAO1 was the wild-type in this study. *P. aeruginosa* from the PA14 background was used for the motility mutants presented in Figure 4.4H-J. *E. coli* wild-type strain was W3110, subtype ZK2686. The following media were used: Luria-Bertani (LB) broth, tryptone broth (TB; 10% w/v tryptone), *Pseudomonas* minimal medium (PMM; 2.5 mM Na-succinate, 1.2 mM $MgSO_4$, 35 mM K_2HPO_4, 22 mM KH_2PO_4, 0.8 mM $(NH_4)_2SO_4$, *E. coli* minimal medium (M63 salts) supplemented with 0.2% (w/v) glucose and 0.5% (w/v) casamino acids ($M63^+$). Unless specified otherwise, the standard growth medium for *P. aeruginosa* was 1% mucin (w/v) in PMM. Mucins were dissolved in the medium by gentle shaking overnight at 4°C.

Constructions of deletion mutants and GFP-labeled strains

Deletions in *P. aeruginosa* strains were obtained using Splicing Over Extension (SOE)-PCR, as described previously [31], and confirmed by PCR. In addition, the inability of the strains Δ*flgE,* Δ*flgK,* Δ*fliD* to swim and swarm, and the incapacity of Δ*pilB* to twitch, was tested as described previously [32]. To facilitate microscopy, we expressed GFP constitutively in each strain. GFP expressing strains were created as described previously [33]. Strains from the PA14 background used in Figure 4.4H-J that express GFP were grown in the presence of carbenicillin (250 μg/ml) as described in [34]. *E. coli* Δ*fliC* was generated using P1 phage transduction [35] from strain JW1908-1 obtained from the Keio collection (Coli Genetic Stock Center) into the

ZK2686 background. Deletion of *fliC* was confirmed by PCR and motility agar assay.

Generation of complementation plasmids

A complementation plasmid containing the *flgE* gene was created using the plasmid pMQ80 [36]. Briefly, the *GFP* gene was removed from the plasmid via restriction enzyme digestion with EcoRI and HindIII. The *flgE* gene was amplified from *P. aeruginosa* PAO1 genomic DNA with primers containing EcoRI and HindIII restriction sites upstream and downstream of *flgE* respectively. After digestion, the *flgE* gene was inserted into the plasmid using T4 DNA ligase. For control plasmids, pMQ80 was treated with Klenow polymerase and blunt end-ligated without an insert. The plasmids were transformed [37] into *E. coli* DH5α cells and plated on LB agar containing 30 μg/mL gentamicin selective media. Resulting colonies were inoculated into overnight cultures and the plasmids were extracted using the GenElute™ Plasmid Miniprep Kit (Sigma Aldrich). The plasmids were transformed into PAO1 strains plated on LB agar plates containing 50 μg/mL gentamicin. Successful transformants were again transformed with the plasmid pSMC21 [34], a constitutive GFP expressing plasmid, to facilitate observation of floc formation (note: the fluorescent strains used in the rest of the study are gentamicin resistant and could not be used with pMQ80 which relies on gentamicin selection). Transformants were selected on LB agar containing 400 μg/mL carbenicillin and 50 μg/mL gentamicin. Floc formation in mucin was performed as described in the main text, with the addition of antibiotics (carbenicillin for GFP expression and gentamicin for complementation plasmids) and 100 mM arabinose to induce pMQ80 complementation vector expression.

Strains and	**Description**	**Reference or**

plasmids		**source**
E.coli		
DH10B	F⁻ *endA1 recA1 galE15 galK16 nupG rps*L Δ*lacX74* Φ80*lacZ*ΔM15 *araD*139 Δ(*ara,leu*)7697 *mcrA* Δ(*mrr-hsd*RMS-*mcr*BC) λ⁻	Invitrogen
SM10 λpir	Km^r, *thi*-1, *thr*, *leu*, *tonA*, *lacY*, *supE*, *recA*::RP4-2-Tc::Mu, *pir*+ pUX-BF13 (Ap^r- Tn7 helper)	[33]
S17-1 λpir	Tp^r Sm^r *recA*, *thi*, *pro*, *hsdR*-M$^+$RP4: 2-Tc:Mu: Km Tn7 λpir	Mark Silby
S17-1 λpir + *gfp*	Tp^r Sm^r *recA*, *thi*, *pro*, *hsdR*-M$^+$RP4: 2-Tc:Mu: Km Tn7 λpir + pBKminiTn7-Gm/Cm-*gfp*	Wook Kim
ZK2686	W3110, Δ(*arg*F-*lac*) U169	[38]
JW1908-1	BW25113, F-, Δ(*ara*D-*ara*B)567, Δ*lac*Z4787(::*rrn*B-3), λ-, Δ*fli*C769::kan, rph-1, Δ(*rha*D-*rha*B)568, *hsd*R514	CGSC
Δ*fliC*	ZK2686, Δ*fli*C769::kan	This Study
P. aeruginosa		
PAO1	wild type, clinical isolate	[39]
Δ*flgE*	PAO1-Δ*flg*E	This study
Δ*fliD*	PAO1-Δ*fli*D	"
Δ*flgK*	PAO1-Δ*flg*K	"
Δ*pilB*	PAO1-Δ*pil*B	"
Δ*flgE* Δ*pilB*	PAO1-Δ*flg*E Δ*pil*B	"
Δ*algD*	PAO1-Δ*algD*	[17], DJ Wozniak
WFPA800	PAO1-Δ*psl*	[13], DJ Wozniak
Δ*algD* Δ*flgE*	PAO1-Δ*algD* Δ*flg*E	This study
Δ*psl* Δ*flgE*	PAO1-Δ*psl* Δ*flg*E	This study
PA14	wild type, clinical isolate + pSMC21	[34]
PA14- Δ*flgK*	PA14-Δ*flgK* + pSMC21	"
PA14- Δ*motAB* Δ*motCD*	PA14- Δ*motAB* Δ*motCD* + pSMC21	"
Plasmids		
pMQ30	pEX18Gm + CENURA, Gm^r, allelic replacement vector	[40]
pBKminiTn7-	Gm^r, Cm^r, transposon delivery plasmid	[33]

Gm/Cm-*gfp*		
pSMC21	Ap^r, Kan^r, $Carb^r$, plasmid containing GFP under the control of P_{tac} constitutive promoter	[34]
pMQ80	Complementation plasmid, GmR	[36], GA O'Toole
pMQflgE	Complementation plasmid containing flgE	This study

Table 4.1. List of strains and plasmids used in this chapter. CGSC, Coli Genetic Stock Center (Yale)

Motility Assay

M63 motility plates supplemented with 0.2% glucose, 1 mM $MgSO_4$ and 0.5% casamino acids were created as described previously [41]. To induce expression from the complementation plasmid, 100 mM arabinose was added to the plates. Wooden inoculation sticks were dipped into overnight cultures of the strains being tested and used to stab the center of the motility plates. The plates were incubated overnight (16 h) at 30°C.

Particle tracking

Exponential phase cells were loaded into chambers for visualization. The chambers were constructed with glass microscope slides and coverslips treated with O_2 plasma for 5 min. Coverslips were adhered to slides using double-sided tape, forming chambers approximately 8 mm wide, 18 mm long and 60 μm tall. Once the chambers were filled, they were sealed with silicone vacuum grease to prevent evaporation. Four videos of 20 s each were acquired within 5 min of loading of the chamber. Videos were analyzed in ImageJ using the Mosaic particle tracking plugin [42].

Floc size measurements

To observe cells growing in mucins, cells from exponential growth phase were added to a 1% mucin gel so that the final concentration was 50-100 cells μL^{-1}. The mix was placed in a 96-well glass bottom plate (MatTek) and incubated at 37°C for 20 h. Images were taken immediately after incubation using an Axiovert 200M (Zeiss). To quantify the dimensions of each colony in a given picture, we used the software ImageJ. We first subtracted the background using the rolling ball algorithm. The image was then thresholded using an iterative procedure based on the isodata algorithm. We defined a group of cells as a floc when it was composed of at least 2-3 cells. Analysis with Minitab 16 (Minitab Inc.) showed that the data were not normally distributed. We therefore plotted the data using box-plots to provide an unbiased overview of the distribution of the floc sizes for each condition. Four pictures from three independent experiments were analyzed for each strain.

Statistical Analysis

Values are reported in the text as value ± SEM. For statistical comparisons between groups with approximately normal distributions, the Student's two-tailed t-test was used. Error bars in figures are either standard deviation or SEM, as indicated in the legends.

BIBLIOGRAPHY

1. Johansson M, Phillipson M, Petersson J, et al. (2008) The inner of the two Muc2 mucin-dependent mucus layers in colon is devoid of bacteria. Proc Natl Acad Sci U S A 105:15064–15069.

2. Morita H, Kettlewell MG, Jewell DP, Kent PW (1993) Glycosylation and sulphation of colonic mucus glycoproteins in patients with ulcerative colitis and in healthy subjects. Gut 34:926–932.

3. Strugala V, Dettmar PW, Pearson JP (2008) Thickness and continuity of the adherent colonic mucus barrier in active and quiescent ulcerative colitis and Crohn's disease. Int J Clin Pract 62:762–769.

4. Venables CW (1986) Mucus, pepsin, and peptic ulcer. Gut 27:233–238.

5. Crater JS, Carrier RL (2010) Barrier Properties of Gastrointestinal Mucus to Nanoparticle Transport. Macromol Biosci 10:1473–1483.

6. Kocevar-Nared J, Kristl J, Smid-Korbar J (1997) Comparative rheological investigation of crude gastric mucin and natural gastric mucus. Biomaterials 18:677–681.

7. Schade C, Flemström G, Holm L (1994) Hydrogen ion concentration in the mucus layer on top of acid-stimulated and -inhibited rat gastric mucosa. Gastroenterology 107:180–188.

8. Kirkham S, Sheehan J, Knight D, et al. (2002) Heterogeneity of airways mucus: variations in the amounts and glycoforms of the major oligomeric mucins MUC5AC and MUC5B. Biochem J 361:537–546.

9. Banerjee I, Pangule RC, Kane RS (2011) Antifouling Coatings: Recent Developments in the Design of Surfaces That Prevent Fouling by Proteins, Bacteria, and Marine Organisms. Adv Mater 23:690–718.

10. Mahenthiralingam E, Campbell M, Speert DP (1994) Nonmotility and phagocytic resistance of Pseudomonas aeruginosa isolates from chronically colonized patients with cystic fibrosis. Infect Immun 62:596–605.

11. Friedman L, Kolter R (2004) Two genetic loci produce distinct carbohydrate-rich structural components of the Pseudomonas aeruginosa biofilm matrix. J Bacteriol 186:4457–4465.

12. Arora S, Ritchings B, Almira E, et al. (1998) The Pseudomonas aeruginosa flagellar cap protein, FliD, is responsible for mucin adhesion. Infect Immun 66:1000.

13. Ma L, Jackson KD, Landry RM, et al. (2006) Analysis of Pseudomonas aeruginosa conditional psl variants reveals roles for the psl polysaccharide in adhesion and maintaining biofilm structure postattachment. J Bacteriol 188:8213–8221.

14. Wozniak DJ, Wyckoff TJO, Starkey M, et al. (2003) Alginate is not a significant component of the extracellular polysaccharide matrix of PA14 and PAO1 Pseudomonas aeruginosa biofilms. Proc Natl Acad Sci U S A 100:7907–7912.

15. Hentzer M, Teitzel GM, Balzer GJ, et al. (2001) Alginate overproduction affects Pseudomonas aeruginosa biofilm structure and function. J Bacteriol 183:5395–5401.

16. Stapper AP, Narasimhan G, Ohman DE, et al. (2004) Alginate production affects Pseudomonas aeruginosa biofilm development and architecture, but is not essential for biofilm formation. J Med Microbiol 53:679–690.

17. Whitchurch CB, Erova TE, Emery JA, et al. (2002) Phosphorylation of the Pseudomonas aeruginosa response regulator AlgR is essential for type IV fimbria-mediated twitching motility. J Bacteriol 184:4544–4554.

18. Moreau-Marquis S, Stanton BA, O'Toole GA (2008) Pseudomonas aeruginosa biofilm formation in the cystic fibrosis airway. Pulm Pharmacol Ther 21:595–599.

19. Connell J, Wessel A, Parsek M, et al. (2010) Probing prokaryotic social behaviors with bacterial "lobster traps."MBio 1:

20. Josenhans C, Suerbaum S (2002) The role of motility as a virulence factor in bacteria. Int J Med Microbiol 291:605–614.

21. Lee A, O'rourke J, Barrington P, Trust T (1986) Mucus colonization as a determinant of pathogenicity in intestinal infection by Campylobacter jejuni: a mouse cecal model. Infect Immun 51:536–546.

22. Yeung ATY, Parayno A, Hancock REW (2012) Mucin Promotes Rapid Surface Motility in Pseudomonas aeruginosa. MBio. doi: 10.1128/mBio.00073-12

23. Vishwanath S, Ramphal R (1984) Adherence of Pseudomonas aeruginosa to human tracheobronchial mucin. Infect Immun 45:197–202.

24. Landry RM, An D, Hupp JT, et al. (2006) Mucin–Pseudomonas aeruginosa interactions promote biofilm formation and antibiotic resistance. Mol Microbiol 59:142–151.

25. Ambort D, Johansson MEV, Johansson M, et al. (2012) Calcium and pH-dependent packing and release of the gel-forming MUC2 mucin. Proceedings of the National Academy of Sciences 109:5645–5650.

26. Berg H, Turner L (1979) Movement of microorganisms in viscous environments. Nature 278:249–251.

27. Turner B, Bansil R, Afdhal N (2007) Expression of cysteine-rich C-terminal domains of pig gastric mucin in Pichia pastoris. FASEB J.

28. Celli J, Gregor B, Turner B, et al. (2005) Viscoelastic properties and dynamics of porcine gastric mucin. Biomacromolecules 6:1329–1333.

29. Lieleg O, Lieleg C, Bloom J, et al. (2012) Mucin biopolymers as broad-spectrum antiviral agents. Biomacromolecules 13:1724–1732.

30. Yates JR 3rd, Eng JK, McCormack AL, Schieltz D (1995) Method to correlate tandem mass spectra of modified peptides to amino acid sequences in the protein database. Anal Chem 67:1426–1436.

31. Schweizer HP (1992) Allelic exchange in Pseudomonas aeruginosa using novel ColE1-type vectors and a family of cassettes containing a portable oriT and the counter-selectable Bacillus subtilis sacB marker. Mol Microbiol 6:1195–1204.

32. O'toole G, Kolter R (1998) Flagellar and twitching motility are necessary for Pseudomonas aeruginosa biofilm development. Mol Microbiol 30:295–304.

33. Lambertsen L, Sternberg C (2004) Mini- Tn7 transposons for site- specific tagging of bacteria with fluorescent proteins. Environmentalist

34. Amiel E, Lovewell R, O'Toole G, et al. (2010) Pseudomonas aeruginosa Evasion of Phagocytosis Is Mediated by Loss of Swimming Motility and Is Independent of Flagellum Expression. Infect Immun 78:2937–2945.

35. Thomason L, Costantino N, Court D (2007) E. coli genome manipulation by P1 transduction. Curr Protoc Mol Biol Chapter 1:Unit 1.17.

36. Shanks RMQ, Caiazza NC, Hinsa SM, et al. (2006) Saccharomyces cerevisiae-based molecular tool kit for manipulation of genes from gram-negative bacteria. Appl Environ Microbiol 72:5027–5036.

37. Choi K-H, Kumar A, Schweizer HP (2006) A 10-min method for preparation of highly electrocompetent Pseudomonas aeruginosa cells: Application for DNA fragment transfer between chromosomes and plasmid transformation. J Microbiol Methods 64:391–397.

38. Danese P, Pratt L, Dove S, Kolter R (2000) The outer membrane protein, Antigen 43, mediates cell- to- cell interactions within Escherichia coli biofilms. Mol Microbiol 37:424–432.

39. Holloway BW (1955) Genetic recombination in Pseudomonas aeruginosa. J Gen Microbiol 13:572–581.

40. Hoang T, Karkhoff-Schweizer R, Kutchma A (1998) A broad-host-range Flp- FRT recombination system for site-specific excision of chromosomally-located DNA sequences: application for isolation of unmarked< .... Gene

41. O'Toole GA, Kolter R (1998) Initiation of biofilm formation in Pseudomonas fluorescens WCS365 proceeds via multiple, convergent signalling pathways: a genetic analysis. Mol Microbiol 28:449–461.

42. Sbalzarini IF, Koumoutsakos P (2005) Feature point tracking and trajectory analysis for video imaging in cell biology. J Struct Biol 151:182–195.

Chapter 5

Paths for future study

Collaborator: Nicolas Vogel

Section 1: *Escherichia coli* flagellar diversity and its relation to surface adhesion

INTRODUCTION

We have shown that *Escherichia coli* cells can adhere to topographically patterned substrates, and they can do this particularly well when aided by their flagella (Chapter 2). Furthermore, we have shown that flagella are most helpful in aiding adhesion to hydrophobic surfaces and may even impede adhesion to hydrophilic surfaces (Chapter 3). This work was carried out using the laboratory strain K12 ZK2686, but we were interested to determine whether these findings were true for other strains as well, and whether this was a broader phenomenon. Interestingly, *E. coli* is a very diverse species in terms of the genetic variation across strains. In fact, only approximately 20% of the genome of a typical *E. coli* strain will be shared as part of the core *E. coli* genome [1]. There are numerous classification schemes for the various strains of *E. coli*, which are typically related to their effects on mammalian hosts. One classification scheme is based on whether the strains are enterohemorrhagic, uropathogenic or enteroinvasive [2]. Another widely used and more specific scheme uses the surface antigens of *E. coli* to classify them based on serotype—i.e., what antibodies are generated by the host in response to these strains. Typically, the O, K and H antigens are used for classifying *E. coli*. The O antigen is a repeating oligosaccharide that forms the outermost part of the lipopolysaccharide surface coating of the cell [3, 4]. The K antigen refers to the cell capsule or in some cases, fimbriae on

the surface of the cell [3]. Finally, the H antigen is flagellin, which is a prominent external feature of the *E. coli* [4].

Because our work focuses on flagella-surface interactions, we chose to focus on flagellar diversity in *E. coli*, as defined by H antigen. Due to the flagellar diversity within the *E. coli*, this H antigen system enables comparisons of different strains of *E. coli* entirely based on their flagella isoforms. There are 53 known H antigens, numbered H1 through H56 (the H13, H22 and H50 designations are not in use). Together, these represent a large diversity of flagellar isoforms. Since these forms are defined by serology, it is their outward-facing components that define the serotype, as these portions act as the epitopes for antibody binding. Importantly, it is these same segments that we might expect to have the most prominent effect on surface binding of flagella, since these are the parts that would interact with environmental interfaces. For this reason, it is reasonable to choose a range of *E. coli* strains with varying H serotypes in order to compare their adhesive properties.

We first wanted to reduce the total number of H antigens to compare, so as to have a tractable set of experiments and data. Because our main concern is surface properties of the various H antigens, we were interested in grouping these various types in a logical manner, so as to capture their diversity, but also to consolidate similar H antigens into groups. Fortunately, in 1977 A. M. Lawn published a system of classification of flagella that divided them into groups by morphotype (Figure 5.1) [5]. Using meticulous and methodical preparation and imaging on TEM, Lawn was able to detect certain similarities among various flagellar serotypes based on the surface texture of flagellar filaments. He divided these into six groups, labeled A through F. Furthermore, for each morphotype A through F, representative serotypes H4, H5, H48, H21,

H12, and H46 were chosen. For our experiments, we decided to work with these representative serotypes, selecting the standard reference strain for each.

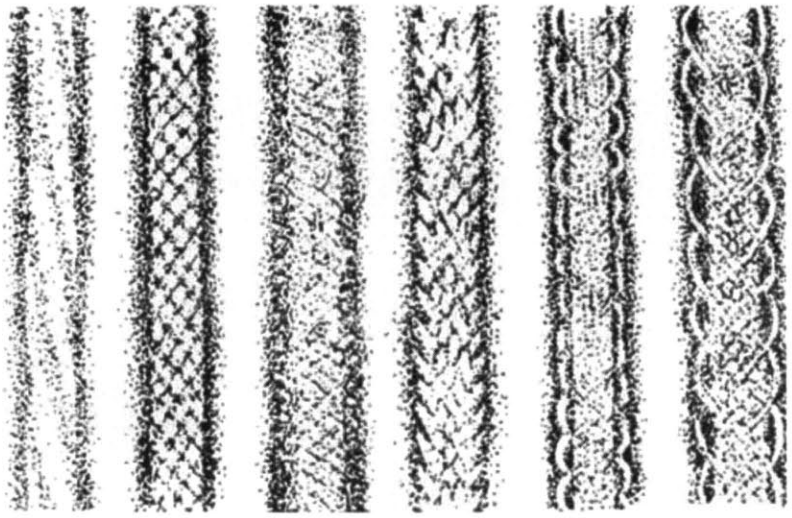

Fig. 1. Diagrams representing the surface structure of the six principal morphotypes.

Morpho-type	Description of morphotype	No. of serotypes	Representative serotype	Diam. of flagella (nm)	Mol. wt of flagellin
A	Thin, long pitch helix pattern	2	H4	19	37000
B	Thin, subunit pattern	8	H5	20	46000
C	Rough subunit pattern	7	H48	23	—
D	Polar subunit pattern	5	H21	22	56000
E	Short pitch loop pattern	8	H12	22	62000
F	Long pitch loop pattern	15	H46	24	56000

Figure 5.1. H antigen diversity. The 53 known H antigens can be classified by morphotype. This was first proposed in 1977, with the creation of six distinct morphotypes from the known H antigens. Each morphotype is drawn to reflect the key features. Representative serotypes are indicated for each morphotype. Figure adapted from Lawn *et al.*, 1977 [5].

In order to compare adhesive properties of our chosen H antigens, we wanted to isolate the H antigen as a single variable in the context of a complex biological system (*E. coli*). Each H antigen has a representative serotype that we wished to use; however these various type-strains of *E. coli* were isolated from sources ranging from human urine (H21) to chicken feces (H46). Making comparisons across these strains is difficult due to the genetic and phenotypic variation among them. Therefore, our strategy was to isolate the flagellin genes from representative

strains corresponding to each morphotype identified by Lawn in his original description. Briefly, we cloned each flagellin gene into a plasmid under control of the native ZK2686 *fliC* promoter and then transformed a ZK2686 Δ*fliC* strain (RSF77) in order to create directly comparable transgenic strains (Figure 5.2). To make comparisons with our previous work, we chose to use strain ZK2686 as our genetic background for these experiments.

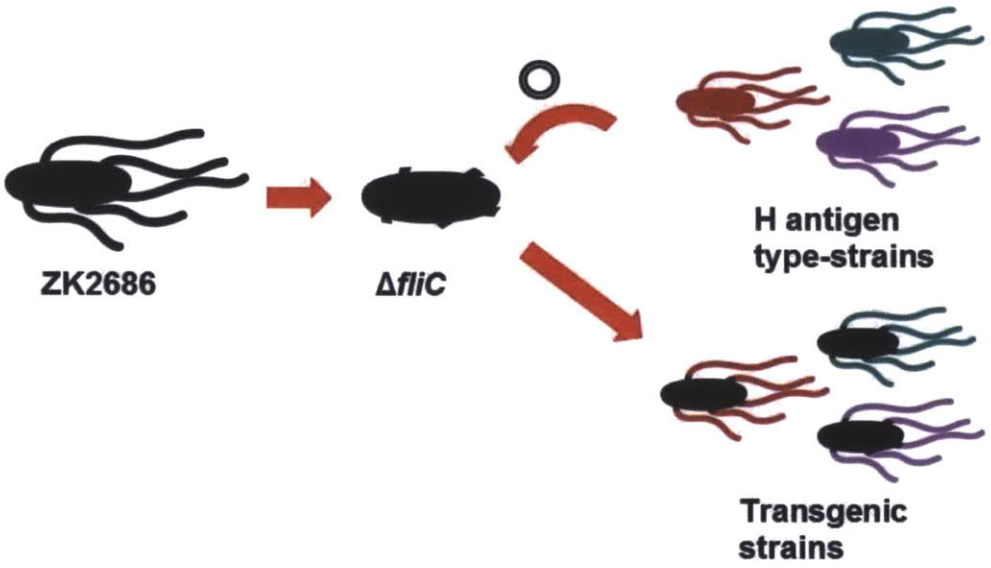

Figure 5.2. Schematic of strategy for comparison of H antigens in adhesion. Using strain ZK2686 as our working strain, we can eliminate its native *fliC* gene and then introduce plasmids bearing the *fliC* genetic sequences encoding H antigens from various H antigen type-strains. If these genes are controlled under the same promoter, comparisons can be made between H antigens expressed in the same genetic background, eliminating genetic variation among the various type-strains themselves.

PRELIMINARY RESULTS AND DISCUSSION

We first aimed to generate plasmids containing *fliC* genes from each of the representative serotypes for each morphotype. To do this, we obtained the type-strains for each representative serotype and created PCR primers to amplify their *fliC* genes. Fortunately, the *fliC* genes for each of these strains have been sequenced, so we aligned the amino acid sequences of H48, H21,

H46, H12 and H4 strains (Figure 5.3). Notably, the N-terminal and C-terminal regions of these sequences are highly conserved across the different strains. As has been previously noted, much of the antigenic diversity among the H antigens results from the central region. The N-terminal, central and C-terminal regions have been named the conserved (C) 1, variable (V) and C2 regions, respectively [4]. The C1 and C2 regions form the central, interior-facing domain of the fliC protein, while the V region forms the exterior-facing domains. For this reason, it is accepted that the high variability of the V region aids in immune evasion, while the conserved central region is required for flagellar structure. The conserved regions allowed us to generate a single primer pair for amplification of the *fliC* genes. Genes encoding for flagella from several H antigen type-strains, including Bi316-42, 5306-56, 323-59 and ZK2686 were PCR-amplified and each inserted into a plasmid under control of the native *fliC* promoter. The resultant expression vector was then used to transform strain RSF77, which has a *fliC* deletion.

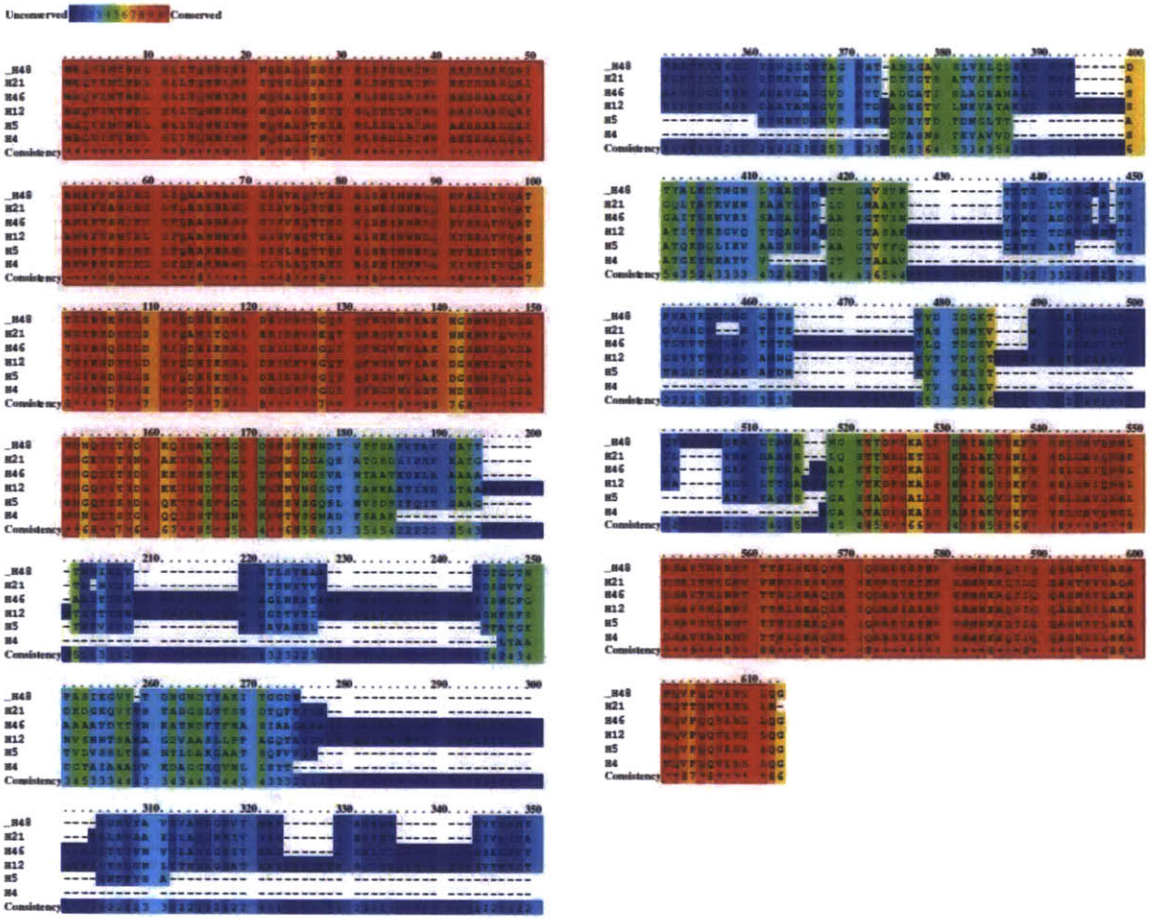

Figure 5.3. Alignment of selected *E. coli* H antigen fliC amino acid sequences. Shown are the alignments of amino acids sequences for H48, H21, H46, H12, H5 and H4. Red areas are maximally conserved and blue areas are not conserved. Clearly, the sequences closest to the N- and C- termini are most conserved. The central sequences vary and are responsible for antigenic diversity.

Once the strains were confirmed to have taken up the plasmid, they were characterized for motility using phase contrast microscopy and motility agar plates (Figure 5.4). These assays indicated that the transgenic strains do express flagella and are motile. Of note, these strains appear to be less motile than the wild-type. This may be due to the presence of antibiotics, as these strains must be grown under constant selection to avoid loss of the plasmid.

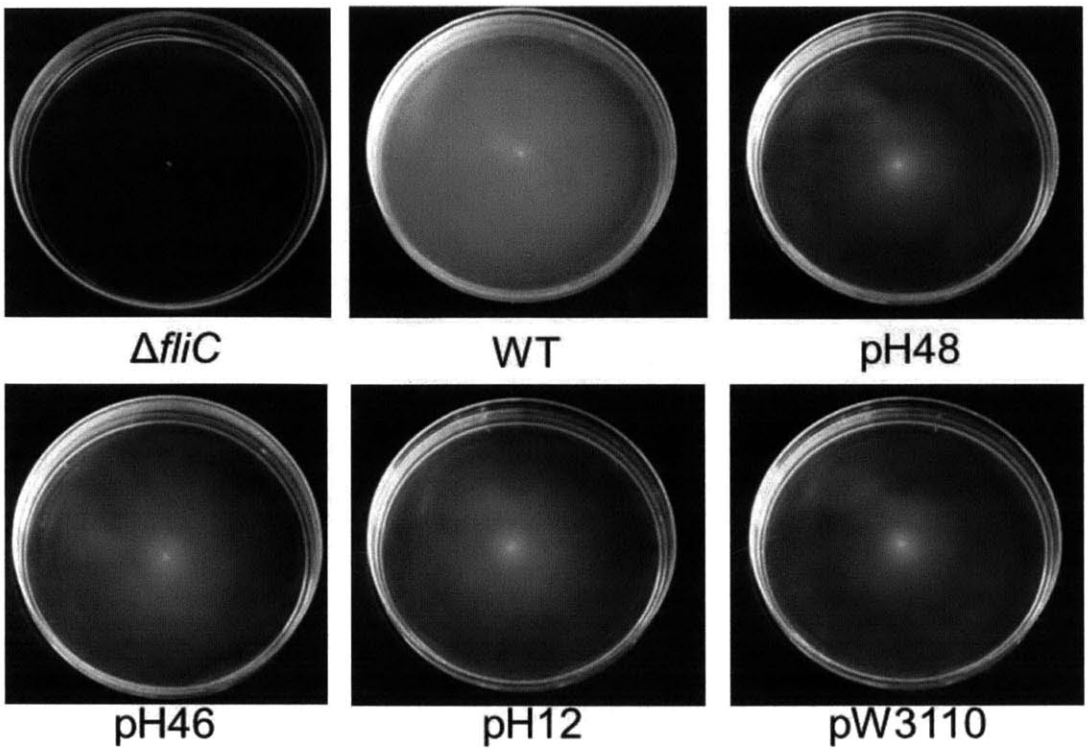

Figure 5.4. Motility of Δ*fliC*, WT, and Δ*fliC E. coli* bearing plasmid-encoded H antigens. Motility agar plates are shown photographed after overnight incubation.

To determine whether the transgenic strains were growing at similar rates, we generated growth curves for each, with and without kanamycin (Figure 5.5). While the strains expressing H46 and H48 grew at rates similar to wild type, the strains expressing H12 and the wild-type flagellin were slower to begin exponential phase. Furthermore, in the presence of kanamycin, all strains except RSF162 (expressing H48) grew more slowly, in many cases not entering exponential phase until 8-10 h after inoculation. In order to have strains grow at similar rates for comparison, larger inocula tended to reduce the lag period; however this requirement makes experimental comparisons more difficult. For future experiments involving transgenic expression of flagella and studies of cell adhesion, an approach that integrates the genes into the chromosome is likely to provide a more satisfactory result.

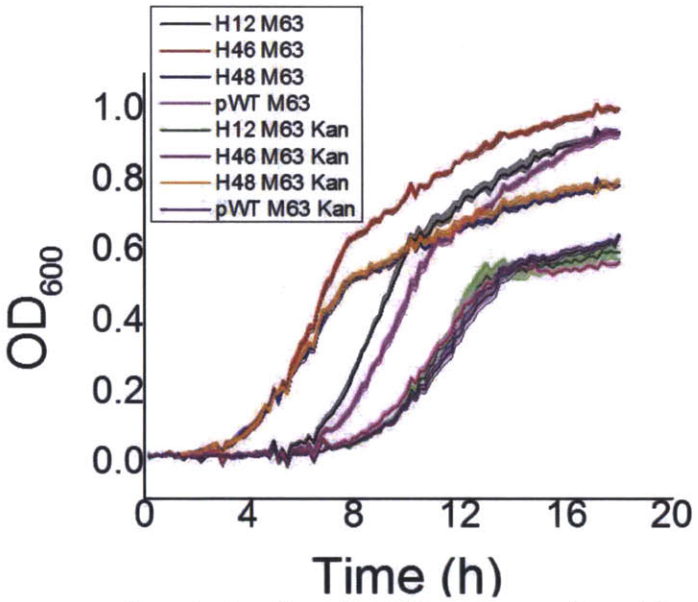

Figure 5.5. Growth curves for strains bearing H antigen plasmids. Strains were grown in M63 medium either with or without kanamycin (plasmid selection). OD_{600} was measured over the course of 18 h. Shaded areas correspond to the standard deviation of 3-4 growth curves.

Using the strains that express H12 and H46, we could purify their flagella for future studies using QCM, similar to those done in Chapter 3. We purified the flagella from each of these strains and confirmed that they were of the expected molecular weight and purity using SDS-PAGE (Figure 5.6). Our yield was somewhat lower for these transgenic strains than for the original ZK2686 flagella purification. This may be related to our observed differences in motility, perhaps due to reduced or delayed expression of flagella. Nonetheless, microscopic observations during purification indicated that cells were highly motile.

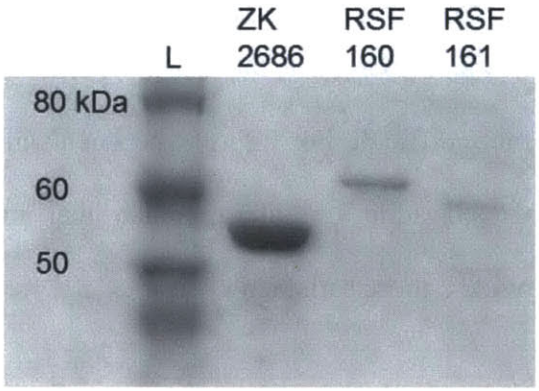

Fig. 5.6. SDS-PAGE of purified fliC from the strains indicated. Gel is stained with Coomassie blue.

We also carried out preliminary flow studies of these flagella isotypes on QCM-D. The H12 and H46 flagella have notably different surface textures, compared with each other and with the original H48 form studied in Chapter 3. Unsurprisingly, the pattern of adhesion to mixed thiol SAMs on quartz crystals is somewhat different than that seen for H48 flagella from ZK2686. As in Chapter 3, we used mixtures of 11-mercapto-1-undecanol and dodecanethiol to achieve a range of hydrophobicities. The overall quantity of flagella adhered to SAM surfaces was similar for all surfaces, as indicated by resonant frequency change of the quartz crystals, ranging from -30 to -50 Hz for both H12 and H46 flagella (Figure 5.7A,B). The most hydrophilic surface did have the lowest adhesion, and the maximum adhesion was seen at intermediate hydrophobicities. Unlike the H48 flagella, the most hydrophobic surfaces did not have the largest frequency changes.

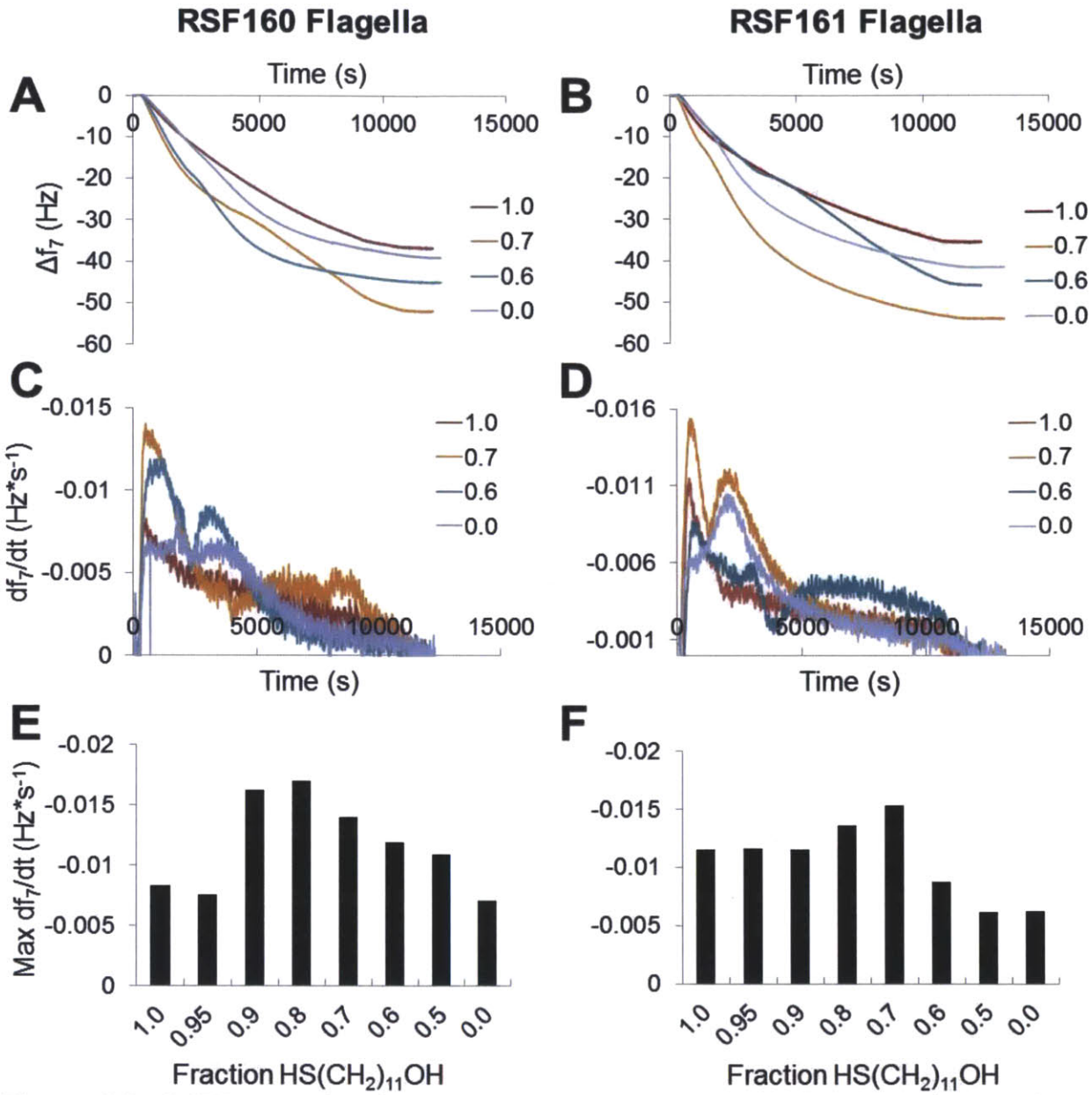

Figure 5.7. QCM analysis of H12 and H46 flagella. (*A*,*B*) Frequency change of QCM resonance (7th overtone) during flow of isolated flagella. Mole fraction 11-mercapto-1-undecanol for each SAM (as in *A*) is indicated for each trace in the legend. (*C*,*D*) Rate of change of QCM resonance frequency during flow of flagella over surface. Molar fraction 11-mercapto-1-undecanol for each SAM is indicated for each trace in the legend. Traces of corresponding colors in each column are from the same experiments. (*E*,*F*) The maximum rate of adhesion of flagella, taken from the first 2000 s of each experiment (i.e. the heights of the initial peaks) for each SAM tested.

When we examined rate of adhesion by taking the time-derivative of frequency change, more complex patterns emerged (Figure 5.7C,D). For both H12 and H46 flagella, the highest rate

of adhesion was observed at intermediate hydrophobicities, corresponding to molar fractions of 0.8 and 0.7 of 11-mercapto-1-undecanol, respectively, in the thiol mixture used to assemble SAMs (Figure 7E,F). Notably, for the most hydrophilic surfaces, we see a simple peak and decay in adhesion rate. As hydrophobicity increases, we begin to see a secondary peak in adhesion rate, which may correspond to a different mode of adhesion and/or a conformational change of adherent flagella. As hydrophobicity increases further, the initial peak is reduced and the later, secondary peak becomes dominant. We may interpret this to mean that there are different domains of the flagellar filaments that preferentially adhere to surfaces of different hydrophobicities. Further study is required to elucidate the underlying mechanism of adhesion.

FUTURE WORK

As noted earlier, the varying growth rates of the transgenic strains make direct comparisons of adhesion difficult. Because we typically inoculate cells in a bath where a surface of interest is immersed, long-term experiments allow cells to grow and adhere. When growth rates are not similar, the number of cells on the surface cannot be compared, as the total number of cells is different. There are ways of accounting for this, including changing the inoculum size, or normalizing adhered cells by total cell number at the time of measurement. However, there are other more complex effects that result from these differences that cannot all be accounted for, such as varying metabolite and nutrient concentrations. Because of this and the fact that antibiotics must be used with our transgenic strains, it is more desirable to generate strains that have genomically integrated *fliC* genes encoding the various flagellar morphotypes. We suggest that generating new strains in this manner will improve the growth curves and enable better comparisons with valid conclusions. We anticipate that such strains can be used to measure

adhesion to SAMs of varying hydrophobicities. This will enable correlation with QCM data and comparisons among the different H antigens for their adhesive properties.

Based on our preliminary QCM results, further investigation of the mechanisms of flagellar adhesion are warranted. One analysis should involve TEM of the purified flagella to enable observation of the surface texture and conformation of the the flagellar filaments. This will allow confirmation that the purified forms are similar to those reported in the literature. It will also enable confirmation that they are in filamentous form. To study modes of adhesion, liquid atomic force microscopy could be used to image flagella after adhesion to hydrophobic, hydrophilic and intermediate surfaces. This would enable observation of the final state of adhesion of the different flagella forms on different surfaces, while maintaining the flagella in a hydrated state. To study and visualize adhesion of the filaments as it happens, we propose using total internal reflection fluorescence (TIRF) microscopy. Purified filaments could be stained using Alexa fluor succinimidyl esters and then column purified to remove excess dye. These fluorescent filaments can be visualized by fluorescence microscopy. By assembling hydrophobic or hydrophilic SAMs on coverglass using silane chemistry, we can generate transparent surfaces suitable for TIRF measurements. Essentially, since TIRF microscopy relies on evanescent waves to illuminate only within approximately 100 nm of the surface, the process of adhesion could be observed as it happens. As filaments approach and attach to the surface, only the adherent and adjacent portions of the flagellar filaments will be excited and emit light that can be detected. Since filaments are several microns long, this will enable the observation of adhesion dynamics. For example, if the tip of a flagellum first adheres, and then the rest of the filament follows, we would observe a dot at the surface, followed by the whole filament. We expect that TIRF could be a powerful tool for studying adhesion dynamics in this system.

Finally, to begin to draw broader conclusions about flagellar adhesion, we would ideally complete measurements on all flagellar morphotypes. This would require the additional cloning of H4, H5 and H21 *fliC* and insertion into the ZK2686 background. As can be seen in Figure 5.9B, not all *fliC* genes could be PCR-amplified, so this would first need to be overcome. If the full complement of flagellar morphotypes could be analyzed in a manner similar to what was done in Chapter 3, adhesive properties could be related to structure and general conclusions about the role of flagella in surface adhesion of *E. coli* could be made. Furthermore, if basic principles relating flagellar properties to surface adhesion can be established, it may aid in prediction of the adhesive abilities of other bacterial strains. This would improve our ability to design anti-adhesive surfaces and to anticipate the types of surface chemistry and topographies that would be most effective in repelling bacteria.

EXPERIMENTAL SECTION

Cloning of ZK2686 *fliC* promoter

To ensure similar expression of the *fliC* genes once they were introduced into the ZK2686 genetic background, we used the native promoter and introduced it into a plasmid vector to act as the promoter for all genes (Figure 5.8). We obtained pCR2.1TOPO from Life Technologies and used it as our general cloning vector (Table 5.1). The strain ZK2686 was used for the *fliC* promoter template. We used primers RF31 and RF32 (Table 5.2) to flank the promoter region for amplification. These primers flank a 270 bp region upstream of the *fliC* gene. Primer RF32 also contains an AflII restriction sequence for later steps. PCR was performed using *Taq* polymerase. The PCR product was checked on an agarose gel (Figure 5.9A) and sequenced to ensure error-free amplification. This product was cloned into a linearized vector, PCR2.1TOPO, using the TOPO TA cloning kit (Life Technologies). This vector comes with

covalently bound topoisomerase I, which enables the PCR product to ligate with the vector, creating circularized DNA. Because *Taq* polymerase naturally leaves behind a 3' overhanging adenine nucleotide, we could insert the PCR product directly into the TOPO TA cloning vector, which has complementary overhanging thymines. This plasmid, bearing the ZK2686 *fliC* promoter, was used to transform chemically competent Mach I cells (Life Technologies). Colonies were selected and grown under kanamycin selection for DNA extraction. Orientation of promoter was confirmed via restriction digest. Those plasmids in the correct orientation were sequenced to confirm error-free PCR products. After this confirmation, this plasmid, pCR2.1TOPO[p^{fliC}], was used in the next step for insertion of the various *fliC* genes.

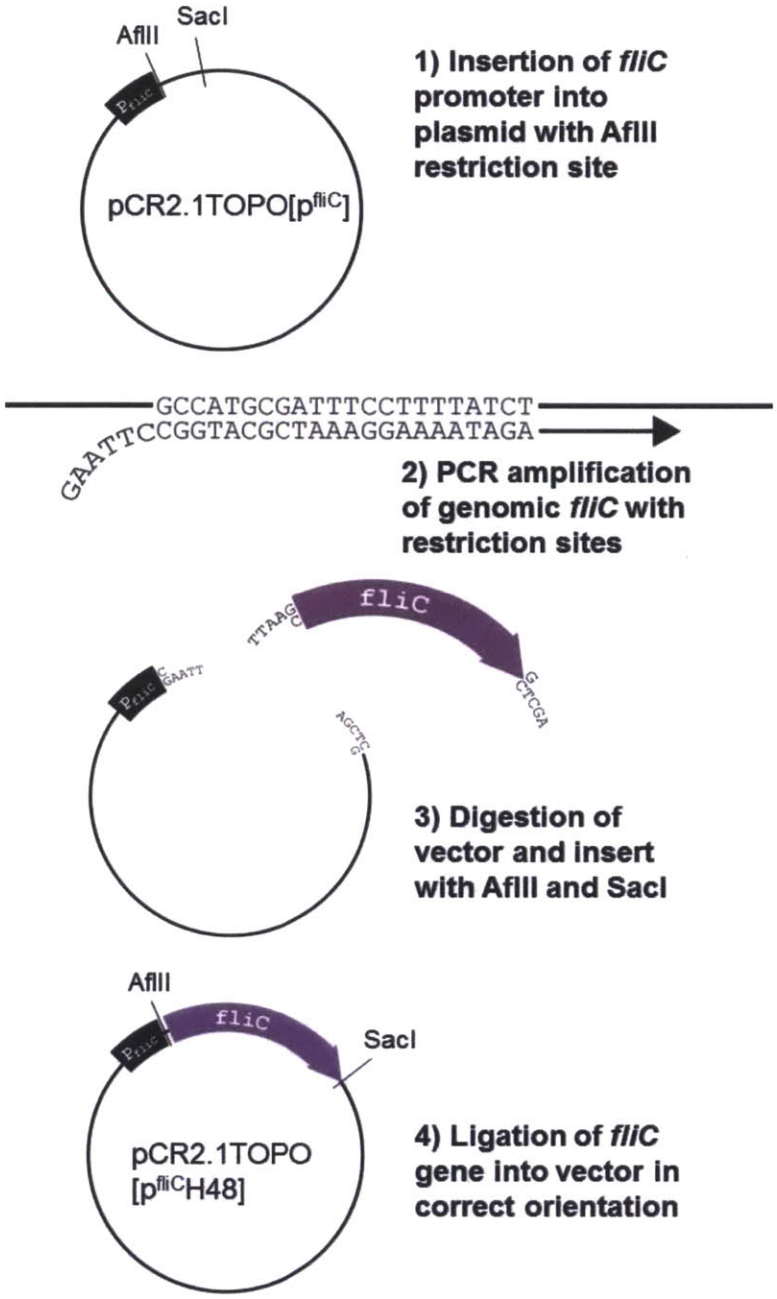

Figure 5.8. Cloning steps for creation of plasmid bearing various *fliC* genes under control of the native K12 *fliC* promoter.

Plasmid or Strain	Description	Reference or source
PLASMIDS		
pCP20	FLP+, λ cI857^{+}, λ p_R Rep^{ts}, amp^R, cam^R	[6]

pCR2.1TOPO	General cloning vector, pUC Ori, kan^R, amp^R	Life Technologies™
pCR2.1TOPO[p^{fliC}]	pCR2.1TOPO, pFliC	This study
pCR2.1TOPO[p^{fliC}H12]	pCR2.1TOPO, pFliC-H12fliC	"
pCR2.1TOPO[p^{fliC}H46]	pCR2.1TOPO, pFliC-H46fliC	"
pCR2.1TOPO[p^{fliC}H48]	pCR2.1TOPO, pFliC-H48fliC	"
pCR2.1TOPO[p^{fliC}H48-ZK2686]	pCR2.1TOPO, pFliC-ZK2686fliC	"
STRAINS		
ZK2686	W3110, Δ(*arg*F-*lac*) U169	[7]
RSF43	ZK2686, Δ*fliC769*::kan	[8]
RSF77	RSF43, kan^S	This study
Mach1™	F-, φ80(lacZ)ΔM15, ΔlacX74, hsdR(r_k^-, mk^+), ΔrecA1398, endA1, tonA	Life Technologies™
Bi316-42	O9:K9:H12, human peritonitis isolate	[5]
5306-56	O26:H46, chicken feces isolate	"
323-59	O16:H48	"
RSF152	Mach1™, pCR2.1TOPO[p^{fliC}]	This study
RSF153	Mach1™, pCR2.1TOPO[p^{fliC}H12]	"
RSF155	Mach1™, pCR2.1TOPO[p^{fliC}H46]	"
RSF156	Mach1™, pCR2.1TOPO[p^{fliC}H48]	"
RSF157	Mach1™, pCR2.1TOPO[p^{fliC}H48-ZK2686]	"
RSF160	RSF77, pCR2.1TOPO[p^{fliC}H12]	"
RSF161	RSF77, pCR2.1TOPO[p^{fliC}H46]	"
RSF162	RSF77, pCR2.1TOPO[p^{fliC}H48]	"
RSF163	RSF77, pCR2.1TOPO[p^{fliC}H48-ZK2686]	"

Table 5.1. Strains and plasmids used in this chapter. Description and sources as indicated. *kan*, kanamycin; *amp*, ampicillin; *cam*, chloramphenicol; Rep, replication.

Primer	Primer sequence (5'-3')	Description

name		
RF31	GCCATGCGATTTCCTTTTATCT	*fliC* promoter forward
RF32	CTTAAGTTATCCTATATTGCAAGTCGTTG	*fliC* promoter reverse w/ overhang containing AflII restriction site
RF33	GGCTACCTTAAGATGGCACAAGTCATTAATA CC	*fliC* forward common primer w/ overhang containing AflII restriction site
RF38	GGTATGAGCTCTTAACCCTGCAGCAGAGAC	*fliC* reverse common primer w/ overhang containing SacI restriction site

Table 5.2. DNA oligonucleotide primers used in this chapter.

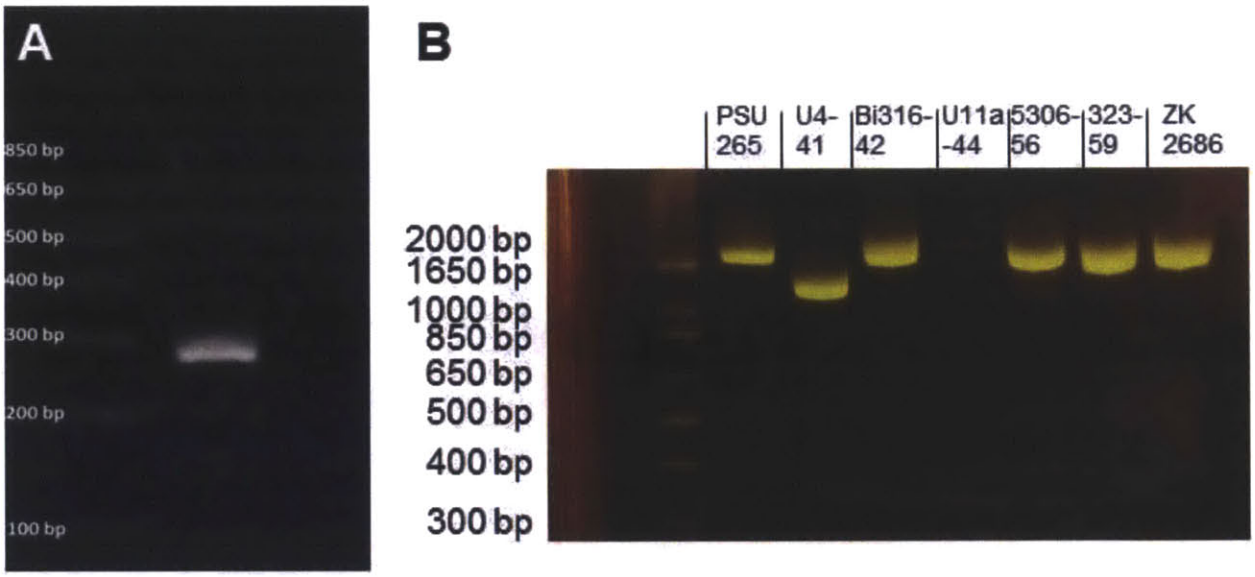

Fig. 5.9. PCR products. (*A*) PCR product of *fliC* promoter region (270 bp). (*B*) PCR product of *fliC* from several H antigen type-strains. Strains are indicated above each lane.

Cloning of *fliC* genes

We began by obtaining H antigen type-strains from J. Keen (University of Nebraska). These were first passaged on MacConkey agar. Strains Bi316-42, 5306-56, 323-59 and ZK2686 were used as sources to amplify *fliC* genes corresponding to H12, H46, H48 and H48

respectively. Because the DNA sequences are identical at either end across the different isotypes, we were able to use common primers (RF33 and RF38) to amplify the *fliC* genes of each strain. It is worth noting that the type-strains for each morphotype chosen for this study have their H antigens encoded on homologous *fliC* genes. Not all H antigens are encoded by *fliC*; some have their flagellin encoded by other genes, such as *fllA* and *flm* [9]. PCR amplification was performed on each strain, with primers providing new restriction sites for AflII and SacI. AflII provides a cloning site for the *fliC* gene adjacent to the previously cloned promoter. SacI provides a restriction site that orients the gene properly, using the unique SacI site on the PCR2.1TOPO vector. Herculase II was used as a high-fidelity polymerase to reduce error. PCR products were checked for length using an agarose gel (Figure 5.9B). These products were then digested with AflII and SacI. The pCR2.1TOPO[p^{fliC}] plasmid was also digested with AflII and SacI, and then two were then ligated using T4 DNA ligase. The ligated plasmids were then used to transform Mach I competent cells. These were grown up in Mach I cells under kanamycin selection and plasmids were isolated. The plasmids were tested for proper orientation and size using restriction digests. The correct isolates were then sequenced to ensure error-free amplification.

Creation of kanamycin-sensitive Δ*fliC* strains

We previously generated the Δ*fliC* strain RSF43 using P1*vir* phage transduction (see Chapter 2). In order to select for strains transformed with the *fliC* expression vectors, they must be grown under kanamycin selection. We therefore first needed to cure strain RSF43 of its kanamycin resistance so that it could be used as a selection agent. Because RSF43 has a kanamycin resistance gene flanked by FRT sites, we could use the Flp recombinase gene encoded by the plasmid pCP20 [6, 10] to excise the kanamycin resistance gene. RSF43 cells

were made chemically competent and transformed with pCP20 (see "Transforming *E. coli*"). We confirmed transformation by growing under ampicillin selection, as pCP20 contains an ampicillin resistance cassette. Excision of the kanamycin resistance gene was confirmed by loss of ability to grow on kanamycin selective plates. The pCP20 plasmid replicates very poorly at temperatures above 37 °C, so cells were grown overnight at 43 °C to remove the plasmid after recombination. This was confirmed by loss of resistance to ampicillin. Once kanamycin resistance was removed and cells were demonstrated to be both kanamycin and ampicillin sensitive, the strain, RSF77, could be used for introduction of new flagellin genes using our expression vectors.

Transforming *E. coli*

RSF43 and RSF77 cells were made chemically competent using the Hanahan protocol [11]. Briefly, cells to be transformed were grown to exponential phase in SOB medium containing 20 mM $MgSO_4$. Cells were centrifuged at 4 °C and washed, and then resuspended in ice-cold transformation buffer, comprised of 10 mM MES pH 6.3, 45 mM $MnCl_2$, 100 mM KCl, 3 mM hexamine cobalt chloride, and 10 mM $CaCl_2$. These cells were kept on ice and immediately transformed with the plasmid of interest.

Creation of transgenic strains expressing H antigens

The plasmids containing the various *fliC* isotypes—pCR2.1TOPO[p^{fliC}H12], pCR2.1TOPO[p^{fliC}H46], pCR2.1TOPO[p^{fliC}H48] and pCR2.1TOPO[p^{fliC}H48-ZK2686]—were used to transform chemically competent RSF77 cells (see "Transforming *E. coli*"), resulting in the creation of strains RSF160-163. The transformed cells were then examined for motility using phase-contrast microscopy and motility agar plates (Figure 5.4).

Growth curves for transgenic strains

To compare the growth rates of the transformed strains of *E. coli*, we measured growth curves for each, both in the presence and absence of antibiotics. Stationary phase cultures (from overnight growth) were inoculated at an effective optical density measured at 600 nm (OD_{600}) of 0.05 in 150 μL of medium of interest per well of a honeycomb well plate (Growth Curves USA). Plates were incubated in a Bioscreen C (Growth Curves USA) plate reader and set to shake continuously at high amplitude at 37 °C for 18 h. OD_{600} readings were taken every 10 minutes (Figure 5.5).

Purification of flagella

Methods for isolating flagella were adapted from Crawford et al., 2010 and Erdem et al., 2007 [12, 13]. Flagella from strains RSF160 and RSF161 were purified as described in Chapter 3. Once purified, flagella were denatured in SDS buffer and run on SDS-PAGE (Figure 5.6).

QCM-D

QCM-D was carried out as described in Chapter 3. In this case, H12 and H46 purified flagella were used.

Section 2: Structured, coated surfaces for the prevention of bacterial adhesion: explorations and future work

INTRODUCTION

By studying the role of flagella in adhesion and examining how hydrophobicity affects flagella- and bacteria-surface interactions, we have established some principles by which to begin designing antibacterial surfaces. We can test some of our basic findings by building substrates that should exploit these principles to reduce adhesion. In Chapter 2, we showed that flagella improved adhesion of *E. coli* to topographically patterned surfaces [8]. The flagella enabled cells to make surface contacts where the cell body could not fit, thus improving the available surface to which the cells could anchor. This work also demonstrated that Cassie-state surfaces could be rapidly forced into the Wenzel state by the action of motile bacteria, thus reducing the effectiveness of superhydrophobic antiadhesive strategies. It is encouraging that cells had a reduction in overall adhesion while the surface remained in the Cassie state, indicating that when flagella could not make contact with the inter-post crevices, the geometric arrangement of the surface was advantageous for reducing adhesion.

The above work was followed up by studies that indicated that flagella could bind well to hydrophobic surfaces, but not hydrophilic ones (Chapter 3). This is consistent with the observations in Chapter 2, since the test substrates were made of PDMS, which is hydrophobic. We also found that once flagella were deleted, the cell bodies could better adhere to hydrophilic surfaces. These findings, while highlighting the resilience of bacteria, also help to define a path forward for generating antifouling substrates. Specifically, the creation of a surface topography that provides minimal contact with the cell body is a good starting point. Further, surface area that is susceptible to anchoring by flagella must be made antiadhesive. We have seen that

hydrophilic surfaces allow reduced adhesion of flagella, thus a hydrophilic coating combined with optimal surface topography is a promising starting point.

One interesting hydrophilic material is mucin, which was examined in Chapter 4. Our work demonstrated that mucins can maintain bacteria in the planktonic state and significantly reduce surface adhesion. We find that this occurs only with purified, native mucins when they are in a three-dimensional gel state. This is in contrast to studies that have shown *P. aeruginosa* cells forming aggregates on surfaces coated with two-dimensional mucin monolayers [14]. In this case, engineered surface topography can provide not only geometric constraints for bacterial adhesion, but also a scaffolding for three-dimensional mucin gels as opposed to surface monolayers (Figure 5.10). We therefore decided to test the ability of purified mucins to prevent bacterial adhesion when used in conjunction with rationally designed surface microtopography.

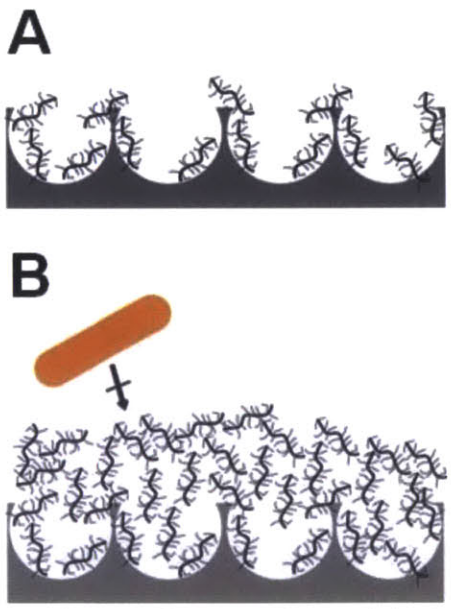

Figure 5.10. Mucins as anti-adhesive surface coatings. (*A*) A monolayer of mucins on a topographical surface. (*B*) Three-dimensional mucin networks may form on an appropriate scaffolding and could reduce bacterial adhesion.

PRELIMINARY RESULTS AND DISCUSSION

To generate topographical surfaces that minimize contact with the cell body, we used the geometry provided by inverse opals, as these provide close-packed pores with minimal surface area between them. These surfaces are highly ordered and are relatively easy to generate reproducibly. If the pores of an inverse opal surface are smaller than the bacterial diameter, the cells will be unable to settle in the spaces between them, thus leaving relatively few contact points for the cell body. If, however, the pores are smaller than necessary, the cell is then provided additional contact points. As the pores become even smaller, the surface begins to approximate a flat surface (Figure 5.11A). An additional consideration is the distance from the cell body to the inner walls of the pore. Since adhesion to these areas would rely on cellular appendages, maximizing this distance would reduce accessibility. This consideration also favors a pore size as large as possible, but without allowing the cell body to enter.

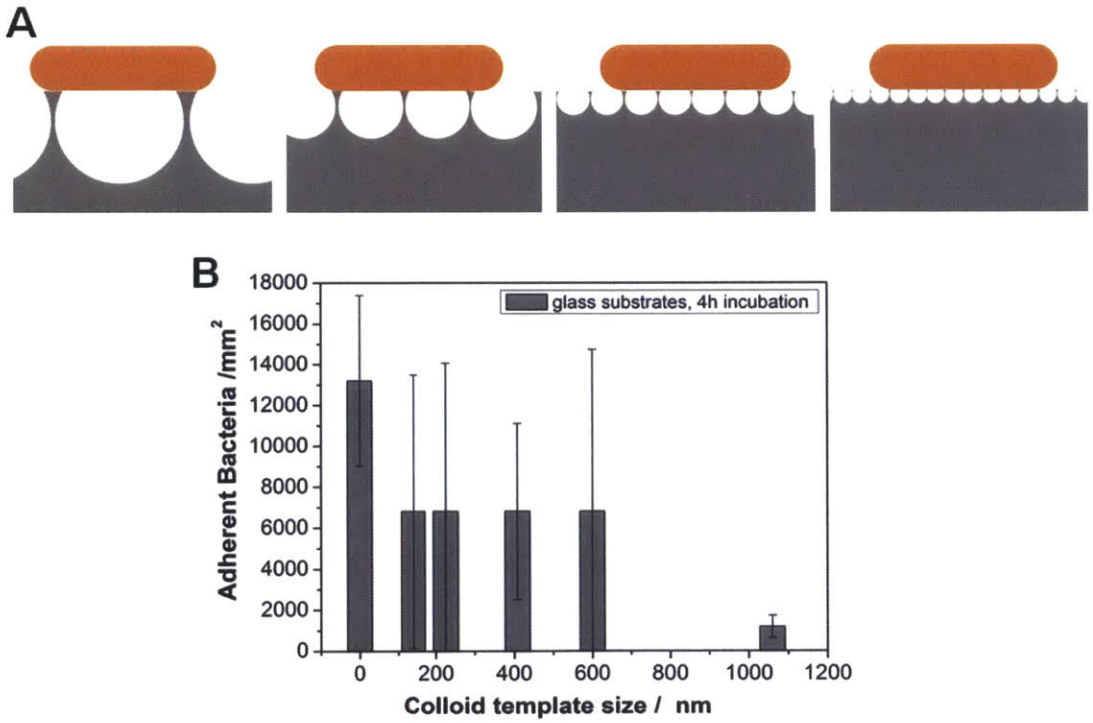

Figure 5.11. Cell adhesion to inverse opal surfaces of varying pore diameter. (*A*) Schematic depiction of a rod-like cell adhering to iMono surfaces of varying pore diameter. Note the number of contact points and overall contact area between the cell and the surface for each example. (*B*) Adhesion of *E. coli* to iMono surfaces in immersed culture after 4 h.

To determine the optimal pore size for these opals, we generated inverse opal monolayer (iMono) substrates comprised of silica. These were assembled on glass coupons and compared to glass alone. Using colloidal templates of 138, 225, 415, 600 and 1060 nm, we generated iMono surfaces of the corresponding dimensions. Each of these was submerged in culture medium and exposed to an inoculum of *E. coli*, which was allowed to grow and adhere during a 4 h stationary incubation. After rinsing and fixation, cells were imaged on counted on each substrate (Figure 5.11B). The flat surface allowed more adhesion than any of the iMono substrates, but among most of the substrates, performance was similar and too variable to determine a clear trend. Importantly, the finding that the iMono surfaces all outperformed the flat surface is consistent with the notion that hydrophilic surfaces with rationally designed topography *reduce* cell adhesion, as opposed to hydrophobic surfaces with topography, that *increase* adhesion (as in Chapter 2). Importantly, one sample stood out as reducing adhesion the most, and that was the 1060 nm diameter pore iMono. Although this is somewhat larger than the average cell diameter, it still performed well. We speculate that within a certain threshold, the cell cannot enter pores larger than its diameter, as precise aiming and application of force are not possible. Another important consideration is the fill fraction during backfilling of the monolayers. Once the colloidal template is assembled, depending on volume of sol-gel fill material, the height of the resulting inverse monolayer relative to the original colloidal template diameter will change, resulting in different pore diameters. At a 50% fill height, the pore diameter will equal the colloidal template diameter (assuming no geometric distortion during preparation). At 100% fill height, the surface will be flat. Between these, the pore size will vary as

$$d_{pore} = 2 \cdot \sqrt{\left(\frac{d_{colloid}}{2}\right)^2 - y^2}$$

where $d_{colloid}$ is the diameter of the colloidal template, y is the height above the equator of the colloidal particles, and d_{pore} is the diameter of the resulting pore in the iMono surface. Knowing that the *E. coli* cell diameter is 600 ± 100 nm (see Chapter 2), then for a 1060 nm colloidal template, a fill height of 437 nm above the equator (or 91% fill height) would result in pores smaller than the bacterial dimensions. The geometry tends to be helpful for reproducibility, as maintaining a ±10% error or less in pore diameter requires only that we stay below a ±21% error in fill height. With this in mind, the variability in results may be due to the difficulty with reproducibility for small pores. Indeed, staying within a 21% error for 225 nm colloids requires a precision of less than 50 nm in height, whereas for 1060 nm colloids, a variation of greater than 200 nm would still provide a pore size within 10% of the colloidal template diameter.

We chose to use 1060 nm pores for our colloidal templates based on their performance and ease of reproducibility. To investigate the effects of the iMono surfaces versus flat surfaces on bacterial adhesion, we extended the time of incubation to 8 h (Figure 5.12). For this comparison, we used flat and 1060 nm iMono substrates with gold coatings, but no additional coatings. In this arrangement, it was clear that the presence of the topography imparted by the iMono surface was beneficial in preventing bacterial attachment at all of the time points measured.

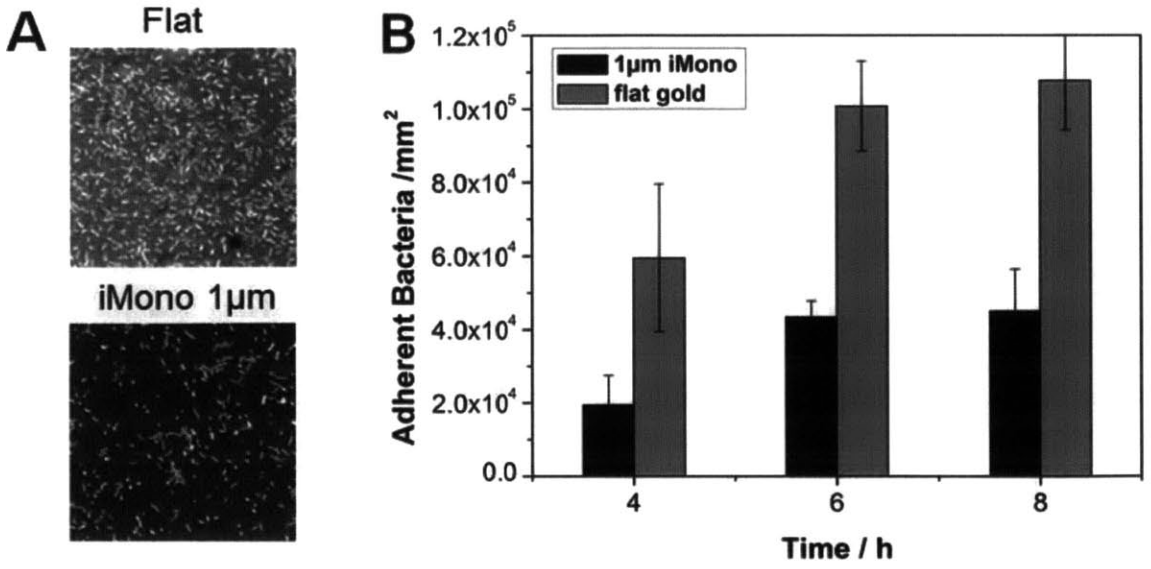

Figure 5.12. Effect of iMono topography on bacterial adhesion. (*A*) Images of adherent fluorescent *E. coli* after a 4 h incubation on the substrates indicated. (*B*) Number of attached *E. coli* after static incubation for up to 8 h to the substrates indicated.

We next wanted to compare mucin coatings to uncoated surfaces for both flat and iMono surfaces. In order to begin to generate coatings for the test surfaces, we chose to use gold coatings to enable linkages via gold-thiol chemistry. Therefore, all surfaces used in these assays were first subject to gold evaporation with a titanium adhesion layer. Once a gold layer was formed, we needed to tether the mucins to the surface. Due to the complexity of mucin glycoproteins, there are a variety of ways in which they can be tethered to a gold surface (Figure 5.13A). Specifically, the hydrophobic portions of the protein backbone can enable mucin tethering to a hydrophobic surface via hydrophobic interactions. A hydrophobic thiol, such as hexanethiol, could create such a surface. This would be similar to methods used previously to generate mucin monolayers [14]. MUC5AC is a negatively charged polymer due to its sialic acids and sulfates [15, 16]. Electrostatic interactions with a positively charged surface is another method of generating mucin coatings. On the protein core of the mucins, amines are available for

covalent tethering, using dithiobis(succinimidyl propionate) (DSP) to link lysine residues with the gold surface. Similarly, the thiols available at cysteine residues enable generation of disulfide bonds. In this case, benzene dimethanethiol could provide the linkage. Finally, the oligosaccharides themselves could be bound to the surface via hydrazide linkages (e.g. Whitesides hydrazides).

For initial tests, we used flat gold-coated substrates and attempted three different methods of tethering mucins. These included using hexanethiol for hydrophobic interactions, cysteamine for electrostatic interactions or DSP for covalent binding via lysine residues (Figure 5.13B). The flat, coated coupons were each incubated with *E. coli* ZK2686 for 4 h under static conditions at 37 °C. In all cases, the presence of mucin reduced adhesion relative to the non-mucin control. Overall, the cysteamine-mediated electrostatic interactions performed best, whereas tethering via hydrophobic interactions resulted in poor performance overall. This is consistent with previous work showing bacterial cell aggregation on mucin monolayers assembled via hydrophobic interactions [14]. These studies were followed up with similar trials, with the addition of iMono substrates and disulfide-bonded mucins (Figure 5.13D). Again, the electrostatically bound mucins showed the least bacterial adhesion after a 4 h incubation, with the iMono surfaces slightly outperforming flat surfaces.

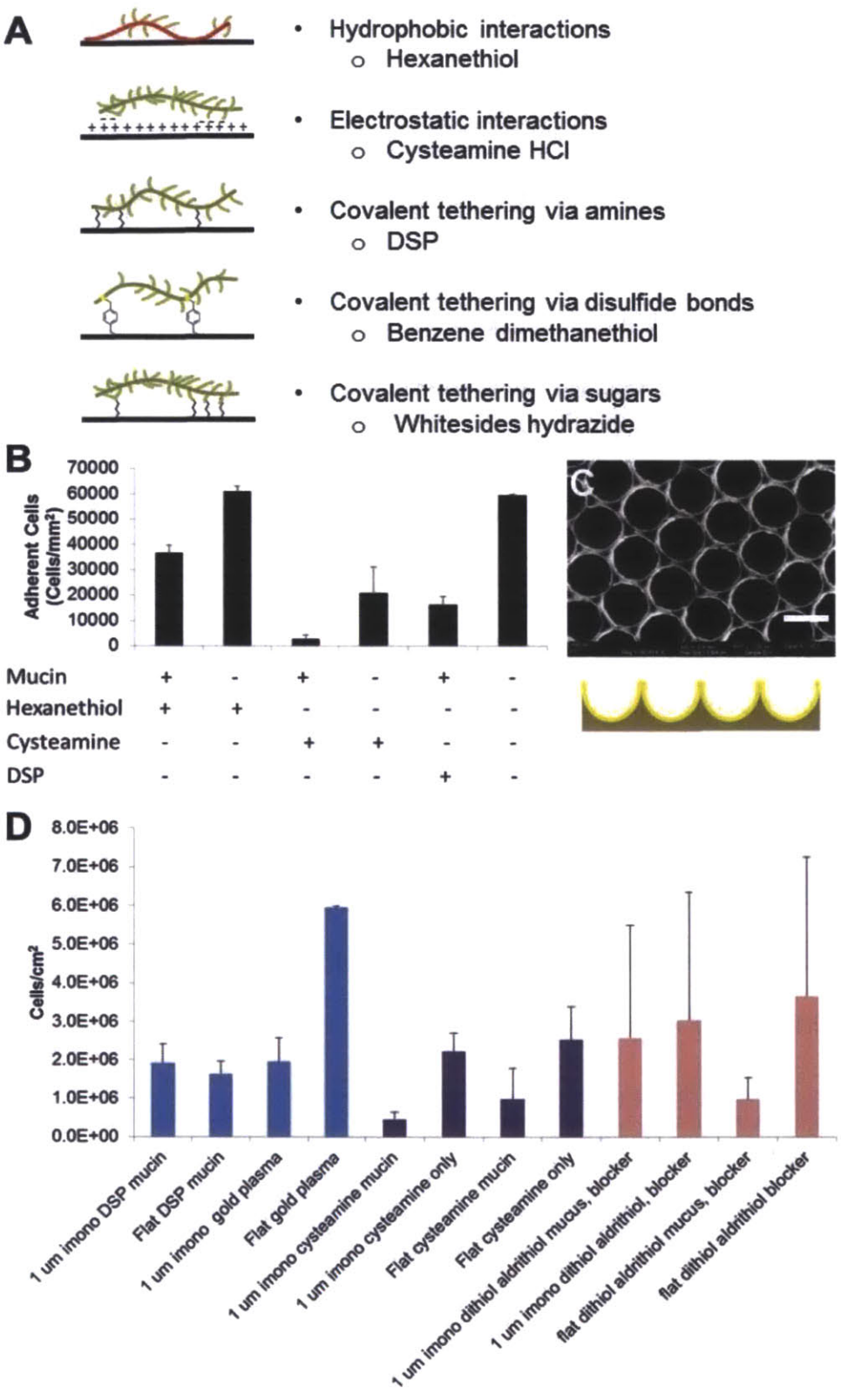
A
• Hydrophobic interactions
o Hexanethiol
• Electrostatic interactions
o Cysteamine HCl
• Covalent tethering via amines
o DSP
• Covalent tethering via disulfide bonds
o Benzene dimethanethiol
• Covalent tethering via sugars
o Whitesides hydrazide
B
Adherent Cells (Cells/mm²)
70000
60000
50000
40000
30000
20000
10000
0
Mucin + - + - + -
Hexanethiol + + - - - -
Cysteamine - - + + - -
DSP - - - - + -
C
D
Cells/cm²
8.0E+06
7.0E+06
6.0E+06
5.0E+06
4.0E+06
3.0E+06
2.0E+06
1.0E+06
0.0E+00
1 um imono DSP mucin
Flat DSP mucin
1 um imono gold plasma
Flat gold plasma
1 um imono cysteamine mucin
1 um imono cysteamine only
Flat cysteamine mucin
Flat cysteamine only
1 um imono dithiol aldrithiol mucus, blocker
1 um imono dithiol aldrithiol, blocker
flat dithiol aldrithiol mucus, blocker
flat dithiol aldrithiol blocker

Figure 5.13. Mucin coatings on iMono substrates. (*A*) Schematic and examples of different methods of tethering mucins to a gold surface. (*B*) Number of cells adhering to flat, gold-coated surfaces with the indicated treatments after a 4 h static incubation. (*C*) SEM image of a 1060 nm iMono substrate (upper panel) and a schematic cross section of iMono surface with conformal gold coating (lower panel). Scale bar, 1 μm. (*D*) Cell adhesion to mucin-coated flat and iMono surfaces after immersion in static culture of *E. coli* for 4 h.

Regardless of coating method, the mucins appeared to somewhat reduce bacterial adhesion. The overall reduction, however, was modest in most cases, so we wished to compare mucin coatings with polyethylene glycol (PEG) coatings, as these have been shown to reduce bacterial adhesion in previous applications [17, 18]. Furthermore, we were interested to see how PEG coatings would perform in conjunction with iMono topography. Using DSP for covalent linkage of PEG-amines, we generated flat and iMono substrates with PEG coatings and incubated them in static *E. coli* culture for 4 h (Figure 5.14). As with mucin surfaces, the PEG coatings had improved performance if applied to iMono surfaces, as compared with flat ones. Furthermore, PEG coatings in general reduced adhesion beyond any of the untreated surfaces. Our initial tests were done using PEG with an average molecular weight of 5000 Da. We also wished to compare long chain PEG surfaces with short chain surfaces, as molecular packing and organization could have an effect on adhesive properties. When we compared PEG5000 with PEG750, performance was similar, though there appeared to be a slight improvement in anti-adhesive performance with PEG5000, particularly on iMono surfaces.

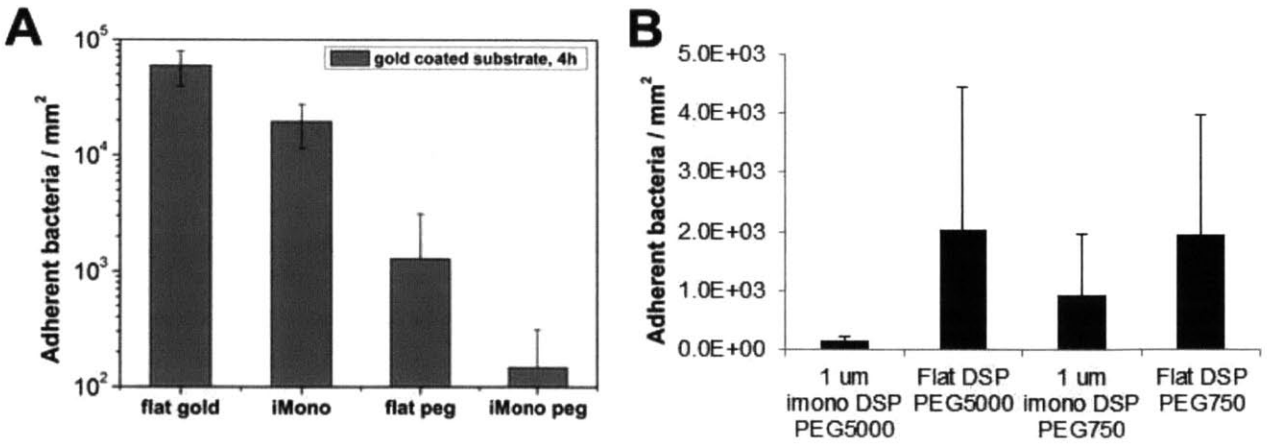

Figure 5.14. PEG coatings reduce bacterial adhesion. (*A*) After a 4 h incubation, *E. coli* adhesion was compared for PEG5000-coated and uncoated surfaces, both flat and 1060 nm iMono. (*B*) Flat and 1060 nm iMono surfaces were coated with PEG5000 or PEG750 and adhesion of *E. coli* during a 4 h incubation was compared.

Noting the excellent performance of PEG-coated surfaces, particularly in conjunction with iMono structured substrates we wished to extend our studies to longer time points and make direct comparisons of mucin coatings with PEG coatings. Examining numbers of adherent cells, it is clear that PEG coatings outperform mucin coatings in any of the configurations we tested (Figure 5.15A). Notably, at later time points the mucin coatings begin to fail and consequently, *increase* adhesion of bacteria. We speculate that none of the tethering methods allowed for proper hydration of the mucin layer and thus, we were not able to observe a reduction in adhesion as we saw in Chapter 4, for three-dimensional mucin gels. Extending time points up to 8 h, we observe that PEG5000 coatings work remarkably well (Figure 5.15B,C). It appears that the additional presence of an iMono topography is beneficial in this system, with only 160 cells adhering per mm^2 of substrate after an 8 h incubation. It appears that combining a reduced available surface area by using engineered surface topographies, with hydrophilic brush polymer coatings is an effective strategy for reducing bacterial adhesion.

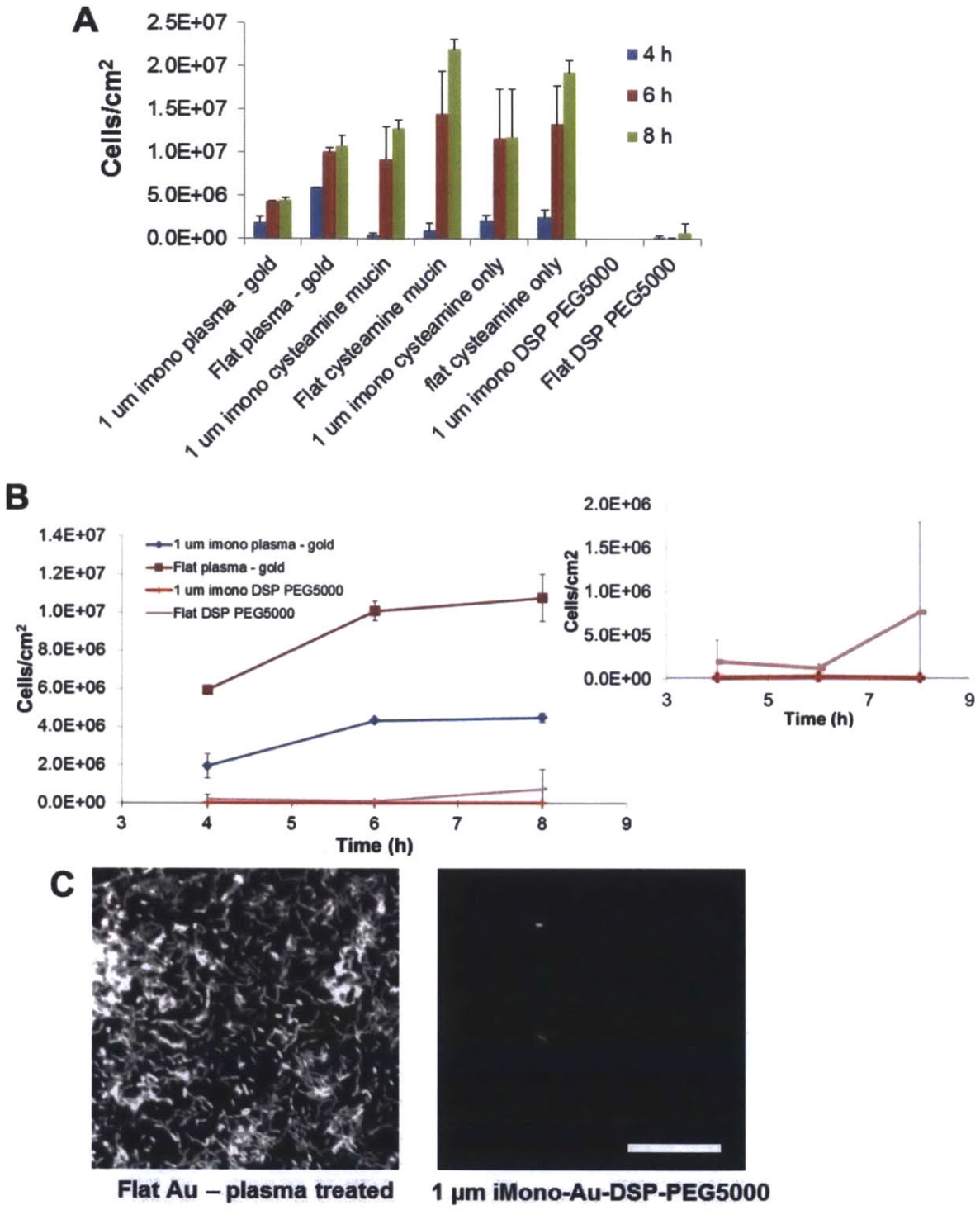

Figure 5.15. Extended trials with PEG coatings. (*A*) Total adhered *E. coli* at the time points indicated for mucin- and PEG-coated substrates of either flat or iMono topography. (*B*) Time-course of cell adhesion to PEG substrates. *Inset*, Flat and iMono PEG-coated substrates plotted on a smaller scale for clarity. (*C*) Images of fluorescent *E. coli* adhering to substrates as indicated after an 8 h incubation period. Scale bar is 25 µm.

FUTURE WORK

Our preliminary data indicates that hydrophilic surfaces with engineered iMono topography reduce bacterial adhesion significantly, as compared with flat, uncoated substrates. Additionally, topography and hydrophilic coatings combined work better than either on their own. Our work with mucins indicates that although they reduce adhesion at early time points, they lose this ability at time points beyond 4 h. Based on our previous work with three-dimensional mucin gels [19], we anticipate that a coating that can maintain the three-dimensional, interwoven structure of native mucins will perform better than the coatings we were able to obtain. Based on the tethering methods depicted in Figure 5.13A, we still have yet to attempt to tether mucins via their oligosaccharide side chains. Future work should attempt to use Whitesides hydrazides to link mucins to gold-coated surfaces via their sugars. Because this type of tethering does not rely on linking the mucin backbone to the surface, it is possible that such a configuration could allow tethering of the molecule without significant dehydration or loss of function.

Using iMono substrates with different colloidal templates revealed that the largest colloidal templates, 1060 nm, performed best. It is possible that even larger colloids would perform even better, however we have not attempted this due to difficulties in assembling colloidal crystal templates of this size. If we are able to overcome these difficulties and generate monolayers of larger colloids with large crystalline domains, these should be used to generate iMono substrates for further testing. We anticipate that an optimal size may be discovered that minimizes adhesion, and above this size, adhesion would begin to increase.

Our findings that PEG-coated iMono surfaces performed better than any other substrate tested warrant further investigation. The extension of the adhesion assays to later time points of

24 h and beyond would be obvious next steps. In order to continue the comparison of adhesion to later time points, we would like to ensure that the dynamic range of our measurements allows comparison with controls. Specifically, flat, gold-coated surfaces can have 10^7 cells/cm^2 attached after 8 h of culture. In comparison, PEG-iMono surfaces only allow 10^2 cells/cm^2 to attach by this time point. The dynamic range of measurement must therefore be quite high. The quantification used here relies on imaging and counting of cells. This is highly accurate and enables quantification of very low cell numbers. However, it is limited to quantification of monolayers of cells, which corresponds to approximately 10^7 cells/cm^2. In order to increase the upper limit of this range, we have begun to test other systems of quantification (Figure 5.16). In order to capture this large, logarithmic range of values, we decided to take test substrates, and sonicate them after attachment and rinsing to remove adherent bacteria. The removed bacteria would be serially diluted and plated for quantification. Our initial attempt involved using test substrates assembled on coverslips and placed in well plates. These resulted in a noise floor at approximately 10^7 bacteria/cm^2. This is likely due to bacteria adhering to the untreated underside of the coverslips. To improve upon this, we then used the coverslips to form the bottoms of wells by attaching stainless steel rings to the coverslips using vacuum grease. In this manner, the underside of the coverslips are never exposed to bacteria and thus cannot contribute noise to the measurement. Nonetheless, this method still had a noise floor at approximately 10^5 cells/cm^2. This is clearly an improvement, but does not reach the low numbers necessary to capture the performance of our least adhesive substrates. Assuming that the vacuum grease itself provided points of attachment for the bacteria, we eliminated this by creating a customized well plate that uses gaskets to seal the base of the well, which is the substrate itself. This requires no gaskets and enables the test substrate to be completely removed for quantification. This modified

stainless steel well plate enabled quantification as low as 10^2 cells/cm^2, which was the lowest cell adhesion number observed in imaging studies. Further, this method is not limited to a monolayer of cells and could thus support a wide dynamic range for comparison. Future work should make use of this apparatus and method of quantification for longer-term studies of cell adhesion. Extending studies on PEG-coated iMono substrates will enable the determination their longevity.

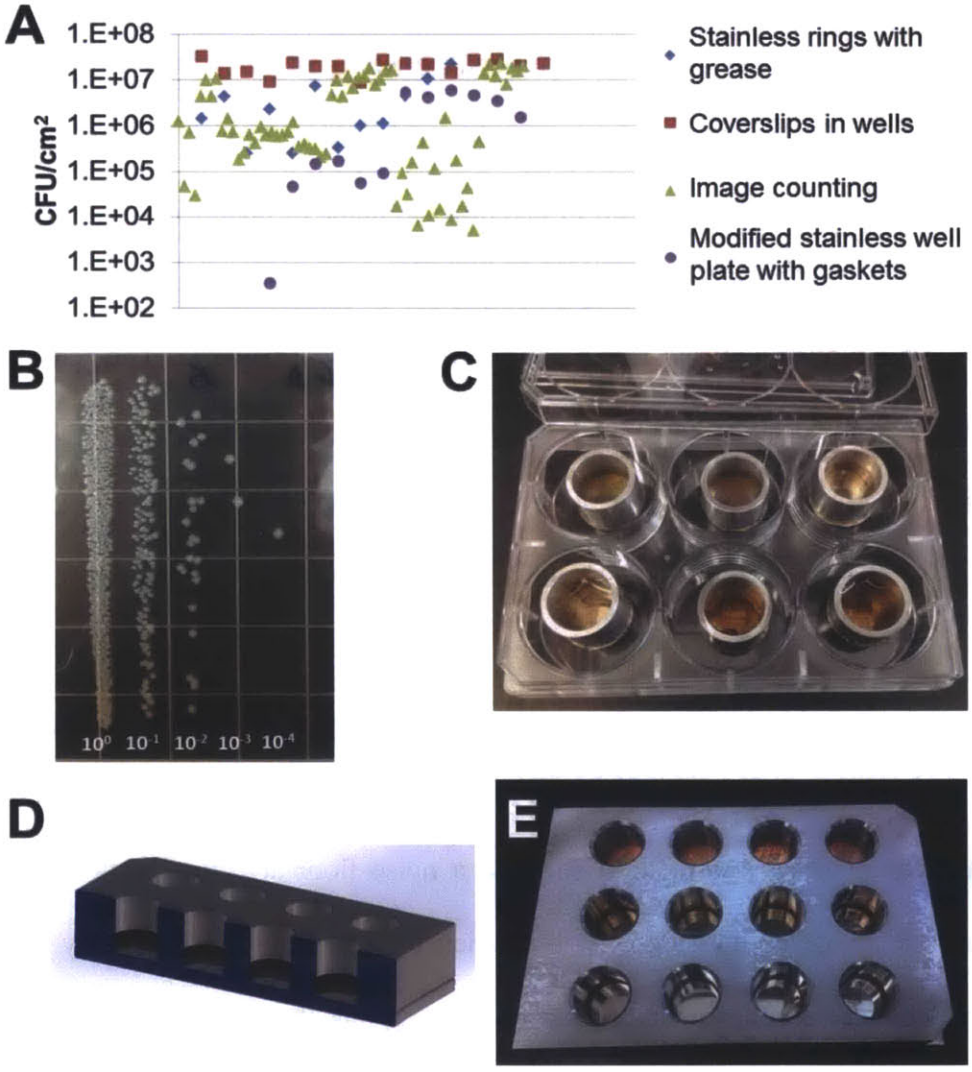

Figure 5.16. Methods of quantification of cell adhesion for long-term assays. (*A*) Apparent cell density numbers for arbitrary substrates using the quantification methods indicated. For each method, we should expect the same range of data points, however due to their inherent limitations, some methods cannot capture this entire range. (*B*) An example of colony counts from serial dilutions after sonication of a substrate. (*C*) Image of stainless steel rings attached to

substrates using vacuum grease. (*D*) Schematic cross section of the modified stainless steel well plate, showing two silicone gaskets at the base of each well, sealing the test substrates. (*E*) Image of a modified stainless steel well plate in use.

EXPERIMENTAL SECTION

Assembly of iMono substrates

Colloidal monolayers are crystallized on the air water interface of a crystallization dish following a protocol from literature [20]. In brief, a colloidal dispersion in 1:1 water/ethanol (solid content approximately 2.5%) is spread onto the interface via a glass slide until the surface is completely covered. The substrate is then inserted into the subphase and the monolayer deposited manually by fishing out the slide. After drying, a closed-packed monolayer uniformly covers the substrate. To form the inverse monolayer, a solution of tetraethylorthosilicate (TEOS), HCl (0.1 mol/L) and ethanol with weight ratios of 1:1:1.5 is prepared and stirred for 1 h. Then, it is diluted with ethanol (dilution ratios see Table 5.3) and spin-coated onto the monolayer-covered substrate (3000 rpm, 30 s). The colloids are removed by combustion at 500 °C (ramped from RT to 500 °C over 5 h, 2 h at 500 °C).

Colloid size	TEOS:Ethanol ratio (volume)
1060 nm	1:0.9
600 nm	1:2
415 nm	1:4
225 nm	1:6
138 nm	1:9

Table 5.3. Mixture ratios between TEOS and ethanol used for spin-coating.

Gold surface coatings

Microscope slides were coated with 2 nm titanium and 30 nm of gold using a Cressington 308 evaporator (Ted Pella, USA). The titanium served as an adhesion promoter to prevent delamination of the gold film.

Mucin and PEG attachment.

For attachment of mucins to gold-coated surfaces, substrates were incubated in thiol solutions as follows: 4 mg/mL DSP in DMSO for 30 min., 0.2% (v/v) hexanethiol in ethanol for 30 min., 2 mg/mL cysteamine for 30 min. All incubations were carried out at room temperature. Following this, surfaces were rinsed in deionized water, then rinsed in the incubating solvent and dried under nitrogen gas. Surfaces were then incubated with 0.1% (w/v) purified mucin in PBS, or PBS alone overnight in a humidified chamber at room temperature. Samples were then removed to PBS and kept hydrated until experiments were begun. For PEG conjugations, gold surfaces were prepared with DSP, as described above. Surfaces were then incubated with 1 mmol/L PEG-amine in toluene (either 750 or 5000 MW) for 18 h. Samples were then rinsed sequentially with toluene, ethanol and water. Samples were then placed in PBS and kept hydrated overnight until experiments were begun.

Adhesion assays and quantification

All strains used in this study are indicated with their sources in Table 5.4. For all adhesion assays, fluorescent *E. coli* strains (RSF84 or RSF85) were inoculated from Luria Bertani (LB) agar plates into LB broth and incubated at 37 °C overnight with agitation. The overnight cultures were diluted 1:100 in M63 salts plus 0.5% (w/v) casamino acids and 0.2% (w/v) glucose ($M63^{+}$). Glass coupons (iMono or flat) were placed at the bottoms of 6-well tissue

culture plates; the overnight cultures diluted in $M63^+$ were used to cover these coupons and the plates were incubated at 37 °C under static conditions for the times indicated in each experiment. The medium was aspirated at the appropriate time point and the coupons were rinsed twice in phosphate-buffered saline (PBS). Then, cells were fixed in a modified Karnovsky's fixative (2% glutaraldehyde, 2.5% paraformaldehyde in 0.08 M Sorenson's phosphate buffer) for 15 min and washed twice in PBS prior to imaging. For quantification, each coupon was examined under a fluorescent microscope, using a dipping water immersion lens to image substrates in their hydrated state. A minimum of four representative images were taken per sample; in cases where cell distribution was highly variable or highly sparse, additional images were captured.

Strain	Description	Reference or source
ZK2686	W3110, Δ(*arg*F-*lac*) U169	[7]
RSF84	ZK2686, glmS::PRNAi-hybrid mKate2-T1 terminator-FRT-kan-FRT::pstS, AmpS, KanR	This study
RSF85	ZK2686, glmS::PRNAi-GFPmut2-FRT-kan-FRT::pstS, KanR, ara+, AmpS	"

Table 5.4. Strain names, genotypes and sources for all *E. coli* strains used in this study. KanR, kanamycin-resistant; AmpS, ampicillin-sensitive.

BIBLIOGRAPHY

1. Lukjancenko O, Wassenaar TM, Ussery DW (2010) Comparison of 61 sequenced Escherichia coli genomes. Microb Ecol 60:708–720.

2. Donnenberg MS, Whittam TS (2001) Pathogenesis and evolution of virulence in enteropathogenic and enterohemorrhagic Escherichia coli. J Clin Invest 107:539–548.

3. Orskov I, Orskov F, Jann B, Jann K (1977) Serology, chemistry, and genetics of O and K antigens of Escherichia coli. Bacteriol Rev 41:667–710.

4. Wang L, Rothemund D, Curd H, Reeves P (2003) Species-Wide Variation in the Escherichia coli Flagellin (H-Antigen) Gene. J Bacteriol 185:2936–2943.

5. Lawn A, Orskov I, Orskov F (1977) Morphological distinction between different H serotypes of Escherichia coli. J Gen Microbiol 101:111–119.

6. Cherepanov P, Wackernagel W (1995) Gene disruption in Escherichia coli: TcR and KmR cassettes with the option of Flp-catalyzed excision of the antibiotic-resistance determinant. Gene 158:9–14.

7. Danese P, Pratt L, Dove S, Kolter R (2000) The outer membrane protein, Antigen 43, mediates cell-to-cell interactions within Escherichia coli biofilms. Mol Microbiol 37:424–432.

8. Friedlander RS, Vlamakis H, Kim P, et al. (2013) Bacterial flagella explore microscale hummocks and hollows to increase adhesion. Proc Natl Acad Sci U S A 110:5624–5629.

9. Ratiner Y (1998) New flagellin-specifying genes in some Escherichia coli strains. J Bacteriol 180:979–984.

10. Datsenko K, Wanner B (2000) One-step inactivation of chromosomal genes in Escherichia coli K-12 using PCR products. Proc Natl Acad Sci U S A 97:6640–6645.

11. Sambrook J, Russell DW (2006) The Hanahan Method for Preparation and Transformation of Competent E. coli: High-efficiency Transformation. CSH Protoc. doi: 10.1101/pdb.prot3942

12. Crawford R, Reeve K, Gunn J (2010) Flagellated but not hyperfimbriated Salmonella enterica serovar Typhimurium attaches to and forms biofilms on cholesterol-coated surfaces. J Bacteriol 192:2981–2990.

13. Erdem A, Avelino F, Xicohtencatl-Cortes J, Girón J (2007) Host protein binding and adhesive properties of H6 and H7 flagella of attaching and effacing Escherichia coli. J Bacteriol 189:7426–7435.

14. Landry RM, An D, Hupp JT, et al. (2006) Mucin–Pseudomonas aeruginosa interactions promote biofilm formation and antibiotic resistance. Mol Microbiol 59:142–151.

15. Paz HB, Tisdale AS, Danjo Y, et al. (2003) The role of calcium in mucin packaging within goblet cells. Exp Eye Res 77:69–75.

16. Kuver R, Klinkspoor JH, Osborne WR, Lee SP (2000) Mucous granule exocytosis and CFTR expression in gallbladder epithelium. Glycobiology 10:149–157.

17. Roosjen A, van der Mei HC, Busscher HJ, Norde W (2004) Microbial adhesion to poly(ethylene oxide) brushes: influence of polymer chain length and temperature. Langmuir 20:10949–10955.

18. Park KD, Kim YS, Han DK, et al. (1998) Bacterial adhesion on PEG modified polyurethane surfaces. Biomaterials 19:851–859.

19. Caldara M, Friedlander RS, Kavanaugh NL, et al. (2012) Mucin biopolymers prevent bacterial aggregation by retaining cells in the free-swimming state. Curr Biol 22:2325–2330.

20. Vogel N, Goerres S, Landfester K, Weiss CK (2011) A Convenient Method to Produce Close- and Non-close-Packed Monolayers using Direct Assembly at the Air–Water Interface and Subsequent Plasma-Induced Size Reduction. Macromol Chem Phys 212:1719–1734.

Chapter 6

Perspective: topographically patterned surfaces for the prevention of bacterial adhesion

INTRODUCTION

The prevention of bacterial adhesion, particularly in biomedical settings, remains a complicated and difficult problem. In our current clinical arsenal, antibiotics are still the best weapons for combating bacterial infection. Even as a prophylactic measure, systemic or topical antibiotics, or antibiotic/biocide-releasing materials are our current best options for preventing infections of implants [1–3]. Unfortunately, with every use of an antibiotic, we increase the selection pressure for resistance. The discovery and synthesis of new antibiotics is of paramount importance; however, new antibiotics do not address the problem of overuse that will lead to their obsolescence. New approaches to eradicating infections in creative ways that do not impose selective pressures will be necessary. Indeed, the last decade has seen the introduction of several approaches that attack virulence traits rather than kill bacteria. Examples include drugs that target quorum sensing [4], bacterial antioxidants [5], pili [6], and bacterial amyloid production [7]. In the realm of implantable biomaterials, a key strategy will be to improve prevention of infection so as to decrease its overall incidence, as well as reduce antibiotic usage. In this thesis, we examined the process of bacterial surface adhesion, specifically focusing on topography, surface hydrophobicity, polymer coatings and bacterial organelles that contribute to adhesion. Here, we examine our findings in the context of existing studies, so as to extract underlying patterns and establish principles by which to design novel surfaces that are effective at repelling bacteria.

BACTERIAL RESPONSES TO SURFACE TOPOGRAPHY

We have shown that the response of *E. coli* to topographically patterned substrates is complex, and relates to bacterial geometry, surface geometry, surface hydrophobicity, surface wetting state and cell expression of surface organelles (see Chapter 2) [8]. Specifically, we generated surfaces with regular features and inter-feature spacings smaller than the diameter of the *E. coli* being tested. For wild-type cells, adhesion after 24 h was enhanced by the presence of topography, indicating that the 440 nm trenches on our test substrates were somehow enabling improved adhesion. Importantly, this discredits any simplified models of the bacterium as an ellipsoid or rod, as far as surface adhesion is concerned. Furthermore, it implies that additional cell surface extensions or appendages play a vital role in adhesion, particularly where non-smooth surfaces are involved. In our case, we demonstrated that the cell's longest appendages, flagella, enabled adhesion to narrow surface trenches. For organisms with peritrichous flagella, it is plausible that this could be an important secondary use for these organelles. Other bacteria, however, may rely on other appendages or secretions to overcome surface topography.

In the process of adhesion and biofilm formation, bacteria secrete exopolysaccharides (eps) and other matrix components such as eDNA and amyloid fibers [9]. Similarly, surface organelles such as flagella and pili play roles in this process. Adhesion and cohesion are important functions imparted by these substances, however overcoming unfavorable surface topography is a plausible additional function for them that should not be overlooked. Numerous publications have examined bacterial adhesion to rough or patterned surfaces. A common finding in these studies is that bacterial adhesion and orientation maximizes contact area between the cells and the substrates [10–13]. Only a small fraction of studies have discussed the interplay

between bacterial surface extensions and adhesion to topographic surfaces and how this serves to increase contact area. One study examined adhesion of *S. epidermidis*, *Deinococcus geothermalis*, *Meiothermus silvanus* and *Pseudoxanthomonas taiwanensis* to carbon-coated, fluoropolymer-coated and bare stainless steel. It was observed that *D. geothermalis*, *M. silvanus*, and *S. epidermidis* expressed thread-like appendages that positively correlated with the overall adhered biomass (Figure 6.1A). The authors pointed out that "the appendages likely represented adhesion tools, as they were only expressed on the non-living substrate. There were no adhesion organelles in planktonic cells" [14]. Similarly, Hsu and colleagues noted that during adhesion to alumina and silica substrates, both *E. coli* and *P. fluorescens* expressed surface appendages that varied depending on substrate material and topography [12]. Making a more direct link between adhesion and surface secretions, Kawai *et al.* examined adhesion of *Streptococcus sobrinus* to porcelain of varying roughness, showing a general trend of increased adhesion and increased synthesis of insoluble glucans on rougher surfaces [15]. Similarly, another study showed that *S. mutans* cells adhered to topographic surfaces and that this was promoted by glucan secretion [16]. Truong *et al.* demonstrated that *P. aeruginosa* and *E. coli* increased eps production on Ti surfaces that were modified to have 100-200 nm undulations (Figure 6.1B) [17].

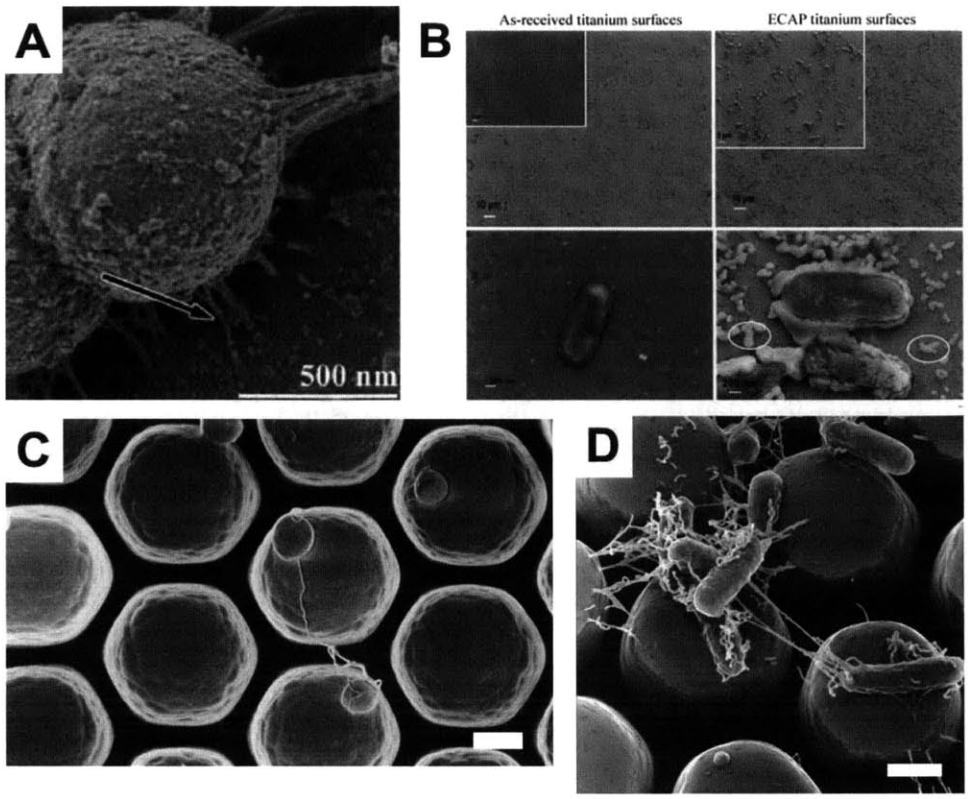

Figure 6.1. Cell surface features aid in adhesion to topographical surfaces. (A) Adhesion threads (black arrow) connecting *D. geothermalis* to a stainless steel surface. Adapted from [14]. (B) Adhesion of *P. aeruginosa* to Ti (left column), or modified Ti (right column) surfaces. White circles highlight eps secreted by the cells. Adapted from [17]. (C) *S. epidermidis* cells adhering to HEX PDMS surfaces. Note the presence of fibers adhering to the substrate and spanning the gaps. (D) *E. coli* adhering to a HEX PDMS substrate. Note the abundance of fibers connecting cells to the substrate and each other.

It appears to be a general phenomenon that bacteria extend substances from their cell surface in order to increase area of contact with rough interfaces. The above studies, however only deal with textured, irregular, rough surfaces. Regular, topographically patterned surfaces possessing translational symmetry are immensely helpful in allowing us to gain a deeper understanding of the underlying bacterial behavior. For example, our studies (in Chapter 2) had well defined topographies with feature spacings smaller than the cell diameters, as well as feature diameters of approximately 3μm. Unlike irregularly patterned surfaces, this enables us to understand that cell appendages must be involved with surface adhesion, as the cell body cannot

fit in between the features. If the features were irregular, such a conclusion would be more difficult to arrive at. In addition to observing flagella as they aid in adhesion of *E. coli* to patterned substrates, we have also observed secretions from *S. epidermidis* during adhesion to patterned substrates (Figure 6.1C). Using regularly spaced silicon nanowire arrays, Jeong *et al.* have demonstrated that *Shewanella oneidensis* cells tether themselves to nanowires via their flagella [18]. It is possible that this recapitulates a process used during adhesion to other rough and smooth substrates as well.

It is clear that bacteria have evolved numerous adaptations to deal with structured surfaces, as the micro-scale environment is rich with structure. By understanding these adaptations we may gain insight into the adhesive process and develop strategies that anticipate the bacterial response. To do this, it is critical that we use well-defined, engineered substrates to probe bacterial behaviors during surface interactions.

SUPERHYDROPHOBICITY AS AN ANTIADHESIVE STRATEGY

An important consideration when working with surfaces structured on the micro- or nano-scale is their surface hydrophobicity. Particularly, hydrophobic surfaces may become superhydrophobic upon introduction of certain micro- or nano-structures. These materials entrap air bubbles between surface features when immersed in aqueous environments. This effect has been exploited in attempts to generate non-fouling surfaces, since liquid bearing bacteria would not even reach the areas occupied by bubbles. A review article by Zhang *et al.* [19] examines the recent uses of superhydrophobic materials for the reduction of bacterial adhesion. Various existing studies have used very different methods for generating superhydrophobic surfaces and have examined broth gram positive and gram negative bacteria. They each report different

findings, which range from nearly no adhesion to biofilm formation on superhydrophobic surfaces. We summarize these studies in Table 6.1. One report, which uses femtosecond laser-ablated Ti substrates, shows both effects: nearly no adhesion of *P. aeruginosa* to nanostructured, superhydrophobic Ti after 18 h of culture, but for *S. aureus*, adhesion to the same substrates is increased, as compared with polished Ti [20]. The authors speculate that the differing shapes of the bacteria play a role in the vastly different findings.

Ref.	Organism(s)	Culture condition	Surface topography	Surface material	CA	Major result
[8]	*E. coli* W3110 and Δ*fliC* mutants	Static; in supplemented minimal medium for ≤24 h	Post array (hexagonal), p=3.4 μm, h=2.7 μm, Ø=3 μm.	PDMS	155° adv.	Flagella aid in attachment to trenches. Increased adhesion by wild type to patterned substrate. Cells accelerate loss of Cassie wetting state.
[21]	*P. aeruginosa* ATCC 9027	Static; in Oxoid nutrient broth for 18 h.	Array of cones with Ø=100 nm at base and 60 nm at cap, p=170 nm, h=200 nm.	Wings of cicada *Psaltoda claripennis*. With or without Au coating.	147° to 172°. 105.5° with Au.	Wing not effective at repelling bacteria. Wing nanopillars penetrated and killed attached cells within 5 min.
[22]	*D. salexigens*	Static; in BioMerieux Bact API 20 solution, under nitrogen, up to 7 days.	Vermiculate patterns of ~300 nm and nanoconvexities of ~50 nm.	Polyelectrolyte multilayers with Ag NPs and fluorosilane on a Cu surface.	152°	Effective at reducing bacterial adhesion. Complementary effects of nanosilver and hydrophobic coatings. Hydrophobicity was reduced over time.
[23]	*M. smegmatis*	Shaking; in tap water for 1.5 h or 13 days.	Agglomerated nano-particles ranging from 24-51 nm, randomly arranged.	Hydrophobic carbon nanostructures on Si wafers or SS mesh.	135.4° 138.3°	Surfaces coated with CNs bound more cells in the short term and formed denser biofilms. Biofilms reduced hydrophobicity substantially.
[24]	*B. subtilis, E. coli, P. stutzeri, P. aeruginosa*	Static; in Oxoid CM3 for	R_q=47.6 nm	Trimethyl-methoxysilane deposited on Si	150°	Greatly increased adhesion to superhydrophobic surfaces as compared with

		24 h.		wafers, with PEG regions.		PEG surfaces.
[25]	*S. epidermidis* ATCC 35984	Shaking at 120 rpm in TSB for 12 h.	2D Mechanically assembled monolayers; R_q= 62.7 to 145.6 nm	PDMS with assembled fluoroalkyl silane.	121° to 128.8°	Roughness increased adhesion, superhydrophobicity decreased adhesion. Surface roughness effects dominated superhydrophobicity.
[26]	*Listeria monocytogenes, Hafnia alvei, P. aeruginosa*	In NaCl for 3 h.	Roughened, sandblasted surface.	Fluorinated, etched, polypropylene and polystyrene	136° to 160°	Adhesion dependent on surface roughness, strain and material. All else being equal, roughness may increase adhesion.
[20]	*S. aureus, P. aeruginosa*	In Oxoid nutrient broth for 18 h (shaking or static not reported).	Hierarchical two-tier surface with 10-20 μm grains bearing 200 nm undulations.	Ti	166°	*S. aureus* had increased attachment to structured Ti, and *P. aeruginosa* had similar, but decreased attachment to structured Ti.
[27]	*E. coli* DH5-α	10 μL drop of LB with exponential phase cells rolled off surface (~s).	Rough, high-aspect, and multiscale structures. Solid fractions ranging from 0.09-0.14.	PS, PC, PE, cast over buckled polyolefin shrink film pattern.	150° to 167°	Significant reduction in adherent bacteria on structured surfaces.
[28]	*S. aureus* CECT239, *P. aeruginosa* ATCC 10145	Immersed in TSB+0.25 % glucose, shaking for 24 h.	Papilla-like protrusions of ~9 μm.	PLLA, roughened by casting with dioxane.	154°	Superhydrophobic surfaces allowed attachment of greater numbers of cells compared with hydrophobic surfaces. These were also more difficult to remove. *S. aureus* showed greater difference.

CA, contact angle. R_q, rms roughness. Ø, diameter. p, pitch. h, height. SS, stainless steel. PDMS, polydimethylsiloxane. PS, polystyrene. PC, polycarbonate. PE, polyethylene. NP, nanoparticle. PLLA, poly(L-lactic acid).

Table 6.1. Selected studies examining bacterial adhesion on superhydrophobic substrates.

The difficulty of attempting to establish broad trends based on superhydrophobicity likely stems from the underlying definition of superhydrophobicity—a surface with an apparent water contact angle of 150° or greater and minimal contact angle hysteresis [29]. This macro-scale

property arises from a combination of surface chemistry and structure. Although two entirely different sub-micron structures can give the same apparent contact angle measurements, the bacterial response to them may be entirely different. In our example, when HEX-patterned substrates are superhydrophobic, adhesion by *E. coli* is reduced. This has much less to do with the superhydrophobicity as an emergent property than the underlying substrate geometry and the wetting state. If the same apparent contact angle were arrived at via a different, random patterning technique, it is likely that the adhesion would have been different. This point is well illustrated by one study, which used radio frequency Ar plasma, followed by CF_4 plasma on polypropylene (PP) samples to generate surface structure and hydrophobicity. By examining the adhesion of *P. aeruginosa*, *L. monocytogenes*, and a strain of *Enterobacter* over the course of 3 h, the authors observed that samples which were "very heterogeneous at the mesoscopic scale show[ed] pro-bioadhesive properties [...] In an opposite manner, PP surfaces with the same surface chemistry but homogeneous at the bacteria scale [...were] anti-adhesion [sic]" [26]. Notably, these two sets of samples, despite their differing structures, had overlapping ranges of water contact angles. It is clear that in order to establish design principles for antifouling surfaces using superhydrophobic materials, their geometries and resultant wetting states must be thoroughly described and followed, as these properties, not simply the contact angle, are relevant on the bacterial size-scale.

In our studies on *E. coli* adhesion to HEX substrates, we found that for the first 2-3 h, HEX substrates could substantially reduce adhesion. During this time period, we showed that the hydrophobic, patterned substrate was in the Cassie-Baxter wetting state. In this configuration, cells could interact with islands of substrate approximately 3 μm wide, separated by a network of air bubbles. Evidently, this reduced the available surface area and acted to reduce cell adhesion.

Unfortunately, this metastable Cassie-Baxter state could only be maintained for up to 4 h, at which point the air bubbles were lost, largely due to the action of the cells themselves, and the substrate transitioned to the Wenzel wetting state. Once the entire substrate became accessible to cells and their appendages, adhesion significantly increased. This is consistent with other studies of superhydrophobic materials that show a loss of superhydrophobicity upon exposure to bacteria, coincident with increased cell adhesion [30, 31]. Interestingly, our finding that adhesion was reduced when the substrate was in the Cassie-Baxter state implies that having small, discontinuous islands for adhesion can reduce cell surface coverage, as compared with a flat surface. It also implies that cells or cell appendages could not pass through the air-water interface to contact the inter-feature trenches. Lastly, this provides evidence that if the cell surface appendages are not able to provide additional surface adhesion, overall adhesion is reduced.

PROSPECTS FOR TOPOGRAPHICAL ANTI-FOULING SUBSTRATES

An obvious direction in surface design, based on the above findings, would be to attempt to extend the period during which superhydrophobicity is maintained. One existing study demonstrates that this might be possible by revealing differences in time to loss of superhydrophobicity for different substrates. It was found that surfaces made with PTFE particles and having an initial contact angle of 150° became fully wetting after 1 day of exposure to mixed cultures in tap water, whereas a roughened polysiloxane surface having an initial contact angle of 169° was only 50% wetting (by surface area) after six months [30]. This difference is ascribed not to the contact angle itself, but to the nano-scale, hierarchical structure of the latter sample.

In order to reduce the likelihood or rate of wetting, we can design surfaces with reentrant

curvature [32, 33], hierarchical structure [34], and/or closed-cell features [35]. Our use of iMono substrates (see Chapter 5§2), while not introducing structural hierarchy, does provide reentrant curvature and closed-cell, non-communicating features. Our previous studies of wetting of open-cell structures (Chapter 2) showed that once the meniscus advances to the base of the substrate, it can continue to travel horizontally between communicating features. By using non-communicating features, even if there is a surface defect allowing local loss of air pockets, the meniscus has no further means of advancing to neighboring features. We used a SAM of tridecafluoro-1,1,2,2-tetrahydrooctyl trichlorosilane to make the iMono surfaces superhydrophobic. Initial observations of these iMono substrates indicate that they do not wet, even when subject to 90% (v/v) ethanol in water, corresponding to a surface tension of approximately 23 mN/m [36]. These iMono substrates are iridescent when in the Cassie-Baxter wetting state, but lose this property when in the Wenzel state, due to refractive index matching. This provides a convenient readout for determining the wetting state during a bacterial adhesion experiment.

Experiments with superhydrophobic iMono substrates with pore diameters of 1060 nm revealed a substantial quantity of adherent bacteria after 4 h (55900 ± 9900 cells/mm^2). Importantly, we continued to observe iridescence, indicating that the sample remained in the Cassie-Baxter wetting state, even when experiments were extended to 8 h (Figure 6.2). The adherent *E. coli* must therefore have adhered to the upper substrate areas surrounding the wells. In this case, unlike for HEX substrates, the maintenance of the Cassie-Baxter state did not reduce overall adhesion. In closed-cell systems, the solid fraction of the surface available to the cells is continuous, whereas in open-cell systems, this fraction is comprised of discontinuous islands. We propose that the availability of continuous stretches of substrate allowed cells to adhere.

Unfortunately, this reveals two antagonistic design parameters: (1) stabilizing the Cassie-Baxter state and (2) reducing the largest continuous area of the substrate to a size that makes adhesion difficult. The use of closed-cell structures to stabilize the Cassie-Baxter state implies that the solid fraction of the surface must be contiguous, thus providing surface area for bacterial adhesion. The only strategy that would accomplish both (1) and (2) would be using open-cell, overhanging hierarchical structures to stabilize the Cassie-Baxter state, which would be prone to mechanical failure, as open-cell micro-posts or similar structures are not as damage tolerant as closed-cell structures.

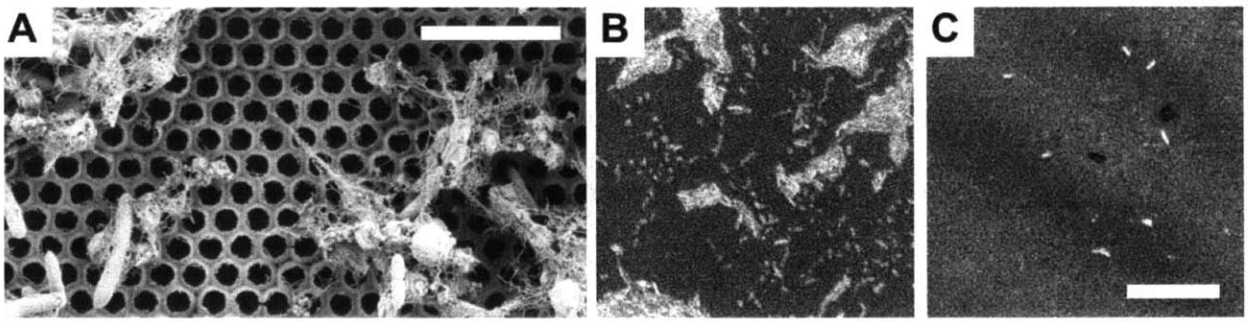

Figure 6.2. Adhesion of *E. coli* to superhydrophobic iMono substrates. (*A*) SEM image of adherent cells on a superhydrophobic iMono surface (templated from 1060 nm colloids). Scale bar is 5 μm. (*B*) Optical micrograph of *E. coli* adherent to a superhydrophobic iMono substrate after 4 h of culture. (*C*) Optical micrograph of *E. coli* adherent to an untreated (hydrophilic) iMono substrate after 4 h of culture. Scale bar is 25 μm. The background stippling in *B* and *C* is due to the pattern of the iMono surface.

Returning to the general concept of superhydrophobicity, the main motivation for attempting to find a non-adhesive superhydrophobic surface is that aqueous solutions make minimal contact and do not readily adhere to the substrate, implying that suspended bacteria would similarly have difficulty making surface contact. However, examination of these surfaces on the bacterial scale reveals a more complex situation, with dependencies on micro-scale geometry, surface energy and bacterial surface properties. When we consider these dependencies individually, topography that limits bacterial contact appears to be a valid approach, but the use

of hydrophobic materials to generate this topography may promote adhesion. We have shown that once the Cassie-to-Wenzel transition is complete (over the course of 4-6 h), adhesion is *promoted* on topographically patterned PDMS [8]. Additionally, we have shown that the flagella that help to anchor *E. coli* to patterned surfaces adhere best to hydrophobic substrates (Chapter 3, Chapter 5§1). Therefore, a patterned *hydrophilic* substrate that minimizes contact with the cell body, but also reduces the ability of flagella to adhere might be the best approach. We and others have demonstrated that highly hydrophilic PEG coatings reduce bacterial adhesion (Chapter 5§2) [37–39]. Furthermore, we have preliminary data that indicates the combination of high molecular weight PEG coatings with iMono surface topography reduces adhesion more than PEG coatings alone (Chapter 5§2). This may point a way toward an antiadhesive strategy that can be explored and optimized for mechanical robustness, longevity and specific environments of application.

CLOSING REMARKS

The development of anti-adhesive surfaces for biomedical applications requires not only a deep understanding of material properties, but also an understanding of the bacterial lifestyle and the process of bacterial adhesion. Furthermore, the specific context of application is critical, as it plays a role in the temperature, nutrient composition, conditioning film, moisture level and exposure to microbes. For these reasons, the close collaboration of biologists, materials scientists and clinicians is required for such a material to be successful. Due to the diversity of bacteria, a pragmatic approach to antifouling might be to choose an area of application, along with the most relevant microbes to that application. The use of model systems that best model the intended environment can provide the best laboratory-level insight into materials performance. For example, we can expose materials intended as urinary catheters to artificial urine at appropriate flow rates. Nonetheless, the complexity of true biological environements, such as the urinary

tract or oral cavity will likely require animal and/or human trials. For example, testing materials for oral applications would benefit from trial placement in the mouths of volunteers. Using such models captures the complexity of the various proteins and diversity of organisms that a material would encounter, as well as the temporal dynamics of nutrient availability, pH and mechanical forces. While the complexity of biological systems seems daunting, it seems likely that a targeted approach to materials design that focuses on specific applications and specific organisms, informed by clinical data and biological insight, will rapidly begin to benefit patients.

BIBLIOGRAPHY

1. McHugh SM, Collins CJ, Corrigan MA, et al. (2011) The role of topical antibiotics used as prophylaxis in surgical site infection prevention. J Antimicrob Chemother 66:693–701.

2. Niska JA, Shahbazian JH, Ramos RI, et al. (2012) Daptomycin and tigecycline have broader effective dose ranges than vancomycin as prophylaxis against a Staphylococcus aureus surgical implant infection in mice. Antimicrob Agents Chemother 56:2590–2597.

3. Francolini I, Donelli G (2010) Prevention and control of biofilm-based medical-device-related infections. FEMS Immunol Med Microbiol 59:227–238.

4. Hentzer M, Givskov M (2003) Pharmacological inhibition of quorum sensing for the treatment of chronic bacterial infections. J Clin Invest 112:1300–1307.

5. Liu C-I, Liu G, Song Y, et al. (2008) A cholesterol biosynthesis inhibitor blocks Staphylococcus aureus virulence. Science 319:1391–1394.

6. Pinkner JS, Remaut H, Buelens F, et al. (2006) Rationally designed small compounds inhibit pilus biogenesis in uropathogenic bacteria. Proceedings of the National Academy of Sciences 103:17897–17902.

7. Cegelski L, Pinkner JS, Hammer ND, et al. (2009) Small-molecule inhibitors target Escherichia coli amyloid biogenesis and biofilm formation. Nat Chem Biol 5:913–919.

8. Friedlander RS, Vlamakis H, Kim P, et al. (2013) Bacterial flagella explore microscale hummocks and hollows to increase adhesion. Proc Natl Acad Sci U S A 110:5624–5629.

9. Flemming H-C, Wingender J (2010) The biofilm matrix. Nat Rev Microbiol 8:623–633.

10. Hochbaum A, Aizenberg J (2010) Bacteria Pattern Spontaneously on Periodic Nanostructure Arrays. Nano Lett 10:3717–3721.

11. Epstein A, Hochbaum A, Kim P (2011) Control of bacterial biofilm growth on surfaces by nanostructural mechanics and geometry. Nanotechnology

12. Hsu L, Fang J, Borca-Tasciuc D, et al. (2013) The Effect of Micro- and Nanoscale Topography on the Adhesion of Bacterial Cells to Solid Surfaces. Appl. Environ. Microbiol.

13. Verran J, Packer A, Kelly P, Whitehead K (2010) The retention of bacteria on hygienic surfaces presenting scratches of microbial dimensions. Lett Appl Microbiol 50:258–263.

14. Raulio M, Järn M, Ahola J, et al. (2008) Microbe repelling coated stainless steel analysed by field emission scanning electron microscopy and physicochemical methods. J Ind Microbiol Biotechnol 35:751–760.

15. Kawai K, Urano M, Ebisu S (2000) Effect of surface roughness of porcelain on adhesion of bacteria and their synthesizing glucans. J Prosthet Dent 83:664–667.

16. Park JW, Song CW, Jung JH, et al. (2012) The effects of surface roughness of composite resin on biofilm formation of Streptococcus mutans in the presence of saliva. Oper Dent 37:532–539.

17. Truong VK, Rundell S, Lapovok R, et al. (2009) Effect of ultrafine-grained titanium surfaces on adhesion of bacteria. Appl Microbiol Biotechnol 83:925–937.

18. Jeong HE, Kim I, Karam P, et al. (2013) Bacterial Recognition of Silicon Nanowire Arrays. Nano Lett 13:2864–2869.

19. Zhang X, Wang L, Levänen E (2013) Superhydrophobic surfaces for the reduction of bacterial adhesion. RSC Adv 3:12003–12020.

20. Fadeeva E, Truong VK, Stiesch M, et al. (2011) Bacterial retention on superhydrophobic titanium surfaces fabricated by femtosecond laser ablation. Langmuir 27:3012–3019.

21. Ivanova EP, Hasan J, Webb HK, et al. (2012) Natural Bactericidal Surfaces: Mechanical Rupture of Pseudomonas aeruginosa Cells by Cicada Wings. Small 8:2489–2494.

22. Liu T, Yin B, He T, et al. (2012) Complementary Effects of Nanosilver and Superhydrophobic Coatings on the Prevention of Marine Bacterial Adhesion. ACS Appl Mater Interfaces 4:4683–4690.

23. Mazumder S, Falkinham J, Dietrich A, Puri I (2010) Role of hydrophobicity in bacterial adherence to carbon nanostructures and biofilm formation. Biofouling 26:333–339.

24. Miyahara Y, Mitamura K, Saito N, Takai O (2009) Fabrication of microtemplates for the control of bacterial immobilization. J Vac Sci Technol A 27:1183.

25. Tang H, Cao T, Liang X, et al. (2009) Influence of silicone surface roughness and hydrophobicity on adhesion and colonization of Staphylococcus epidermidis. J Biomed Mater Res A 88:454–463.

26. Poncin-Epaillard F, Herry JM, Marmey P, et al. (2013) Elaboration of highly hydrophobic polymeric surface — a potential strategy to reduce the adhesion of pathogenic bacteria? Materials Science and Engineering: C 33:1152–1161.

27. Freschauf LR, McLane J, Sharma H, Khine M (2012) Shrink-induced superhydrophobic and antibacterial surfaces in consumer plastics. PLoS One 7:e40987.

28. Sousa C, Rodrigues D, Oliveira R, et al. (2011) Superhydrophobic poly(L-lactic acid) surface as potential bacterial colonization substrate. AMB Express 1:34.

29. Wang S, Jiang L (2007) Definition of Superhydrophobic States. Adv Mater 19:3423–3424.

30. Zhang H, Lamb R, Lewis J (2005) Engineering nanoscale roughness on hydrophobic surface—preliminary assessment of fouling behaviour. Sci Technol Adv Mater 6:236.

31. Truong VK, Webb HK, Fadeeva E, et al. (2012) Air-directed attachment of coccoid bacteria to the surface of superhydrophobic lotus-like titanium. Biofouling 28:539–550.

32. Tuteja A, Choi W, Ma M, et al. (2007) Designing superoleophobic surfaces. Science 318:1618–1622.

33. Tuteja A, Choi W, Mc Kinley GH, et al. (2008) Design Parameters for Superhydrophobicity and Superoleophobicity. MRS Bulletin 33:

34. Xue Y, Chu S, Lv P, Duan H (2012) Importance of hierarchical structures in wetting stability on submersed superhydrophobic surfaces. Langmuir 28:9440–9450.

35. Bahadur V, Garimella SV (2009) Preventing the Cassie-Wenzel transition using surfaces with noncommunicating roughness elements. Langmuir 25:4815–4820.

36. Vazquez G, Alvarez E, Navaza JM (1995) Surface tension of alcohol water+ water from 20 to 50. degree. C. Journal of chemical and

37. Cunliffe D, Smart CA, Alexander C, Vulfson EN (1999) Bacterial adhesion at synthetic surfaces. Appl Environ Microbiol 65:4995–5002.

38. Roosjen A, van der Mei HC, Busscher HJ, Norde W (2004) Microbial adhesion to poly(ethylene oxide) brushes: influence of polymer chain length and temperature. Langmuir 20:10949–10955.

39. Park KD, Kim YS, Han DK, et al. (1998) Bacterial adhesion on PEG modified polyurethane surfaces. Biomaterials 19:851–859.